Investigation of the Effect of MWCNT Filled Epoxy Adhesives in Enhancing the Quality of Dissimilar Material Bonded Joints

Maria Konstantakopoulou

Doctor of Philosophy

School of Mechanical and Systems Engineering

Newcastle University

Abstract

Achieving a high quality adhesive bond between any two parts (also called adherends) requires the presence of a strong adhesive and a strong adhesive/adherend interface, which are both capable of sustaining the stresses that arise within the bonded joint during its service life. The objective of this study is to improve the bond of metal-to-composite joints by modification of the adhesive properties and the adhesive/adherend interface through the addition of multi-wall carbon nanotubes (MWCNTs).

MWCNT/epoxy composites of various weight fractions, i.e. 0.1, 0.3, 0.5 and 1% were manufactured and characterised via a series of mechanical tests in order to assess the effect of different dispersion methods and CNT loadings. Once the mechanical properties were optimised, the MWCNT reinforced epoxy was utilised for the manufacturing of metal-to-metal and metal-to-composite adhesively bonded joints.

Co-cured carbon fibre reinforced laminate to steel (CFRP/Steel), glass fibre reinforced laminate to steel (GFRP/Steel) and glass fibre reinforced laminate to aluminium (GFRP/Aluminium) single lap joints with three overlap lengths, namely 25, 40 and 60 mm, were tested in order to investigate how the MWCNT reinforced epoxy adhesive in relation to the overlap length variation affected the joint performance. Finite element analysis (FEA) was employed to determine the stress field along the overlap length of all dissimilar material joints. The resistance to crack propagation with respect to the different weight fractions of the MWCNT epoxy adhesive was also evaluated via the Mode-I fracture toughness test. Virtual crack closure technique (VCCT) simulation was finally used for the calculation of the critical strain energy release rate.

Lap shear strength is found to increase up to 40% when MWCNTS are incorporated into the epoxy adhesive used to bond the two substrates. The utilisation of the MWCNT reinforced epoxy adhesive is also proved to be beneficial for the critical strain energy release rate. The latter increases with the increase of the CNT loading, yielding the highest values for the case of GFRP/Aluminium joints. The results suggest that the addition of MWCNTs enhances the interfacial properties of the joints resulting in the improvement of the joint strength and adhesive fracture energy.

To my brother, Vasilis

Acknowledgements

I would also like to thank my supervisors Dr. George Kotsikos and Prof. Geoff Gibson for their guidance throughout this research work. Especially I would like to thank Dr. Kotsikos for his support in overcoming the obstacles I faced through my research.

I would like to express my gratitude to my fellow doctoral students Aikaterini Deligianni, Wan Wan Jusoh, James Humphrey, Ayad Mahuof, Dr. Sandra Christke and Dr. Johannes Linden for creating a friendly and inspiring office atmosphere. I also thank the laboratory technicians and especially Brian Stoker, Adam Richardson and Michael Foster for offering valuable assistance during the experimental activities.

My special thanks go to my friends in Newcastle for being always willing to listen to my PhD stories while giving me strength to continue. I also thank my friends from Greece who despite the distance, they were always keen to know what I was doing and how I was proceeding even if it was impossible for them to understand it.

A very special gratitude goes to my partner Dr. Angelos Mintzas for his support, encouragement and patience throughout these years and especially during the writing-up period.

Last but not least, I am grateful to my mum Martha and the rest of my family for always providing emotional support along the way.

Table of Contents

List of Figures

List of Tables

Nomenclature

Abbreviations	Description
2D	Two-dimensional
3D	Three-dimensional
BCP	Block Copolymer
BYK	Disperbyk 2150
CCVD	Catalytic Chemical Vapour Deposition
CFRP	Carbon Fibre Reinforced Polymer
CNTs	Carbon Nanotubes
CVD	Chemical Vapour Deposition
CZM	Cohesive Zone Modelling
DCB	Double Cantilever Beam
DMA	Dynamic Mechanical Analysis
DMF	N-dimethylformamide
DLJ	Double Lap Joint
DSC	Differential Scanning Calorimetry
DWCNT	Double-wall Carbon Nanotubes
EPFM	Elasto-plastic fracture mechanics
FEA	Finite Element Analysis
FESEM	Field Emission Scanning Electron Microscopy
FPL	Forest Products Laboratory Etching

FRP	Fibre Reinforced Polymers
GFRP	Glass Fibre Reinforced Polymer
HLU	Hand Lay-up
LEFM	Linear Elastic Fracture Mechanics
MWCNT	Multi-Wall Carbon Nanotubes
OM	Optical Microscopy
PAA	Phosphoric Acid Anodising
RS	RS-L135/ RS-H136 epoxy resin
SEM	Scanning Electron Microscopy
SENB	Single Edge Notched Beam
SERR	Strain Energy Release Rate
SIF	Stress Intensity Factor
SLJ	Single Lap Joint
SWCNT	Single-wall Carbon Nanotubes
TAST	Thick Adherend Shear Test
TEM	Transmission Electron Microscopy
TGA	Thermogravimetric Analysis
TW	Technowrap 2K L.T. Epoxy Resin
VCCT	Virtual Crack Closure Technique

Symbols	*Description*
a	crack length
B	specimen thickness

E_C	Young's Modulus of Composite Adherend
E_M	Young's Modulus of Metal Adherend
$f(x)$	Geometric Calibration Factor
G_{IC}	Mode-I Critical Fracture Energy
G_I	Mode-I Fracture Energy
G_{II}	Mode-II Fracture Energy
K_{Ic}	Critical Stress Intensity Factor
P	Applied Load
T_g	Glass Transition Temperature
v	Poisson's ratio
W	Specimen Width
x	Longitudinal Coordinate in the Middle of the Overlap

Chemical Formulas	*Description*
Al_2O_3	Aluminium Oxide
H_2SO_4	Sulphuric Acid
H_3PO_4	Phosphoric Acid
Fe_3O_4	Iron (II, III) Oxide
$K_2Cr_2O_7$	Potassium Dichromate
NaOH	Sodium Hydroxide

Chapter 1. Introduction

1.1 Structural Adhesive Bonding

Multi-material structures are essential in the transportation sector where designers are constantly examining techniques to reduce weight and hence, reduce fuel consumption and emission of greenhouse gases. Nevertheless, weight reduction has to be achieved without compromising structural integrity. Composite materials can efficiently meet the aforementioned requirements due to their excellent strength-to-weight and stiffness-to-weight ratios allowing them to replace conventional materials, such as steel and aluminium. However, lightweighting cannot be limited to "single" material structural designs. By joining different materials, each possessing unique properties, an optimised structure can be obtained with a performance that would not have been possible if made by a single material. When it comes to joining fibre reinforced polymers (FRP) with metal parts in order to either strengthen or repair existing structures, adhesive bonding alone or in combination with other mechanical fastening techniques is the preferred technology.

Such hybrid structures are being used in a variety of sectors, namely aerospace, railway, automotive and marine. A fine example of the widespread application of composite-to-metal joints can be found in aerospace industry, where 50 wt.% of the Boeing 787 Dreamliner is manufactured from composite materials, which are joined with other metallic parts to form the fuselage (Figure 1.1).
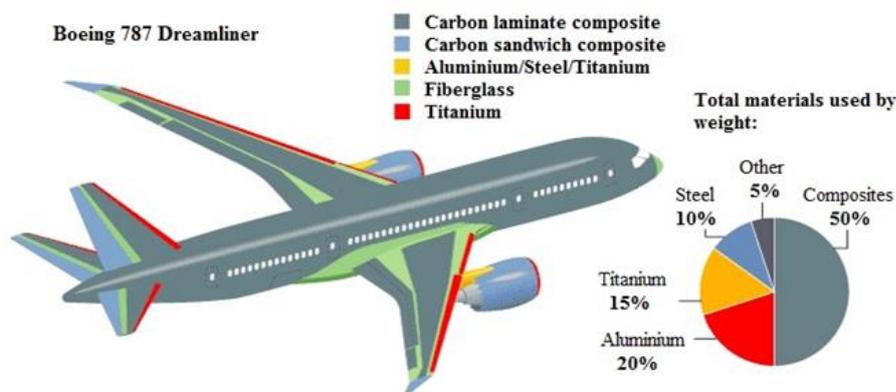
Figure 1.1: Detailed material breakdown for a Boeing 787 Dreamliner [1].

Joining dissimilar materials is also a requirement for the railway sector, where composites have been mostly utilised for the fabrication of the interiors of the train, such as doors,

window frames, flooring, luggage storage and ceilings. In Figure 1.2, a composite roof bonded onto the metal carriage is illustrated.
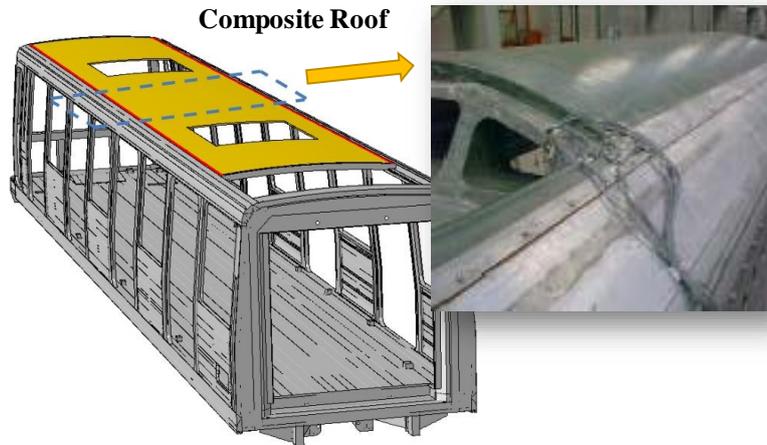
Figure 1.2: Composite roof bonded on metal frame.

Besides weight and fuel saving, the replacement of steel parts with composites is also beneficial for the marine sector, because it reduces the maintenance costs due to the high corrosion resistance of composite materials. The Visby class is the latest class of corvette to be adopted by the Swedish Navy (Figure 1.3a). The hull is constructed with a sandwich design consisting of a PVC core with a carbon fibre and vinyl laminate. Another example of this technology is the La Fayette frigate of the French Navy, which is made of light alloy, glass fibre reinforced polymer and Kevlar (Figure 1.3b).
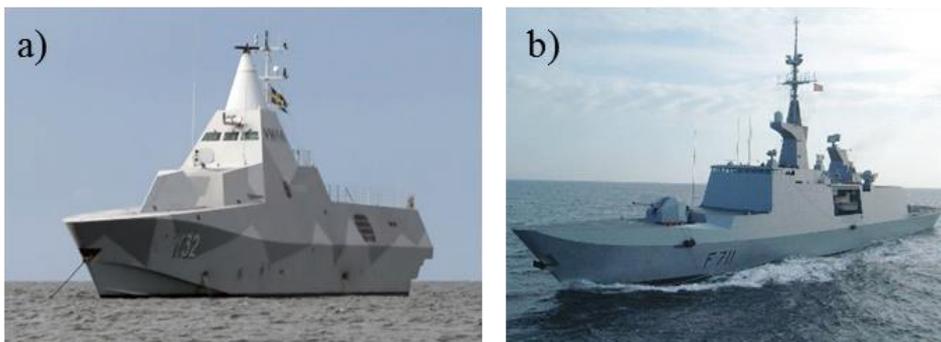
Figure 1.3: a) Visby class naval vessel and b) La Fayette frigate [2, 3].

Another application of dissimilar material joints is pipeline composite repairs. Repairs are engineered, so that even if the metal substrate corrodes away, the composite can sustain the pressure. Composites can be also used in order to join different parts of the metal pipe (Figure 1.4).

Figure 1.4: Pipe composite repair at Walker Technical Ltd.

1.2 Aims and Objectives

Although adhesive bonding allows more flexibility in structural design, joining dissimilar materials presents a great challenge. This is because the materials that are to be joined often have different mechanical, thermal and chemical properties. Therefore, the adhesive and the adhesive/adherend interface must be tailored such as to achieve chemical compatibility between the adhesive and both of the adherends and also have the structural strength to carry the stresses that develop during the joint's service life.

In the literature, the addition of nanomaterials in polymer matrices has been found to improve their mechanical, thermal and electrical properties. One of the most investigated nanofillers are the carbon nanotubes (CNTs), which have been shown to enhance the adhesion of the fibres to the resin. The reason for the improved adhesion is believed to be the better chemical compatibility between the modified polymer and the fibre as well as the ability of the nanotubes to toughen the polymer and the polymer/fibre interface by triggering energy dissipation mechanisms, such as crack deflection. The successful transfer of these unique properties to the adhesive used to bond similar or dissimilar materials can potentially improve the load carrying capacity of the joints.

The aim of this work is to develop strong joining techniques for metal-to-metal and composite-to-metal joints by utilising the characteristic properties of multi-wall carbon nanotubes, which are introduced at the joint interfacial region via mixing with an epoxy resin adhesive. Steel/Steel, Aluminium/Aluminium, CFRP/Steel, GFRP/Aluminium and GFRP/Steel joints are assessed in terms of joint strength and fracture toughness, while considering different overlap lengths and CNT loadings of the nano-reinforced adhesive.

There is a vast amount of studies investigating the performance of polymers reinforced with SWCNTs, DWCNTs, MWCNTs and functionalised CNTs [4-7]. There are also many studies investigating the performance of adhesively bonded joints with similar and dissimilar material adherends bonded with reinforced adhesives. Albeit some of these studies show an

improvement on the adhesive joint strength and fracture toughness, in many cases it is not clear which mechanisms lead to such an improvement[8-11]. This work attempts to address the latter, through a systematic study, which starts from the investigation of the properties and failure modes of the CNT reinforced bulk adhesives and then, moves on with the investigation of the properties and failure modes of the resulting adhesively bonded structures. In this way, it is attempted to link the failure modes from the material level up to the adhesively bonded structural level.

Chapter 2. Adhesively Bonded Joints

2.1 Introduction

The purpose of a joint is to efficiently transfer tensile and/or shear loads, between two adherends [12]. Joints represent one of the greatest challenges in the design of structures, because they entail both geometrical and material discontinuities, which give rise to stress concentrations [13]. Two types of load carrying joints are mostly used:

- Mechanically fastened joints
- Adhesively bonded joints

In engineering applications, adhesively bonded joints often substitute mechanical joints, because they provide many advantages over the conventional mechanical fasteners. Among these advantages are the improved damage tolerance and lower fabrication cost and structural weight. Adhesive joints are also structurally more efficient than mechanically fastened joints [13], because they present better opportunities for eliminating stress concentrations due to the absence of holes providing greater load carrying area compared to bolted joints [4]. Thus, a more uniform stress distribution along the overlap area is obtained, which leads to higher stiffness and load transfer. Due to the polymeric nature of the adhesive, adhesive joints provide good damping properties achieving high fatigue strength [14]. Adhesives can also bond dissimilar materials with different coefficients of thermal expansion due to the adhesive flexibility that can compensate for the difference between the adherends.

However, adhesives are quite sensitive to environmental factors, such as humidity and temperature, which affect the long-term durability of the joint. Another drawback of the manufacturing process of adhesively bonded joints is the requirement of surface preparation of the areas to be bonded prior to the application of the adhesive, a process not required for mechanically fastened joints. Moreover, adhesive bonding is usually not instantaneous and entails the use of fixtures in order to align and maintain the substrates in position. In addition, the solidification of some adhesives occurs at certain temperature, which can further complicate the bonding process. Finally, mechanically fastened joints are preferred over adhesively bonded joints when either disassembly of a joint or replacement of a damaged structure is required, processes that are not feasible when utilising the adhesive bonding technology.

An overview of the parameters that affect the joint performance as well as the analytical methods that have been developed over the years will be presented in this chapter.

2.2 Adhesively Bonded Joint Configurations

Depending on the structural requirements, a wide variety of adhesively bonded joints exists, e.g. single lap joints, double lap joints, scarf joints, step joints etc. In Figure 2.1, some of the most common joint configurations are shown.
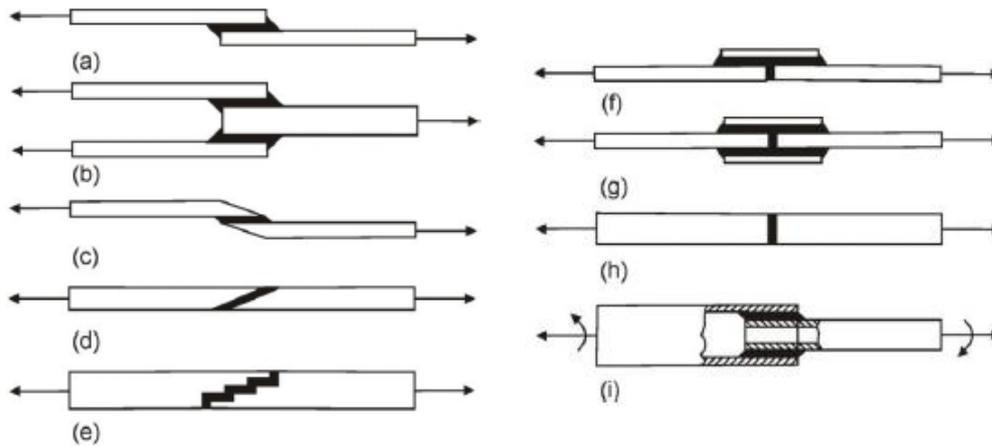
Figure 2.1: Typical configurations for adhesively bonded joints: a) single lap, b) double lap, c) scarf, d) bevel, e) step, f) butt strap, g) double butt strap, h) butt and i) tubular lap joints [15].

The single lap joint is one of the most widely used joint configurations, because of its design simplicity, low-cost manufacture and simple testing procedure. Due to the eccentricity of the loading path caused by its structure, a complex stress state arises within the adhesive (Figure 2.2), which is also representative of that found in many structural applications.
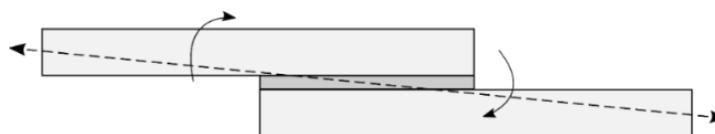
Figure 2.2: Load path eccentricity of single lap joint.

The external load in single lap joints is primarily transferred through shear stresses in the adhesive and due to the fact that the adhesives are much more resistant to shear than direct tension, single lap joints are favoured over other joint configurations (i.e. butt, scarf joints) in most structural joining applications. Single lap joints are also used in order to characterise different types of adhesives.

2.3 Failure Modes in Adhesively Bonded Joints

The failure modes observed in single lap joints depend on the quality of the bond, specimen geometry (i.e. adhesive and adherend width and thickness) and loading and they have to be determined in order to gain full understanding of the properties of the adhesive and joint under investigation [16]. The main failure modes suggested by the ASTM D5573-99 standard [17] are shown in Figure 2.3.

a) Adhesive Failure (ADH)   b) Cohesive Failure (COH)

c) Thin-Layer Cohesive Failure (TLC)   d) Fibre-Tear Failure (FT)

e) Light Fibre-Tear Failure (LFT)   e) Stock-Break Failure (SB)
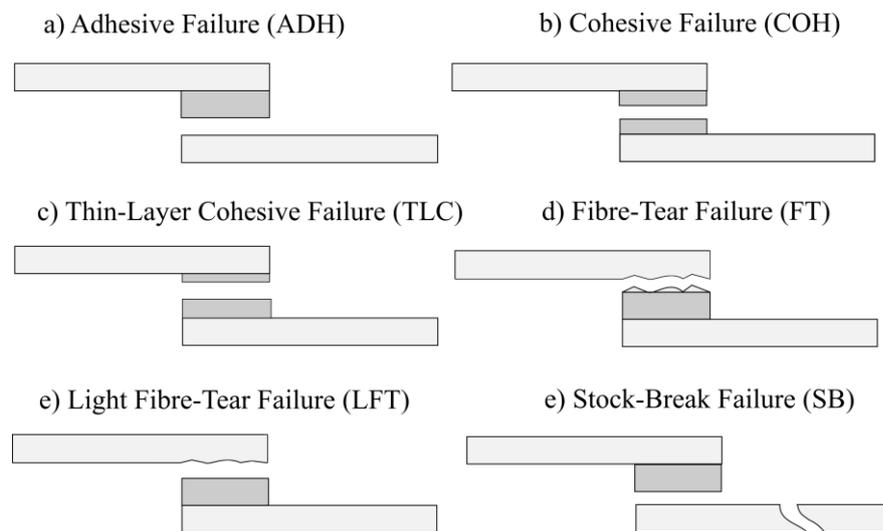
Figure 2.3: Possible failure modes of FRP composite bonded joints.

Adhesive failure (Figure 2.3a) occurs at the adhesive/adherend interface and indicates manufacturing problems, which often suggest poor surface preparation or existence of impurities at the adherend surface. Cohesive failure (Figure 2.3b) takes place within the adhesive. It is more common in joints with metal adherends, because the adhesive tends to fail first due to its lower tensile and shear strength compared to the corresponding strengths of the substrates. Thin-layer cohesive failure (Figure 2.3c) is similar to cohesive failure, however, in the former case, failure occurs very close to the adhesive/adherend interface and it is characterised by light dusting of the adhesive on one adherend surface and a thick layer of adhesive left on the other [18]. Stock-break failure (Figure 2.3f), i.e. failure outside the bonded region can occur in joints with composite substrates, however, fibre-tear and light fibre-tear failure (Figure 2.3d and e) are the most common failure modes in composite joints. Fibre-tear failure is characterised by the appearance of exposed fibres on the fracture surface of the substrate. On the contrary, light fibre-tear failure occurs within the FRP adherend, but close to the adhesive/adherend interface. It is characterised by a thin layer of the FRP matrix visible on the adhesive with few or no fibres on the adhesive fracture surface. Defects in the composite substrate, such as air bubbles and poor impregnation of the fibres favour the fibre-

tear and light fibre-tear failure modes initiating the failure process in the region close to the adhesive/adherend interface. Another reason for failure initiation at the adhesive/adherend interface apart from the manufacturing defects is the lower in-plane shear strength and through the thickness strength of the composites compared to the corresponding shear and tensile strength of the adhesive and adhesive/composite interface. Failure is a complicated phenomenon and can entail a combination of the aforementioned failure modes, thus leading to a mixed mode failure. However, cohesive failure is preferred to adhesive failure, since more energy is required for the crack to propagate, hence one can design the joint (overlap length) to ensure that failure will occur at the adherend (metal or composite), once the most probable failure mechanism is known.

2.4 Single Lap Joint Parameters

The main factors that determine joint strength are the following [15]:

- Specimen preparation process (i.e. surface treatment, spread of adhesive, curing temperature)
- Geometry of the specimen (i.e. specimen size, thickness of adherends and adhesive)
- Physical parameters of the adherends and the adhesives (i.e. elastic modulus, cohesive strength, volume contraction during curing procedure)
- Testing conditions (i.e. magnitude of load applied, temperature, relative humidity, loading speed)

The effect of these parameters on the joint performance has been extensively investigated in the literature and some of the studies focused on the geometrical parameters and the substrate surface preparation techniques are presented below.

2.4.1 Overlap Length

The influence of the overlap length variation on the lap shear strength has been investigated by many researchers. da Silva et al. [19] examined the effect of the overlap length (12.5mm, 25mm and 50mm) on joints with three types of steel adherends (i.e. low, intermediate and high strength steel) bonded with three different adhesives (i.e. ductile, intermediate and brittle adhesive). It was found that when the overlap length increased and provided that the adhesive was sufficiently ductile and the adherends did not yield, lap shear strength increased almost linearly. For substrates that yielded, lap shear strength reached a plateau with the increase of the overlap length, which was defined by the yielding of the adherend. The increase of the failure load with the increase of the overlap length for flexible adhesives was also reported in

[20]. In another study [21], an increase by 45.5% in lap shear strength of joints with steel adherends was shown when the overlap length increased from 12.5mm to 50mm. Karatzas et al. [22] investigated the effect of the overlap length variation (12.5mm, 100mm, 200mm and 300mm) on the joint strength of CFRP/steel single lap joints. It was found that the failure load of the joints increased with the increase of the overlap length and the magnitude of this increase depended on the quality of the bond.

Song et al. [23] investigated how various overlap lengths (12.7mm, 19.05mm, 25.4mm, 38.1mm and 50.8mm) influenced the lap shear strength of the corresponding composite joint configurations. The results suggested that by increasing the overlap length, the obtained failure load increased, because the overall stress level, i.e. von-Mises stress along the mid-surface of the adhesive including the peak stresses at the end areas, decreased as shown from FEA. This is because the stresses are distributed over a larger area. However, the increase of the overlap length was effective up to a threshold, since the reduction rate of the peak stresses at the ends decreased with the increase of the overlap length. Similar findings were reported in [24], where the overlap length varied from 15mm to 60mm. The maximum shear strength of aluminium single lap joints was obtained for 40mm overlap length with further increase of the overlap length leading to reduction of the lap shear strength.

Seong et al. [25] studied how the variation of the overlap length (15mm, 20mm, 25mm, 30mm, 35mm, and 40mm) of adhesively bonded CFRP to aluminium single lap joints affected the joint strength. The failure load was found to increase with the increase of the overlap length, while the bonding strength decreased as the overlap length increased. It was also shown that the failure load was not linearly proportional to the overlap length and hence, it did not increase substantially when the overlap length was greater than 25mm or when the overlap length-to-width ratio was greater than 1. It was therefore concluded that when the overlap length-to-width ratio of single-lap bonded joints is much greater than 1, further increase of the overlap is not beneficial.

2.4.2 Adhesive Thickness and Type

The thickness and type of the adhesive, i.e. brittle or ductile, play a critical role in joint performance. Crocombe [26] proposed that the strength of a joint bonded with ductile adhesive should increase with the decrease of the bondline thickness, whereas for the case of brittle adhesive, the strength should increase with the adhesive thickness. Experimental results in various studies, such as in [27] showed that lap joint strength increased as the bondline got thinner (ranging from 0.05mm to 0.5mm). However, this observation might vary depending

on the type of loading (shear or peel), the adherend behaviour (elastic or plastic) and the type of the adhesive (ductile or brittle).

da Silva et al. [27] investigated the discrepancy between the classical elastic analyses and the experimental results regarding the effect of the adhesive type and thickness on the bond strength. They used three different types of adhesive (i.e. brittle, intermediate and ductile) with strain to failure ranging from 1.3% to 44% and varied the thickness according to the following values: 0.2mm, 0.5mm and 1mm. High strength steel adherends were used as substrates in order to remain in the elastic region and avoid plastic deformation. It was reported that lap shear strength increased as the bondline thickness decreased and the adhesive toughness increased. For the case of joints with low strength steel adherends, it was found in [19] that the failure load was independent of the adhesive. In [20], two different types of flexible adhesives, i.e. polyurethane and RTV silicone rubber were investigated under the influence of temperature. For the polyurethane adhesive, the failure load and the overall stiffness of the single lap joints decreased as the bondline got thicker, whereas for the RTV silicone rubber adhesive, the failure load increased as the bondline got thicker.

The influence of the adhesive in terms of toughness (namely very ductile, intermediate and very brittle) and thickness (0.5mm, 1mm and 2mm) on the lap shear strength was also examined by da Silva et al. [21]. Lap shear strength decreased by 18.9% as the adhesive thickness increased. An increase of the joint strength up to a specific adhesive toughness was observed, followed by a decrease for higher toughness values. This variation indicated that the peak joint strength achieved corresponded to the best combination of adhesive thickness and toughness. Arenas et al. [28] applied a statistical analysis based on Weibull distribution and proposed the optimum adhesive thickness aiming to the best mechanical performance and reliability. Aluminium single lap joints with various adhesive thicknesses were manufactured and tested to determine the influence of the thickness on the mechanical behaviour of the joint. It was found that for thicknesses between 0.4mm and 0.8mm, where cohesive failure was observed, shear strength increased with the reduction of the adhesive thickness. On the contrary, for adhesive thicknesses less than 0.4mm, where cohesive/mixed failure mode was observed, shear strength exhibited higher values compared to those obtained for adhesive thickness greater than 0.4mm, but with high deviation. By correlating the experimental results with the statistical analysis, 0.5mm was suggested as the optimum adhesive thickness.

Bak et al. [29] varied the adhesive thickness (0.2mm and 0.4mm) of GFRP single lap joints in order to investigate the impact on the lap shear strength and failure mode of the joint. They

then compared the experimental results against acoustic emission and finite element analysis (FEA). In both experimental and numerical results, the failure load decreased with the increase of the adhesive thickness. Davies et al. [30] characterised aluminium joints bonded with epoxy adhesive of different thicknesses by testing them under three different types of loading using the Arcan fixture. It was reported that for shear loading, there was a small reduction in joint strength and failure strain with the increase of the adhesive thickness, whereas under tensile loading, there was a significant drop of the aforementioned properties. This variation was explained via numerical analysis, which showed a change in stress when thicker adhesives were used. Stress concentration was higher for tension than tension/shear loading and lower for shear loading, but in all cases it increased with the adhesive thickness. It was proposed that for this Arcan test, the adhesive thickness should be limited to 0.6mm to characterise the joints in tension and below 0.8mm for tension/shear and pure shear. It was finally concluded that as the adhesive thickness decreased, the edge effects, i.e. stress concentration decreased as well.

Stress concentration at the ends of the overlap length also depends on the stiffness of the adhesive. Therefore, the so called *bi-adhesive* (Figure 2.4), i.e. two adhesives with different stiffnesses can be used as an alternative along the overlap length. Stress distribution is not uniform within the bonded area. It peaks at the edges of the overlap length and obtains its minimum value at the middle of the overlap length. In order to promote uniform stress distribution, a high stiffness adhesive is used at the middle part of the overlap, while a low modulus adhesive is applied at the edges.
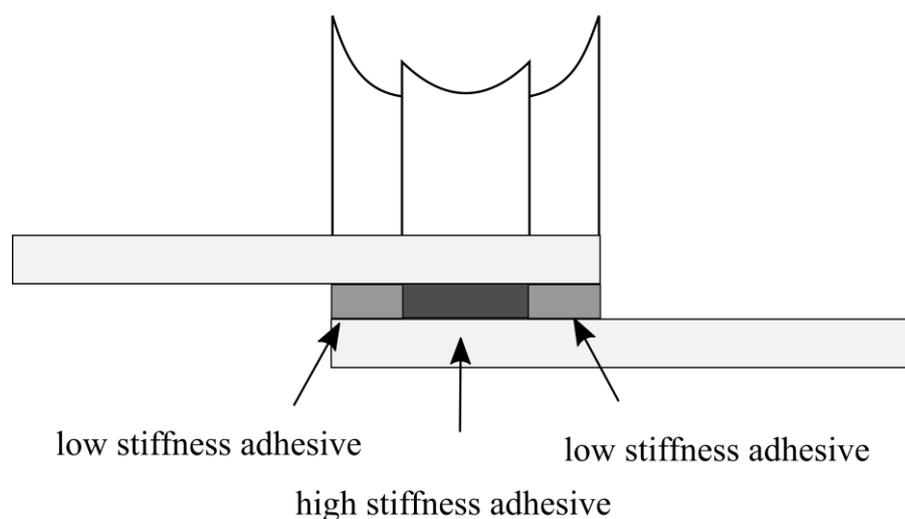
Figure 2.4: Bi-adhesive in single lap joints and schematic adhesive shear stress distribution.

Pires et al. [31] studied how the joint strength was affected when a high stiffness adhesive, a low stiffness adhesive and a bi-adhesive were used to bond single lap joints. Although there was a significant difference between the high and low Young's moduli of the two adhesives, 5.9GPa and 1.8GPa respectively, the joints exhibited similar strength when either of the two was used. This might be attributed to the fact that a high stiffness adhesive can sustain high loads, whereas the low stiffness adhesive is capable of distributing the stresses more uniformly. Nevertheless, when the bi-adhesive was used, the shear stress peaks at the overlap ends were lower compared to the other cases leading to an increase of 22% in joint strength.

2.4.3 Adherend Thickness and Type

Another parameter that has to be considered when adhesively bonded joints are fabricated is the material of the adherend in combination with its thickness. According to Gledhill et al. [32], adherend thickness is critical for the joint strength with the latter being also affected by the adherend material. For high strength adherends, increase of adherend thickness, results to an increase on the applied bending moment (due to higher eccentricity of the loading path), which consequently results to a decrease in the joint strength. On the other hand, when the thickness of low strength adherends increases, the adherends become more robust preventing them from plastic deformation. The aforementioned observations were also validated in [19] and [21], where the lap shear strength increased as the yield strength of low and high strength steel adherends increased. For the case of low strength steel and CFRP adherends [23], lap shear strength also increased when their thickness increased. Pinto et. al [33] evaluated the joint strength of single lap joints between similar and dissimilar adherends (PE=PE, PE=PP, PE=CFRP, PE=GFRP, PP=PP, CFRP=CFRP and GFRP=GFRP) bonded with an acrylic adhesive. The experimental results were in good agreement with the numerical results obtained from a mixed-mode (I+II) cohesive damage model. From the stress analysis of shear and peak stresses in the adhesive layer along the overlap length, it was concluded that as the adherend stiffness increased, the joint bending reduced and thus, the stresses at the overlap ends decreased resulting in the increase of the joint strength.

Owens and Sullivan [34] tested aluminium-to-aluminium and composite-to-aluminium single lap joints bonded with a rigid and a flexible adhesive. They found that the joint stiffness was primarily affected by the stiffness of the respective adherends rather than the modulus of the adhesive. The joints with less stiff adherends significantly decreased the overall joint stiffness. Anyfantis and Tsouvalis [35] investigated CFRP-to-steel joints with two overlap lengths (25 and 75mm), two adhesive thicknesses (0.5 and 0.85mm) and two composite

adherend thicknesses. They found that the effect of the adhesive thickness and stiffness ratio[2] on the strength and overall stiffness of the joints was not as important as the overlap length.

2.4.4 Spew Fillet

Stress concentrations arising due to the abrupt change of geometry at the overlap ends affect the strength of single lap joints. Therefore, many geometric solutions, such as the use of spew fillets[1] and adherend profiling have been proposed in order to provide a smoother transition in joint geometry and minimise the peel stresses. For instance, spew fillets have been used in many studies in order to redistribute the stresses at the overlap ends and therefore, reduce stress concentration (Figure 2.5).
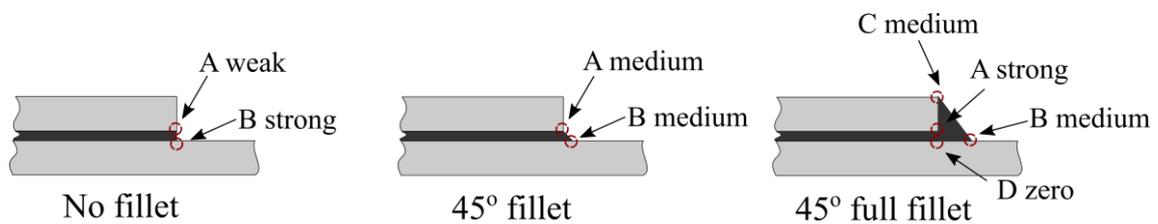
Figure 2.5: Strength of singularities with and without fillet.

Tsai et al. [36] reported that the spew fillet can significantly reduce the adhesive shear and peel stress concentrations. Lang and Mallick [37] also presented similar results. da Silva and Adams [38] compared different designs of double lap joints (titanium/CFRP/titanium), where tapers and/or fillets were used. Dissimilar material double lap joints, which either had an outside or an inside taper and joints with a fillet combined with an inside taper, were investigated. Experimental and numerical results showed that the highest value of lap shear strength was obtained when the internal adherend taper was combined with an adhesive fillet design (Figure 2.6).
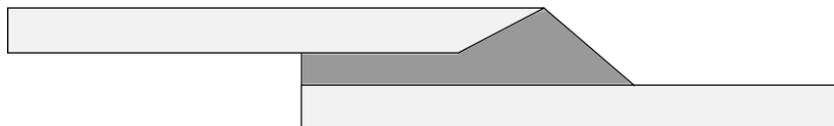
Figure 2.6: Inside taper and adhesive fillet in single lap joints.

---

[1] Spew fillets are formed by the excess of adhesive squeezed out of the lap region during the joint manufacture.
[2] Stiffness ratio is defined as $E_C t_C / E_m t_m$, where E_C and E_m are the Young's moduli of the CFRP and steel adherends respectively, and t_C and t_m are the CFRP and steel thicknesses.

2.4.5 Substrate Surface Preparation

Substrate surface preparation [39] is essential for the successful implementation of adhesive bonding technology. Both short-term bond strength and long-term durability depend on the interaction between the polymer (adhesive or primer) and the pre-treated surface of the substrate. Therefore, the surfaces to be bonded must be prepared in a way, so that the adhesion between the substrate and the adhesive is optimised. Hence, the quality of the bond is improved and eventually a load bearing structure is achieved.

A clean surface is a necessary condition for adhesion, but not sufficient for bond durability [16]. The key-requirements that can guarantee good surface preparation are listed below [14]:

a) The surface must be clean from any contamination that can interfere with the adhesive bond.
b) The adhesive or primer must wet the adherend surface.
c) The surface preparation must enable and promote the formation of chemical and/or physical bonds across the adherend/adhesive interface.
d) The interface must be stable under the service conditions during the service life of the bonded structure.
e) The surface formed by the treatment must be reproducible.

Aviation and aerospace industry have developed and used protective treatments and processes in order to obtain good durability of adhesively bonded joints and ensure that the integrity of the structure is not degraded during service and under extreme environmental conditions. There are many surface pre-treatment methods that a metal substrate can undergo prior to the application of the adhesive and they can be divided into three general categories:

a) Abrasion, i.e. grit blasting, sanding, shot blasting: it exposes the metal surface which is free of contaminants, such as grease and oil.
b) Chemical treatment, i.e. etching in acidic (e.g. Forest Products Laboratory) or alkaline solutions: it deoxidises the metal surface and provides some roughening. However, corrosion of the metal due to entrapped acid might occur.
c) Electrochemical treatment, i.e. anodising in acidic solutions (e.g. Phosphoric Acid Anodising and Chromic Acid Anodising): during this process, mechanical interlocking is promoted at the adhesive/adherend interface via the flow of adhesive into the pores created on the metal surface.

Surface Pre-treatments for Aluminium Substrates

The most widely applied surface treatments on aluminium substrates are the following:

- Forest Products Laboratory Process (FPL)
- Phosphoric Acid Anodising Process (PAA)
- Chromic Acid Anodising Process (CAA)

Acid etching process (e.g. sulphuric acid sodium dichromate processes) can be used as standalone treatment [39] prior to bonding or as pre-treatment prior to anodising process. Etching creates morphologies, i.e. protrusions on the aluminium surface without the use of electrical current. Due to the development of these protrusions the interfacial area available for chemical bonding increases by 10% [40]. However, the structures obtained from etching process [39] are generally not as robust as those from anodising and do not provide the same level of mechanical interlocking of the polymers with the pore structure.

During phosphoric acid anodising process (PAA) [41], the natural oxide layer on the aluminium surface grows thicker via an electrolytic process. The final oxide film produced consists of two layers: a thin, dense barrier layer at the metal surface and a thicker, porous outer layer. The pore size and coating thickness are dependent on the bath temperature and the applied voltage. However, interlocking occurs only when the polymeric adhesive wets and penetrates the pores of the oxide film. This wetting process is realised by the nanoscale pores that create capillary forces and assist the adhesive penetration. The main advantage of this process is that the anodic film acts as protective barrier, isolating the metal substrate from the environment ensuring the long-term durability of the bond. Long-term durability is mostly determined by the degree of stability of the aluminium oxide in a humid environment. Moisture transforms the oxide to hydroxide with an accompanying morphological change. The resulting material, called boehmite, which is a form of aluminium hydroxide, adheres poorly to the aluminium beneath it. Therefore, once it forms, the overall bond strength is severely degraded [42].

Etching and anodising pre-treatment processes are often combined. Firstly, abrasion and immersion of the aluminium substrate in an alkaline solution take place in order to remove the weak oxide layer. Then, etching followed by anodising are applied, which produce porous oxide films with a certain degree of roughness on the metal surface. The oxide protrusions [40, 43] created, increase the contact area and mechanically interlock with the adhesive. The microscopic interlocking [43] is a critical factor that affects adhesion at the epoxy oxide

interface and results in the formation of much stronger bonds and thus, enhanced bond strength. In case of good adhesion, the long-term durability of metal/polymer bonds, which depends a lot on the environmental lack of stability (i.e. moisture intrusion), also improves. It is the dissolution of the protective phosphate layer during the hydration process that gives PAA aluminium surface its superior hydration resistance and hence, its long-term durability [42].

According to Venables et al [40], the comparison between the aforementioned surface preparation processes shows that while the FPL surface is characterised by protrusions (Figure 2.7a), the PAA surface has well-developed hexagonal cells and protrusions, which are much longer (Figure 2.7b). The oxide layer of the PAA treated surface is also considerably thicker [43].
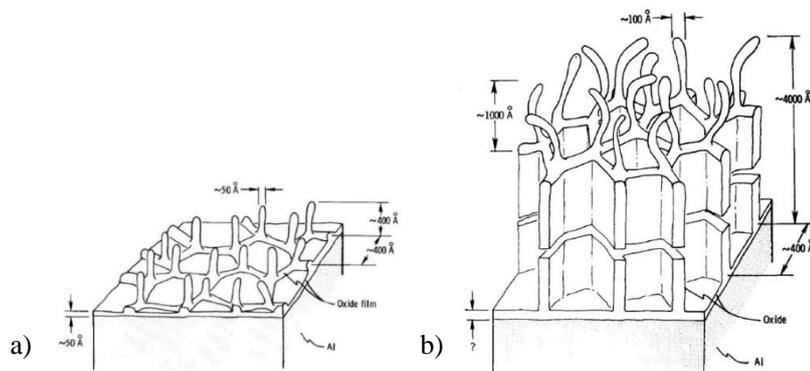
Figure 2.7: Isometric drawing of oxide structure on: a) FPL and b) PAA surface [40].

On the other hand, CAA, which is mostly used in Europe, because it is a more environmental friendly process comparing to the other two processes [44], is characterised by a densely packed thick oxide layer. In spite of some porosity on the oxide film formed during this process, it lacks the microscopic protrusions that characterise the other two surfaces (Figure 2.8).
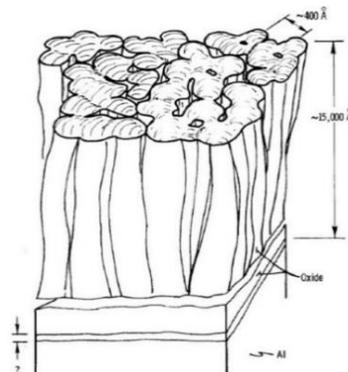
Figure 2.8: Isometric drawing of oxide structure on CAA surface [40].

This observation suggests that the initial bond strength resulting from the use of the CAA process may not be as good as that obtained when FPL or PAA methods are employed, because it lacks the high degree of mechanical interlocking. Nevertheless, the greater thickness and denser structure of the CAA surface may provide an increased corrosion protection for those structures, where long-term durability is required. To sum up, PAA surface treatment provides better mechanical interlocking with the epoxy and therefore, exhibits stronger bond than that of the FPL surface, whereas the thicker oxide film of the CAA surface provides better corrosion resistance.

Surface Pre-treatments for Steel Substrates

For steel substrates unlike the aluminium substrates, no general surface pre-treatments have been developed. This is due to following reasons [14]:

- Industries, like the automotive have been focused on developing adhesives and processes that require minimal surface preparation.
- Unlike aluminium and titanium, it is difficult to grow a stable film with the fine micro- or nano-roughness needed for good adhesion on steel.
- Different alloys can require different pre-treatments, therefore, a process that might be suitable for one alloy, it might give different results for another alloy.

Although several chemical etchants, such as nitric and chromic acid have been used for the surface preparation of steel samples, grit blasting has been proved to be superior to chemical processes and hence, it is the most commonly used pre-treatment.

2.4.6 Co-curing and Secondary Bonding

There are two ways of manufacturing adhesively bonded joints: co-curing and secondary bonding. Both methods present advantages and disadvantages. In secondary bonding, an additional adhesive is used to bond the cured substrates, which introduces new parameters that need to be taken into account, such as substrate surface preparation, adhesive thickness, use of fillets etc. For co-cured joints, the two most important parameters are the substrate surface preparation and the type of the adhesive. Co-cured joints can be manufactured with or without the use of adhesive (usually adhesive film). When no adhesive film is used, the same resin used for the composite manufacturing is also used for bonding and therefore, the curing of the composite substrates and the adhesive occur at the same conditions (time and temperature). Hence, the design and analysis of co-cured joints for composite structures are simpler than those where additional adhesive is utilised [45]. Although co-curing is usually

preferred to secondary bonding, it can be impractical in cases where assembly of large and complex composite structures is required.

Park et al. [46] investigated the effect of different manufacturing methods for carbon/epoxy composite single lap joints for different environmental conditions: a) room temperature and dry, b) elevated temperature and wet and c) cold temperature and dry. The four different bonding methods studied were the following: co-curing without adhesive, co-curing with additional adhesive, secondary bonding during which additional adhesive was used to bond the cured laminates and co-bonding during which additional adhesive was used between the cured laminate and the uncured prepreg. In all environmental conditions, co-cured single lap joints exhibited the highest strength. Kim et al. [47] also compared different bonding methods for CFRP/CFRP single lap joints, namely co-curing with or without adhesive and secondary bonding. The highest joint strength value was obtained for the co-cured joints without adhesive and the lowest values for the co-cured joints with adhesive. Differences in failure modes between the three cases were also observed. Catastrophic delamination occurred for both cases of co-curing, whereas progressive failure along the adhesive layer took place for secondary bonding. Song et al. [23] investigated four different methods for bonding composite single lap joints, i.e. co-curing with (prepreg + adhesive + prepreg) and without adhesive (prepreg + prepreg), secondary bonding (laminate + adhesive + laminate) and co-bonding (prepreg + adhesive + laminate). Experimental findings showed that the highest strength was obtained for co-cured joints without adhesive and secondary bonded joints. Co-bonded joints yielded the lowest strength.

2.5 Dissimilar Material Joints and Nano-modified Adhesives

Most of the structural adhesives, such as epoxies, exhibit lower strength than the adherends they bond resulting in failure of the bondline. Therefore, a means of improving the adhesive properties through the reinforcement of the adhesive with nanofillers is an approach often adopted. Carbon nanotubes have been used to a great extent due to their exceptional mechanical properties, i.e. Young's modulus=0.9TPa and tensile strength=150GPa [48]. Hedia et al.[49] showed that the use of 1 wt.% of organic MWCNT adhesive increased the ultimate stress of neat resin by 29% for both tensile and single edge notched specimens consisting of white iron substrates. The residual strength and fracture toughness were also increased by 56% and 265% respectively due to the increased number of features on the surface, which increased fracture surface and hence, the energy absorption. A few of the

studies that include the utilisation of CNTs and other nanofillers in adhesives are mentioned below.

Khalili et al. [18] investigated the effect of adhesive reinforcements on the properties of lap joints subjected to tension, bending, impact and fatigue. In this study, glass fibre reinforced laminates were bonded with an epoxy resin reinforced with unidirectional, chopped glass fibres (30 vol.% with fibre orientation: 0°, 45°, 90°) and micro-glass powder (20, 30, 40 vol.%). Apart from the case of 90° fibre orientation, joint strength increased when the adhesive was reinforced with either glass powder or fibres. The fatigue life increased by 125%, the ultimate joint strength in tension increased by 72%, the ultimate bending joint strength increased by 112% and the impact joint strength increased by 63%. Srivastava [8] examined the use of epoxy resin containing 3 wt.% of MWCNTs in order to bond carbon/carbon (C/C) and carbon/carbon-silicon carbide (C/C-SiC) composites. It was reported that MWCNTs increased the strength and toughness of the bulk adhesive, resulting in an increase of the strength of the lap joints bonded with the MWCNT reinforced epoxy adhesive. Kwon et al. [9] investigated the potential of improving the bond strength of CFRP scarf joints through the addition of CNTs along the interface of the joint. The CNT reinforced joints exhibited 10% higher strength.

Gude et al. [50] assessed the strength and toughness of CFRP composite joints after the incorporation of carbon nanotubes (0.25 wt.%) and carbon nanofibres (0.5 wt.%) to the epoxy resin adhesive. It was found that both nano-reinforcements increased the critical fracture energy, G_{IC}, of the joints without however, affecting the lap shear strength. Carbon nanotubes also improved the interfacial shear strength between the adherend and the adhesive and prevented the crack from propagating along the adhesive layer by changing the failure mode from fully adhesive to partly cohesive. Hsiao et al. [51] investigated the effect of the inclusion of multi-wall carbon nanotubes (i.e. 1 and 5 wt.%) in epoxy resin used to bond graphite fibre/epoxy composite adherends. After the addition of 5 wt.% of MWCNTs into the adhesive, lap shear strength increased by 45.6% compared to the values obtained for the pure epoxy resin adhesive. Another interesting finding was that the failure mode shifted from adhesive (along the bonding interface) for the epoxy adhesive to cohesive for the MWCNT reinforced adhesive, where the graphite fibres of the adherends were exposed on the fracture surface.

Various nano-reinforced epoxy resin adhesives have been also used to bond metal-to-metal and metal-to-composite joints. In [52], Goh et al. developed adhesives with improved

strength, which were used to bond aluminium substrates. Al_2O_3 nanofillers in combination with silane additives incorporated in the adhesive were found to improve the lap shear strength and changed the failure mode from adhesive to cohesive. The mechanical performance of aluminium single lap joints bonded with aluminium powder filled epoxy (10, 25, 50 wt.%) was studied by Kahraman et al. [53]. It was found that joint strength increased with the increase of the aluminium filler content and all joints failed cohesively indicating good adhesion at the metal surface. Yu et al. [10] studied the adhesion properties of carbon nanotube reinforced epoxy (i.e. 0.5, 1, 2, 3.5 and 5 wt.%) used for the bonding of aluminium alloy substrates. The fracture toughness of all CNT reinforced bonded joints increased compared to the unreinforced ones. However, the highest value was achieved for 1 wt.% and further increase of the CNT content led to the decrease of the fracture toughness due to agglomeration. Carbas et al. [54] added different amounts of carbon black (0, 1, 5, 10, 20 vol.%) in the adhesive used to bond steel substrates in order to improve the stress distribution along the overlap length and thus, increase the joint strength. Joints with functionally graded bondline exhibited higher joint strength than the cases where the carbon black was either homogeneously dispersed along the overlap length or not used at all.

Tensile and shear properties of composite interfaces reinforced with two types of nanofillers, i.e. carbon nanotubes and alumina nanopowder (up to 15 wt.%) were studied by Meguid and Sun [11]. CFRP substrates were bonded with aluminium alloy substrates using the reinforced epoxy adhesives. Both shear and tensile properties (strength and modulus) increased with the increase of the weight percentage of the nanofillers. However, further increase of nanofillers above 10 wt.% degraded the properties. Kang et al.[55] incorporated 2 wt.% of CNTs into epoxy resin in order to use it as adhesive for CFRP/Aluminium single lap joints. Lap shear strength decreased by 36.62%, whereas fatigue strength increased by 12.8% compared to the joints without carbon nanotubes. Finally, the addition of 1 wt.% MWCNTs increased Mode II critical strain energy release rate by approximately 20% [56]. An interesting observation was that for the samples with higher G_{IIC} values, failure occurred mainly through the steel/adhesive interface, while for the samples with lower G_{IIC} values failure was noticeable at the composite/adhesive interface.

2.6 Analyses of Adhesively Bonded Joints

There are two basic mathematical approaches for the analysis of engineering structures and hence, for adhesively bonded joints: a) closed-form analyses or analytical methods [16, 57, 58] and b) numerical methods (i.e. finite element analyses) [59, 60]. In order to achieve closed-form solutions, a number of simplifications on the geometry as well as assumptions on

the material behaviour are required, whereas numerical methods can handle complex structures and nonlinear material properties. Despite their limitations, closed-form solutions are useful especially when parametric studies are required [14].

In the simplest and most widely used analysis for the single lap joint (SLJ), which is also adopted in the ASTM and ISO standards, the adhesive is considered to deform only in shear and the adherends to be rigid (Figure 2.9). The adhesive shear stress (τ) is thus assumed to be constant across the overlap length and is given by the equation below:

$$\tau = \frac{P}{bl} \quad (1)$$

Where P is the applied load, b is the joint width, l is the overlap length and τ is the average shear stress acting on the adhesive layer.
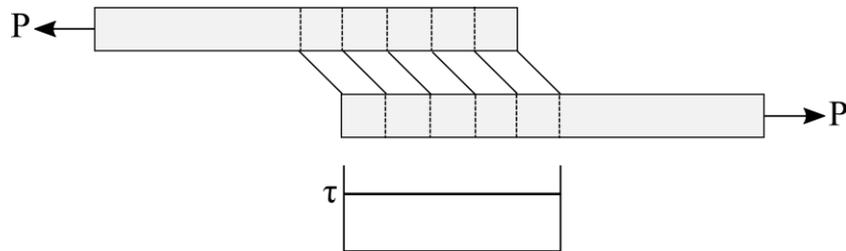
Figure 2.9: Deformation in single lap joint with rigid adherends.

Volkersen's analysis [61] for adhesively bonded joints, which is also known as shear lag analysis was presented in 1938 and it assumes that the adherends deform only in tension and the adhesive only in shear (Figure 2.10).
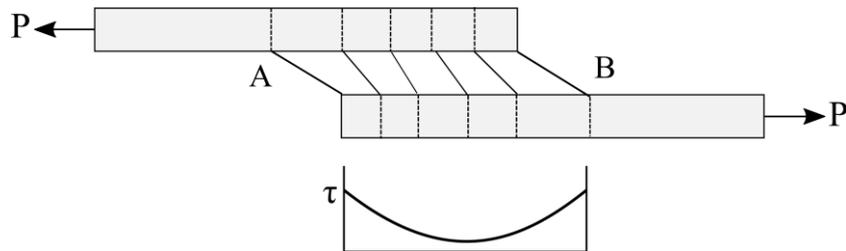
Figure 2.10: Single lap joint with elastic adherends.

The tensile stress in the upper adherend is maximum at A and decreases to zero at B (free surface), so the strain must progressively reduce from A to B resulting to non-uniform shear stress distribution in the adhesive layer. If the joint bending is not critical and the adhesive is brittle, Volkersen's analysis is sufficient. However, if the adhesive and/or the adherends yield and peeling stresses are present, a more complex model is required [57].

Goland and Reissner [62] extended this study by taking the lap joint rotation into account. They introduced a bending moment factor which related the bending moment acting at the overlap end to the in-plane loading and the dimensions of the joint. The result of the adherend bending was to induce direct stresses in the adhesive, the so-called peel stresses (Figure 2.11) in the through-thickness direction [12]. They assumed constant peel and shear stresses across the adhesive thickness and they calculated the transverse peel stresses, but neglected the shear deformation of the adherends. The joint was considered to be wide, i.e. plane strain condition.
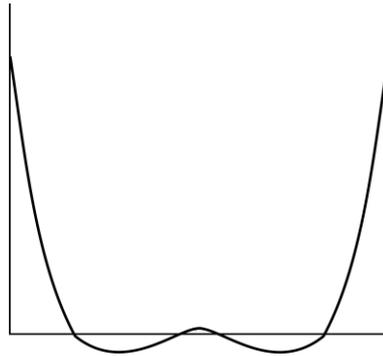
Figure 2.11: Peel stresses in a single lap joint.

The joint rotates due to the bending moment and therefore; the direction of the loading line becomes more concentric (Figure 2.12). As the joint rotates, the bending moment will decrease, giving rise to a nonlinear geometric problem, where the effects of the large deflections of the adherends must be accounted for [57].

a) Bending Moment $= Pt/2$

b) Bending Moment $= kPt/2$
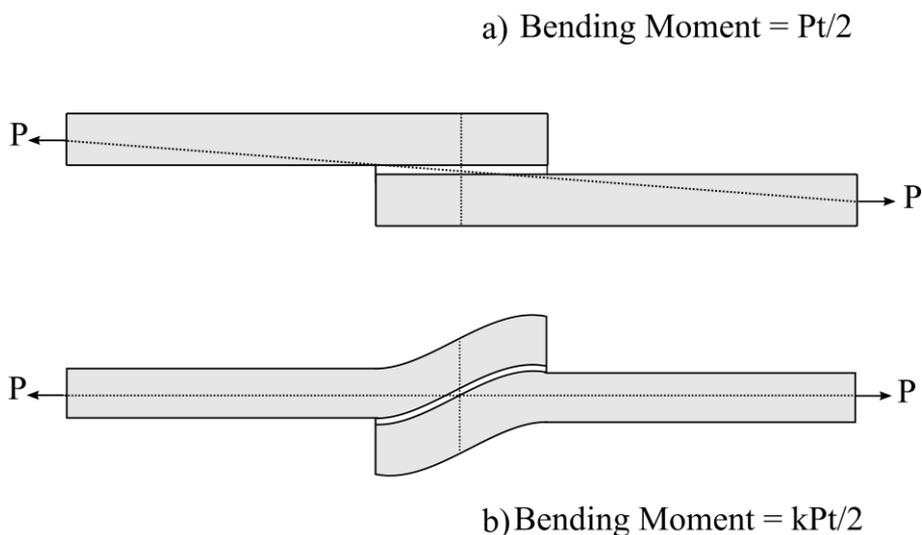
Figure 2.12: Geometrical representation of bending moment factor: a) undeformed single lap joint, b) deformed single lap joint.

Hart-Smith [63] proposed a simple analytical model by considering that the adhesive layer had perfect elastoplastic behaviour. This approach allowed for a better prediction of the mechanical behaviour of joints with ductile adhesives.

However, the effect of transverse (through-thickness) shear and normal deformations on the adherends, which is particularly important for composite adherends due to their relatively low shear modulus compared to metals, is not included in the analyses described above. The most important earlier analyses to account for the aforementioned deformations assumed that the adhesive stresses were constant across the thickness neglecting the adhesive longitudinal normal stresses, are summarised below.

Renton and Vinson [64] developed an analytical solution of the single lap joint geometry in order to account for the shear deformation of the composite adherends and determine the linear elastic response for the adherends and adhesive. This model satisfied the adhesive shear stress-free boundary condition at the ends of the overlap. Srinivas [65] developed a similar method for single and double lap joints, which included shear deformation as part of the analytical solution, while attempting to approximate the nonlinear geometric effects. Using an alternative approach, Allman [66] expressed the stresses in the joint as a set of stress functions while minimising the strain energy in the joint. The developed solutions satisfied the adhesive stress-free boundary condition and allowed the satisfaction of the full equilibrium equations for the adherends. Adams and Mallick [67] used Allman's approach to develop an one-dimensional finite element solution including the nonlinear adhesive behaviour. The adherends could be dissimilar with different material properties and/or different thicknesses. This model also allowed the variation of the adhesive stresses through the thickness.

All the analyses presented above assume linear elastic behaviour for the adherends. Some analyses assume plastic behaviour only for the adhesive layer and some others include variations in the distribution of the adhesive through-thickness stresses. The majority of the analytical models are also two-dimensional. However, the analysis becomes very complex if material nonlinearity is to be taken into account. Thus, numerical methods (finite element models) are also used, so that the effect of bending, adherend shear, end effects and nonlinear behaviour of the adhesive and adherends can be included in the analysis.

A vast amount of linear and nonlinear finite element analyses on a wide variety of adhesive joints can be found in the literature. The approaches for predicting the joint strength can be divided in three main categories: a) continuum mechanics approach, b) fracture mechanics and c) damage mechanics approach and are described in the following section.

2.7 Failure Analyses

2.7.1 Continuum Mechanics

According to the continuum mechanics approach, the adhesive and adherends are modelled using continuum elements and assuming that the adhesive is perfectly bonded onto the adherends. Under the assumption of a perfect bond, the adhesion properties of the interface are not taken into account. Average stress, maximum stress (shear, normal or von-Mises) and maximum strain criteria are often used to predict failure [68-71]. However, when linear elastic material behaviour is assumed, singular stresses arise at the bi-material junctions, which make the stress values at these points highly mesh dependent [72]. Moreover, the aforementioned stress criteria can be applied only when their values are taken at a distance from the singular corner or are averaged over an area with the latter being a function of the material properties and the geometry of the joint.

2.7.2 Fracture Mechanics

Fracture mechanics can be divided in linear elastic fracture mechanics (LEFM), which is based on linear elasticity and the elasto-plastic fracture mechanics (EPFM), which takes nonlinearity and plasticity into account. In the fracture mechanics approach, either stress intensity factor (SIF) or strain energy release rate (SERR) is used to study crack propagation along a pre-existing crack path (Figure 2.13). According to the stress intensity approach, the stress field near the tip of a sharp crack depends on the SIF [73, 74] and fracture occurs when the latter reaches a critical value.
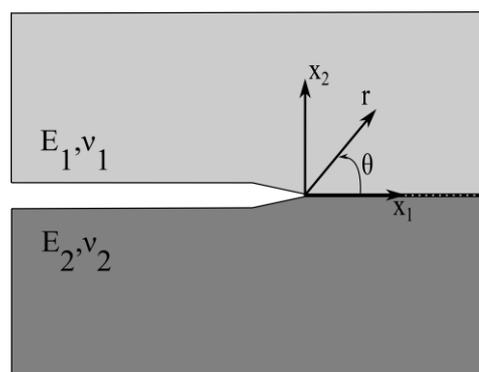
Figure 2.13: Geometry and coordinate definitions for an interface crack.

The SERR, an energy parameter can be also used for the failure criterion. If the local strain energy release rate exceeds a critical value, then failure occurs [75].

Virtual Crack Closure Technique

There are three ways to apply a remote load to enable a crack to propagate, namely mode-I, II and III, as illustrated in Figure 2.14. During the opening mode (mode-I) which is associated with local displacement, the crack surfaces move apart (Figure 2.14a). The sliding mode, mode-II, is developed when crack surfaces slide over each other in a direction perpendicular to the leading edge of the crack (Figure 2.14b) and the tearing mode (mode-III) is characterised by crack surfaces sliding with respect to each other in a direction parallel to the leading edge of the crack (Figure 2.14c) [76]. An adhesive layer typically fails under mixed-mode conditions [77].

a) Mode-I   b) Mode-II   c) Mode-III
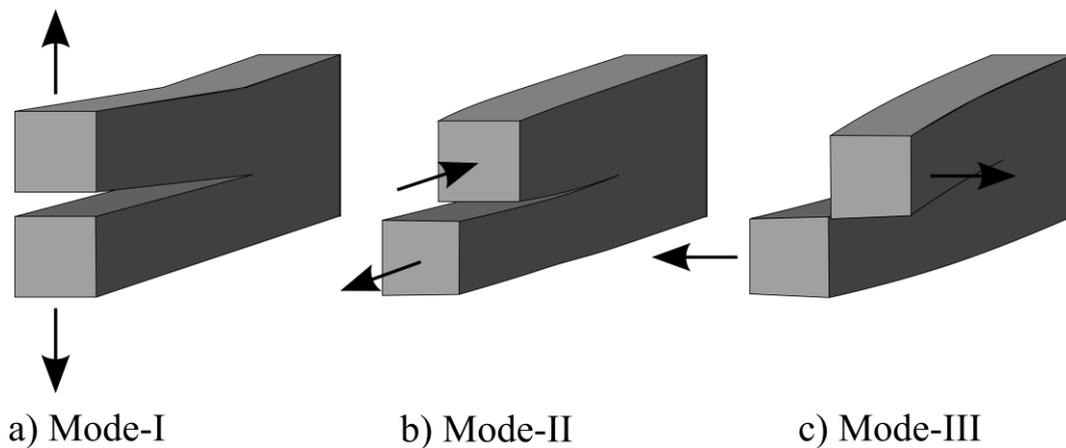
Figure 2.14: Fracture modes: a) Mode-I: tension, b) Mode-II: in-plane shear and c) Mode-III: out-of-plane shear.

Within the framework of linear elastic fracture mechanics, virtual crack closure technique (VCCT) has been utilised for the numerical simulation of the failure behaviour of adhesive joints. VCCT was initially developed to calculate the energy release rate of a cracked body and it has also been widely used for the interfacial crack growth simulation of laminate composites [78]. The crack can be located in a single material or along the interface of two materials. The VCCT crack growth simulation involves the following assumptions [79]:

- pre-defined crack path via interface elements
- quasi-static analysis
- linear elastic (isotropic, orthotropic or anisotropic) materials

Crack closure technique assumes that the energy released to separate a surface, i.e. to extend a crack from a to $a+ \Delta \alpha$, is the same as the energy needed to close the same surface (Figure 2.15). The modified or virtual crack closure method assumes that the stress states around the

crack tip do not change significantly when the crack grows by a small amount (*Δa*). This in effect means that when the crack tip is located at node *k*, the displacements at the node *i,* behind the crack tip are approximately equal to the displacements behind the crack tip at node *l*, when the crack tip is at node *i* [79, 80].
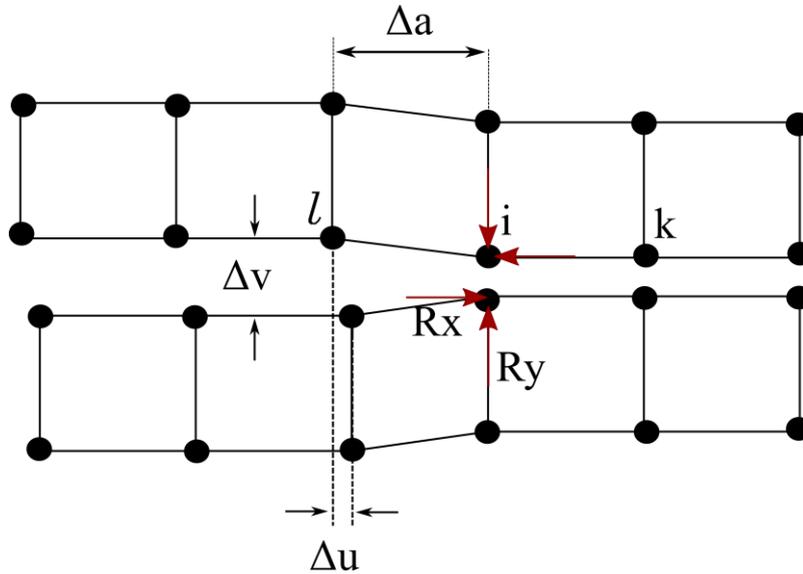
Figure 2.15: VCCT for four-noded element.

VCCT uses nodal forces and displacements from a finite element model in order to calculate the current energy release rate for a particular mode. The sum of all current energy release rates is the total energy release rate. The mode-I and mode-II components of the strain energy release rate for a 2D crack geometry can be calculated as follows [80]:

$$G_{\mathrm{I}} = \frac{1}{2\Delta\alpha} R_y \Delta v \ (2) \qquad \text{and} \qquad G_{\mathrm{II}} = \frac{1}{2\Delta\alpha} R_x \Delta u \ (3)$$

Where, G_{I}, G_{II} are the mode-I and II strain energy release rates, *Δv* and *Δu* are the relative displacements between the top and bottom nodes of the crack face in local coordinates *y* and *x* respectively, R_y and R_x are the reaction forces at the crack tip node and *Δα* is the crack extension.

VCCT is the technique also employed in this study (Chapter 7) for the calculation of the strain energy release rate of metal-to-composite joints, because:

a) it can be used for dissimilar materials and

b) the crack path is pre-defined, since the crack lengths are determined from the DCB tests. One of the assumptions mentioned above is therefore satisfied.

2.7.3 Damage Mechanics

Damage mechanics modelling approach is also used to simulate fracture and debonding process in adhesively bonded joints. Damage can be modelled over a finite region (continuum approach) or can be confined in zero volume lines (2D) and surfaces (3D) (cohesive zone approach). Cohesive Zone Modelling (CZM) simulates the progressive damage along a pre-defined crack path by specifying a traction-separation response between initially coincident nodes on either side of the crack path. The traction-separation laws are such that with increasing interfacial separation, the traction across the interface reaches a maximum (crack initiation) then, decreases (softening) and finally, the crack propagates leading to interfacial debonding (Figure 2.16) [16, 81, 82].
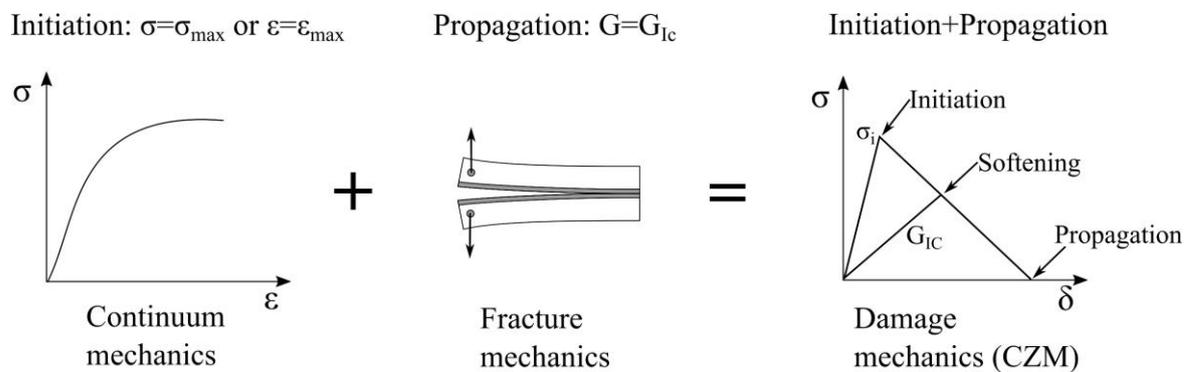
Figure 2.16: Schematic traction-separation law used to describe mode-I fracture.

In other words, CZMs combine strength and energy fracture criteria within a particularly shaped traction-separation law (cohesive law) [83]. The main limitation of cohesive models compared to continuum mechanics models is that the critical zones where damage occurs, must be known, so as to place the cohesive elements accordingly [84].

Chapter 3. CNT Filled Composites

An overview of the studies aiming to investigate the effect of carbon nanotubes on the mechanical, electrical and thermal properties of polymer matrices is presented in this chapter. Various techniques to improve dispersion, such as mechanical mixing and chemical/non-chemical treatments are also reviewed.

3.1 Introduction to CNTs

In 1991, Iijima [85] discovered the tubular structure of carbon, known as carbon nanotubes (CNTs). Nanotubes are members of the fullerene structural family and their name is derived from their long, hollow structure with walls being formed by one atom thick sheets of carbon, called graphene. These sheets are rolled at specific and discrete ("chiral") angles. The combination of the rolling angle and radius determines the properties of nanotubes. Iijima produced carbon nanotubes using direct current arc discharge evaporation of carbon in an argon filled vessel. Apart from the arc discharge method, carbon nanotubes can be produced by several techniques such as laser ablation, thermal and plasma enhanced chemical vapour deposition (CVD) and many others, a review of which can be found in [86].

Depending on the fabrication process, there are two types of CNTs: single-wall CNTs (SWCNTs) and multi-wall CNTs (MWCNTs) [87]. SWCNTs consist of a single graphene layer rolled up into a seamless cylinder (Figure 3.1A), whereas MWCNTs consist of two or more concentric cylindrical shells of graphene sheets (Figure 3.1B) coaxially arranged around a central hollow core with van der Waals forces connecting the adjacent layers.
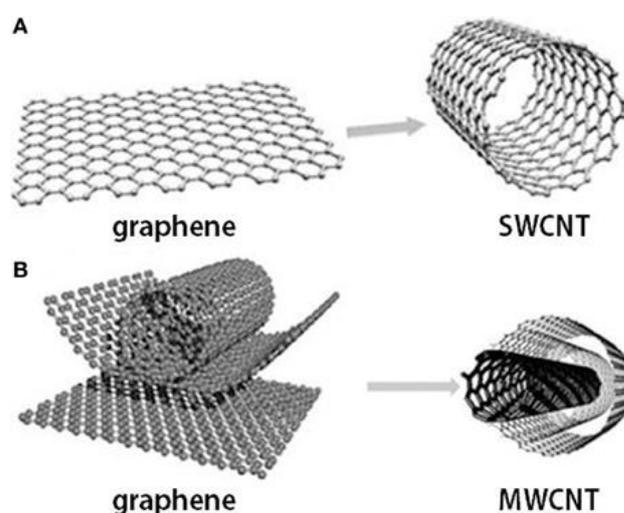
Figure 3.1: Different types of CNTs: A) SWCNTs and B) MWCNTs [88].

CNTs are one dimensional carbon materials with an aspect ratio (length-to-diameter) greater than 1000. Hence, they have an extremely large surface area, which leads to large interaction sites between the matrix and the filler [89, 90]. Carbon nanotubes also exhibit high Young's modulus (0.9TPa), tensile strength (150GPa) [48] and elongation to failure (20-30%) [90]. Apart from their remarkable mechanical properties, they also present good electrical, thermal and optical properties. Extensive research has been therefore carried out in order to exploit their properties and successfully transfer them into composite materials.

Homogeneous dispersion of individual CNTs in the polymer matrix and strong interfacial bonding between the matrix and the filler in order to ensure efficient load transfer, are the critical requirements that need to be satisfied, so as to develop high performance CNT reinforced composites.

3.2 Dispersion of CNTs in Epoxy Resin

Carbon nanotubes have the tendency to aggregate and form bundles or ropes that are difficult to disrupt due to the strong interaction between them. The attractive forces originate from their extended π electron system and because these structures are polarisable, a large amount of van der Waals forces exists between them, which are responsible for the phenomenon of aggregation [90]. However, the key factor in order to achieve good composite properties is homogeneous dispersion of CNTs in the matrix. A good dispersion not only makes more filler surface area available for bonding, but it also prevents the aggregated fillers from acting as stress concentrators. Such aggregates can be detrimental to the mechanical performance of the composite and lead to premature failure [91].

Many techniques have been developed to assist dispersion and they can be generally classified into three categories [92]:

i. *Mechanical - Direct mixing*: CNTs are dispersed in the polymer matrix via mechanical forces. Common methods are shear mixing and ultrasonication.

ii. *Chemical surface modification (covalent treatment)*: It is the covalent chemical bonding (grafting) of polymer chains to the functional groups of CNT surfaces, attained by treating them with strong acids, e.g. nitric acid or other strong oxidizing agents, such as H_2SO_4. The CNT/matrix chemical compatibility is therefore enhanced and results in strong CNT/matrix interface and good dispersion [90]. The downside of this method is that the oxidative treatment might introduce structural defects on the CNTs, such as disruption of the conjugated electronic structure and decrease of the

CNT length, which lead to the degradation of their electrical and mechanical properties. According to [92], trifluoroacetic acid (TFA) not only helped dispersing carbon nanotubes and doping conjugated conducting polymers in organic polymer matrices, but it was also highly effective at purifying CNTs by eliminating carbonaceous particles and metal catalysts without oxidising the nanotubes.

iii. *Physical surface modification (non-covalent treatment)*: Physical methods involve the adsorption and/or wrapping of a third component onto the CNT surface aiming to assist the dispersion of CNTs in solvents and polymer matrices. The third component might be surfactants, polyelectrolytes and surfactant-like block copolymers [93]. These chemicals adsorb onto the walls of CNTs during sonication and then, they stabilise the dispersion due to repulsive electrostatic interactions between the surfactants adsorbed on the nanotubes [92].

Although all the aforementioned methods are usually combined together to achieve optimum dispersion, more emphasis will be given on the mechanical mixing, which is an imperative step of the nanocomposite manufacturing and can be also used as a standalone dispersion method.

Mechanical Dispersion Methods

The most widely used mechanical dispersion methods are ultrasonication, calendering, ball milling and shear mixing. A brief description of the fundamental principles of each technique is given below.

- *Ultrasonication*: During ultrasonication, an ultrasonic bath or an ultrasonic horn/probe is used, which generates ultrasound that propagates via a series of compressive waves. Attenuated waves are induced in the molecules of the medium through which it passes. The production of these shock waves promotes the ''peeling off'' of the individual nanoparticles located at the outer part of the agglomerates and thus, it leads to the separation of individual nanoparticles from the bundles [89, 94]. However, CNT structure might be impaired if either too aggressive or too long sonication takes place, because it can produce high energy inter-particle collisions (implosion of shock waves and micro jets) that damage the particle surface [95]. Another drawback of this technique compared to calendering ,which is described below, is that it cannot be used on an industrial large-scale production owing to the limited amount of material that can be mixed [96].

- *Calendering* [89]: Calender or three roll mill applies high shear forces created by the rollers in order to disperse the nanoparticles in the matrix. The machine consists of three adjacent cylindrical rollers which run at different velocities. The first and third roller are the feeding and apron roller respectively and rotate in the same direction, whereas the centre roller rotates in the opposite direction. The material to be mixed is fed into the hopper, where it is drawn between the feed and centre rollers (Figure 3.2). When pre-dispersed, the material sticks to the bottom of the centre roller, which transports it into the second gap. In this gap, the material is dispersed into the desired degree of fineness. Upon exiting, the material that remains on the centre roller moves through the second nip, between the centre roller and apron roller, which subjects it to even higher shear forces due to the higher speed of the apron roller. A knife blade then scrapes the processed material off the apron roller and transfers it to the apron. This milling cycle can be repeated several times to maximise dispersion. The narrow gaps between the rollers combined with the mismatch in angular velocity of the adjacent rollers, result in locally high shear forces with short residence time. One of the advantages of this technique is that the gap width between the rollers can be adjusted according to the size of the particles to be mixed. The applied high shear stresses can disentangle the CNT bundles and disperse them into the polymer matrix, while the short residence time limits the breakage of individual nanotubes.
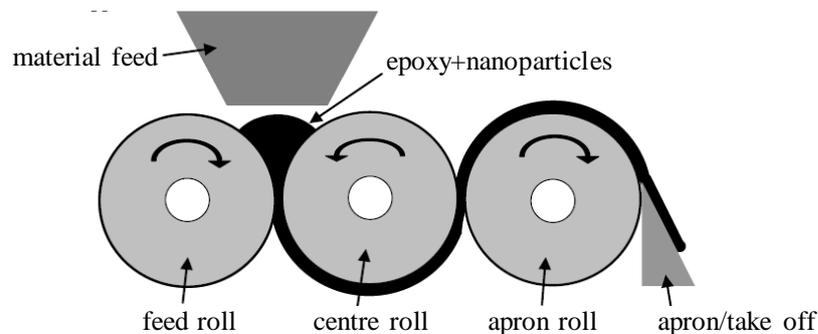
Figure 3.2: Calendering.

- *Ball milling*: Ball milling is a type of grinding method used for the exfoliation of graphitic materials [97]. During ball milling, a high pressure is generated locally due to the collision between the rigid balls in a concealed container (Figure 3.3a). The high energy mechanical impact introduced by ball-milling can modify the CNT morphologies [98] or decrease their length [99].
- *Shear mixing*: A common technique used to disperse nanoparticles is shear mixing according to which the fluid undergoes shear, because the fluid velocity at the outside

diameter of the impeller is higher than the velocity at the centre of the impeller (Figure 3.3b). This velocity difference creates high flow and shear forces in the medium that can disentangle severely the CNT agglomerates [89]. Shear mixing depends on the size and shape of the impeller and the mixing speed.
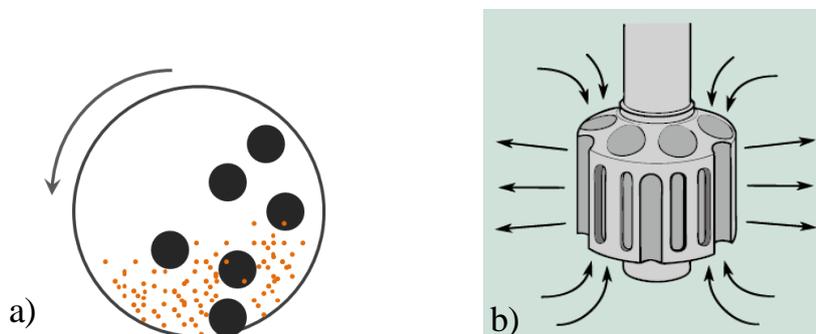
Figure 3.3: a) Ball milling and b) Shear mixing.

Although these techniques may appear very different, they all share a common characteristic; the transfer of physical shear stresses onto the CNTs, which break down the bundles [100]. According to the study in [101], the shear stress energy delivered to the particles during mixing has to exceed the van der Waals forces of attraction in the contact region. Below this shear energy density, proper dispersion cannot be achieved irrespective of the mixing duration.

The dispersion methods mentioned above are usually combined to optimise dispersion, e.g. ultrasonication and ball milling [102]. Caneba et al. [103] used an ultrasonic probe and bath to disperse carbon nanotubes in dimethylformamide (DMF). The dispersion obtained was significantly enhanced by superimposing the two methods compared to using either of them alone. In addition, mechanical stirring with ultrasonication has been proved to be an effective way to uniformly disperse carbon nanotubes without any use of solvents [10].

3.3 Mechanical Properties

The effect of covalent or non-covalent functionalisation in relation to the dispersion methods employed for different types of CNTs has been extensively investigated. An overview of studies found in the literature which study how the incorporation of carbon nanotubes influences the mechanical, electrical and thermal properties of the nanocomposites is outlined in the following sections.

3.3.1 Sonication and Calendering

The CNT content in combination with the dispersion method are the key factors that determine the properties of nanocomposites. Therefore, the objective is to reduce the number of aggregates to the minimum and ensure efficient load transfer between the matrix and the filler by optimising dispersion. Sonication is the dispersion method that has been used the most by researchers in order to exfoliate the CNT bundles. Gkikas et al. [94] manufactured 0.5 and 1 wt.% MWCNT filled and unfilled epoxy composites, which were tested in tension and single edge notched 3-point bending in order to assess the loading effect on the mechanical properties. The dispersion conditions, such as sonication time and total energy input were also investigated. Tensile strength showed an increase for intermediate levels of sonication duration, i.e. between 1h and 2h, whereas the influencing parameter for fracture toughness was sonication energy. The best results were obtained for 2h of sonication and 50% sonication amplitude. It was suggested that this level of sonication allowed appropriate dispersion of the CNTs into the epoxy matrix without disrupting the CNT structure. Zhou et al. [4] assessed the loading effect, i.e. 0.1, 0.2, 0.3, and 0.4 wt.% on the mechanical properties of MWCNT epoxy composites. A high intensity ultrasonic processor was used. Flexural modulus was found to increase with higher CNT loading percentages. The maximum flexural strength and fracture toughness enhancement was obtained for 0.3 wt.% CNT loading. However, further increase of the CNT loading to 0.4% decreased the strength and fracture toughness due to poor dispersion of CNTs in the matrix.

Khashaba et al. [104] used various nanofillers, including MWCNTs to modify the Epocast 50-A1/946 epoxy, which was primarily developed for joining and repairing composite aircraft structural components. MWCNTs were ultrasonically dispersed in the epoxy resin at 30% sonication amplitude and for 30min to avoid damage of the CNT structure. Tensile and in-plane shear tests were performed to characterise the specimens. The highest improvement in tensile and shear properties was obtained for 0.5 wt.% CNT loading. Shear strength and modulus increased by 5.5% and 10.3% respectively and tensile strength and modulus by 7.5% and 18.2% compared to pure epoxy. Song and Youn [105] investigated the effects of different dispersion states of MWCNTs on rheological and mechanical properties of epoxy nanocomposites. The dispersion states were controlled by sonicating MWCNTs (0.5, 1 and 1.5 wt.%) in ethanol or not, prior to the dispersion in epoxy resin. The morphological observation of the samples via field emission scanning electron microscopy (FESEM) and transmission electron microscopy (TEM) showed that when ethanol was not used, aggregates of pristine CNTs remained in the nanocomposites. Regarding the mixture viscosity, it was

found that the poorly dispersed CNT nanocomposites exhibited a more solid-like behaviour. The tensile strength of the composite filled with well dispersed CNTs increased as CNT loading increased, whereas that of the composite filled with poorly dispersed CNTs, decreased due to the agglomerates that assisted the crack initiation and propagation. On the contrary, tensile modulus of epoxy composites with poorly dispersed CNTs showed a higher increase than the well dispersed CNT epoxy samples. This was explained by the fact that the agglomerates, which acted as large particles in the poorly dispersed CNT nanocomposites, trapped polymer resin in the voids between the CNTs and thus, the nanocomposites behaved as if the volume fraction of the polymeric matrix was lower. Finally, when the CNT loading was increased, the elongation at break of both CNT/epoxy composites was reduced, with poorly dispersed CNTs showing larger reduction. In [5], it was found that the average fracture toughness of 1 wt.% and 3 wt.% MWCNT/epoxy composites prepared by sonication was greater than pure epoxy by 1.29 and 1.62 times respectively. Furthermore, the fatigue lives of 0.5 wt.% MWCNT/epoxy composites were 10 times greater than the average fatigue life of pure epoxy.

Lau et al. [6] dispersed 0.5% of SWCNTs in three solvents, namely DMF (N-dimethylformamide), acetone and ethanol via sonication, which were then incorporated in epoxy matrix. Only the acetone-dispersed nanocomposites exhibited improvements in flexural strength over the pure epoxy. Another interesting finding was that due to the high boiling point of the solvents, it was difficult to remove them completely from the final sample. Therefore, differential scanning calorimetry (DSC) results indicated small traces of residual solvent that had a great impact on the cure reaction and the endothermic behaviours of the nanocomposites. The solvent effects found were in the order of DMF > ethanol > acetone, which was consistent with the order of their boiling points.

Many studies have been also carried out in order to gain in depth knowledge of the influence of the CNT dimensions, e.g. length and diameter on the performance of the CNT filled composites. Thostenson and Chou [106] investigated how the structure/size of aligned MWCNTs influence the elastic properties of polystyrene matrix. The experimental results were also compared with numerical predictions and it was shown that the elastic properties of the nanocomposites were particularly sensitive to the nanotube diameter with the larger diameter nanotubes showing lower effective modulus and occupying greater volume fraction in the composite. Bai and Allaoui [107] investigated the effect of nanotube length and aggregate size on the mechanical properties of composites reinforced with 0.5, 1 and 4 wt.% CNT. Three treatments were applied on the MWCNTs in order to attain the following lengths:

50μm, 10μm and 1μm. The 0.5 wt.% CNT loading was the threshold of the improvement efficiency and further increase did not enhance the results. Finally, they concluded that good compromise of aggregate size and aspect ratio, i.e. the case of 10μm length was the key factor for good mechanical performance.

Despite the extensive use of sonication treatments to debundle and disperse CNTs, it has been reported in many research papers that sonication process damages the outer graphitic layers of CNTs and shortens their length. This can also be detrimental for the mechanical, electrical and thermal properties of the CNT reinforced nanocomposites. Rossell et al. [108] investigated the impact of sonication pre-treatment on the structure of MWCNTs attached to Fe_3O_4 nanoparticles. It was found that sonication altered the sp^2 CNT structure by introducing defect sites at their sidewalls and partially removing graphitic layers, which in some cases led to open holes. The damage of CNTs was also addressed in [109] and [110], where bending and buckling defects were introduced to CNTs. The number of defects was analogous to the duration of sonication time.

Calendering process as already described above, prevents CNTs from rupture. Gojny et al. [7] compared the dispersion of 0.1 wt.% of DWCNTs (amino-functionalised and not) in epoxy matrix produced by calendering technique to the dispersion obtained by sonication process. Transmission electron microscopy (TEM) was used to determine dispersion qualitatively. When calendering was employed, only some small agglomerates with exfoliated structure were observed, whereas after sonication the agglomerates did not exfoliate and maintained their condensed structure. A possible advantage of this dispersion method is the homogeneous introduction of shear forces over the whole volume of the nanocomposite in contrast to sonication, which introduces the energy locally.

3.3.2 Covalent and Non-Covalent Functionalisation

Surface functionalisation of CNTs and addition of surfactants in the CNT solution during mixing also have a significant influence on the mechanical behaviour of nanocomposites. In [7], Gojny et al. investigated the impact of amino-functionalised DWCNTs on the mechanical properties of the composites. A significant improvement of strength and stiffness was demonstrated when the amino-functionalised DWCNTs were used. The amino groups present on the CNT surface reacted with the epoxy matrix and formed covalent bonds leading to enhanced interfacial adhesion.

After removing the external shear stresses from the CNT solution, CNTs tend to reconfigure themselves into a new equilibrium state of low energy through re-aggregation [111]. The driving force for re-aggregation is provided by the van der Waals attraction. Redispersability, also known as steric stabilisation occurs unless surfactants are added to the solution. Such surfactants provide steric hindrance or static charge repulsion and hence, stabilise the solution (Figure 3.4).
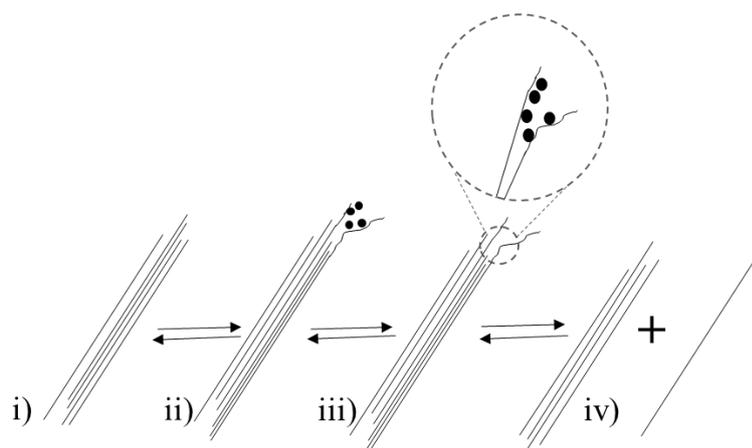
Figure 3.4: Mechanism isolation from bundle obtained by ultrasonication and surfactant stabilisation: i) ultrasonic treatment provides high local shear, ii) spaces/gaps at the bundle ends are formed, iii) propagate by surfactant adsorption and iv) separation of the individual CNTs from the bundle [112].

At low concentrations and for homogeneously dispersed solutions, non-interacting nanotubes appear quite stable against re-aggregation, whereas at concentrations above a threshold of the order of 2-3 wt.%, entangled nanotubes are observed in the dispersed mixture [101]. Various approaches to slow down or to prevent CNT re-aggregation after the shear stress removal are demonstrated in [111]. Amongst them is the kinetic approach of using a highly viscous solution/melt (only for shear mixed samples) and the thermodynamic approach of choosing a compatible solvent or surfactant. Zhao and Gao [93] investigated a way to overcome re-aggregation. It was reported that a suspension of 1 wt.% concentration was stable only when a small quantity of copolymer (Disperbyk-2150) was used as dispersant. An important factor that contributed to the good dispersion of MWCNTs in the ethanol solution was the affinity due to chemical intercalation between the copolymer and the MWCNTs. Steric stabilisation acted as hindrance against the van der Waals adherence between individual and bundles of MWCNTs in the solution. Li et al. [113] managed to achieve strengthening of 0.03 wt.% CNT filled epoxy composites by adding a small amount of copolymer. Young's modulus and tensile strength of the nanocomposites with the copolymer were found to be approximately

50% higher than for pure epoxy resin and about 20% higher than for the nanocomposites without dispersing agent.

Cho et al. [114] incorporated MWCNTs to improve the matrix dominated thermomechanical properties of the composite. Two different CNT lengths, i.e. 1μm and 10μm on average, were considered. The dispersion of the CNTs was enhanced with the block copolymer. More specifically, a noticeable improvement of the composite properties was achieved for 0.5 wt.% MWCNT filled composites irrespective of the CNT length. Whereas, when no block copolymer was used, greater enhancement of composite properties was obtained for the longer nanotubes. The dispersant therefore, worked better with shorter CNTs and lower CNT content. Finally, because of the reduction in fibre volume ratio with the increase of CNT loading, the optimum range of 0.5-1.0 wt.% was suggested.

3.4 Electrical Properties

MWCNTs are very efficient in terms of enhancing the electrical conductivity of nanocomposites, because of their relatively low surface area and high aspect ratio. According to Bai and Allaoui [107], the length of MWCNTs plays the key role for the improvement of the electrical conductivity. Any treatment, e.g. sonication and functionalisation that leads to the decrease of the aspect ratio also results to the increase of the percolation threshold and hence, reduction of the electrical conductivity [90].

Gojny et al. [115] evaluated the effect of the dispersion performed with a mini calender on the electrical conductivity of nanocomposites. Different types and volume fractions of pristine and amino-functionalised carbon nanotubes (SWCNT, DWCNT and MWCNT) were utilised. It was found that the nanoparticles with the highest densities, i.e. MWCNTs exhibited the lowest percolation thresholds. For the non-functionalised nanotubes, electrical conductivity increased with the CNT content, whereas the functionalisation of CNTs reduced their aspect ratio and subsequently, the electrical conductivity. Sandler et al. [116] developed a dispersion process in order to achieve the desirable matrix conductivity for anti-static applications. CNT composites of 0.0225 to 0.15 wt.% were manufactured. Electrical conductivity was achieved for all cases with reduction of the percolation threshold to less than 0.04 wt.%. In [105, 117], a percolation threshold of less than 0.5 wt.% was shown. It was concluded that electrical conductivity benefited from the aggregated phases, which formed a conductive three-dimensional network throughout the whole sample.

3.5 Influence on T_g and Cure Kinetics

The influence of the CNT incorporation on glass transition temperature (T_g) of epoxy resin has also been investigated. Gkikas et al. [94] identified the effect of loading via dynamic mechanical analysis (DMA). Enhancement of glass transition temperature was reported for 0.5 and 1 wt.% CNT loadings and for 1h of sonication. The significant increase of T_g was associated with the improved dispersion and interfacial bonding between the CNTs and the epoxy matrix. Zhou et al. [4] also assessed the loading effect (0.1, 0.2, 0.3 and 0.4 wt. %) on T_g, which was found to increase by 17°C for 0.4 wt.% MWCNT loading. Gojny and Schulte [118] investigated the glass transition temperature of reinforced epoxy with different loadings of functionalised and non-functionalised CNTs. T_g increased with the increase of both types of MWCNTs with the amino-functionalised CNTs showing a stronger influence. The increase of T_g was attributed to the confinement of polymer chains by the nanoparticles, which increased the activation energy of the polymer molecules with temperature [114, 117]. However, in other studies, the glass transition temperature was not affected by the addition of CNTs in the epoxy matrix [119] or even showed a decrease. Fidelus et al. [120] explained that the higher the amount of CNTs (both SWCNTs and MWCNTs), the more likely was to reduce the crosslinking tendency of epoxy resin.

The inclusion of CNTs in epoxy resin has also been proved to alter the cure kinetics of nanocomposites. Puglia et al. [121] studied the effect of SWCNTs on the cure reaction of epoxy resin with dynamic and isothermal differential scanning calorimetry (DSC). It was found that SWCNTs acted as a strong catalyst and accelerated the cure reaction. Tao et al. [122] also studied the cure reaction of SWCNT/epoxy composites using the DSC technique. It was shown that carbon nanotubes initiated curing at lower temperatures. However, the lower total heat of reaction and lower T_g compared to pure epoxy resin suggested that the curing process of nanocomposites was slower.

Kim et al. [123] investigated the relationship between the state of particle distribution and change in the cure kinetics (i.e. heat of reaction) using the DSC method. It was found that the addition of well-dispersed CNTs to epoxy resin reduced the total heat of reaction. This was because CNTs acted as obstacles to the cross-linking reaction. Jahan et al. [124] assessed the influence of carboxyl functionalised MWCNTs (0.1, 0.2 and 0.3 wt.%) on the cure behaviour of epoxy resin using DSC in dynamic scan mode at various heating rates (2, 5, 10 and 15 deg/min). It was shown that CNTs were able to initiate the cure reaction at lower temperature. Small amount of CNTs (0.1 wt.%) caused slight decrease of the peak temperature and activation energy compared to pure epoxy because of their catalytic action. Whereas, higher

CNT loadings did not affect the peak temperature, but increased the activation energy due to the retarding effect. At such high CNT loadings, the specific surface area of CNTs increased and resulted in higher electrostatic repulsion and greater steric hindrance in the cure reaction. Finally, the lower total heat of reaction was correlated to the CNT dispersion state and indicated better CNT/matrix interfacial interaction and thus, better dispersion.

Abdalla et al. [125] compared the impact of carboxyl and fluorine modified MWCNTs on the curing behaviour of epoxy resin with differential scanning calorimetry. It was demonstrated that the cure mechanisms of the pure epoxy resin and fluorinated samples were similar, but different from the carboxyl modified MWCNT/epoxy samples. This difference was associated with the dispersibility. The fluorinated MWCNTs were more uniformly dispersed in the matrix than the carboxylated MWCNTs. The poor dispersion hindered the mobility of the reactive species and hence, changed the cure kinetics. The cure kinetics of MWCNT/ tetrafunctional epoxy composites was studied by Xie et al. [126]. When the MWCNT content increased, the nanocomposites exhibited lower activation energies compared to pure epoxy. The increase in the initial reaction rates and the reduction of the time to the maximum reaction rate with increasing MWCNT content, revealed the acceleration effect of MWCNTs.

3.6 Toughening Mechanisms

Many studies have shown that CNTs are able to deform elastically under relatively large stresses both in tension and compression leading to highly energy-absorbing processes [96]. This unique flexibility gives rise to several micro-mechanical mechanisms that enhance the fracture toughness of CNT reinforced polymers. According to [127], the most important are:

i. localised inelastic matrix deformation and void nucleation
ii. particle/fibre debonding
iii. crack deflection
iv. crack pinning
v. fibre pull-out
vi. crack tip blunting (or crack tip deformation)
vii. particle/fibre deformation or breaking at the crack tip

Numerous researchers have investigated the toughening mechanisms in order to gain full understanding of the relationship between the fracture behaviour and microstructure. A brief review follows in order to explain how the CNT composite performance is affected when a toughening mechanism takes place.

3.6.1 Crack Deflection

Crack path deflection mechanism is a source of energy dissipation during crack propagation. According to this mechanism, the particles cause the crack to deviate from its original path. After the crack front approaches the particle/matrix interface, it is forced to change direction and pass around the particles along the interface [128]. This deflection changes the local stress state from mode-I (crack opening) to mixed-mode. More energy is therefore absorbed in order to propagate a crack under mixed mode conditions than under pure mode I, which results in higher fracture toughness. Although this mechanism does not seem to depend on the particle size, it is believed that uneven spacing provides better results than uniform spacing.

3.6.2 Crack Pinning

During the crack-pinning mechanism [129], particles arrange in lines and act as obstacles for the crack font. Therefore, the crack front has to bow locally between the fillers in order to pass through the line formed by the latter (Figure 3.5).
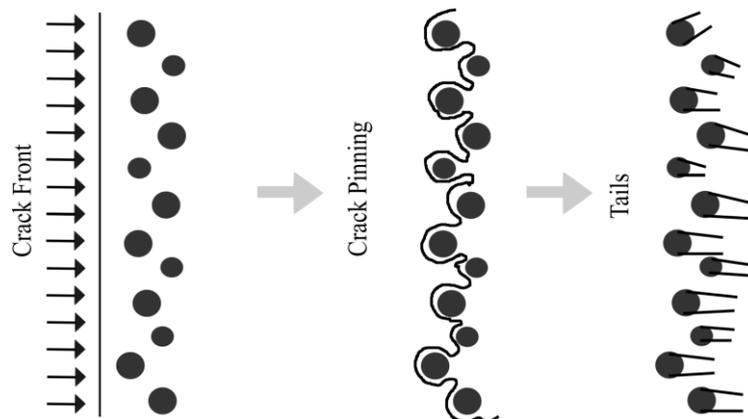
Figure 3.5: Crack pinning process.

The particles are considered to be the toughening agents, because the crack front remains pinned at them resulting to the increase of the crack length. Secondary cracks, which coalesce after passing the particles, can be also generated. As the strain energy increases, local step fracture occurs and the pinned points are released creating a "tail-like" feature on the fracture surface. During this process the propagation rate is slowed down leading to an increase in fracture toughness due to the absorbed amount of energy [128].

3.6.3 Pull-out, Debonding and Crack Bridging

The key factor that highly affects the toughening mechanisms is the nature of the interfacial region between the matrix and the particle. The interface must be of sufficiently low toughness, so that the particle will not be able to slide neither too easily nor with too much

difficulty. In the case of very strong particle/matrix bonding, fracture of the outer layer of the tube or even a complete rupture of the particle can occur. On the contrary, when the particle/matrix bonding is weak, the pull-out mechanism may be favoured (Figure 3.7).
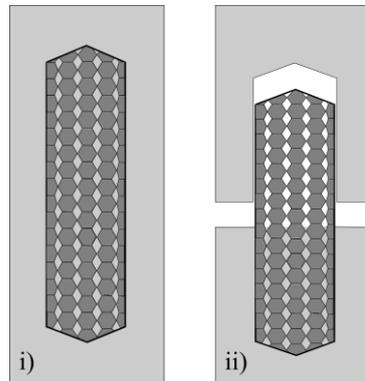
Figure 3.6: i) Initial state of the CNT and ii) Pull-out caused by CNT/matrix debonding in case of weak interfacial adhesion.

In the latter case, the particle is pulled out of the matrix leading to a partial interfacial debonding (Figure 3.7a) [130]. The debonding of the particles allows subsequent plastic void growth within the polymer, which is another key energy dissipation mechanism (Figure 3.7b) [128].
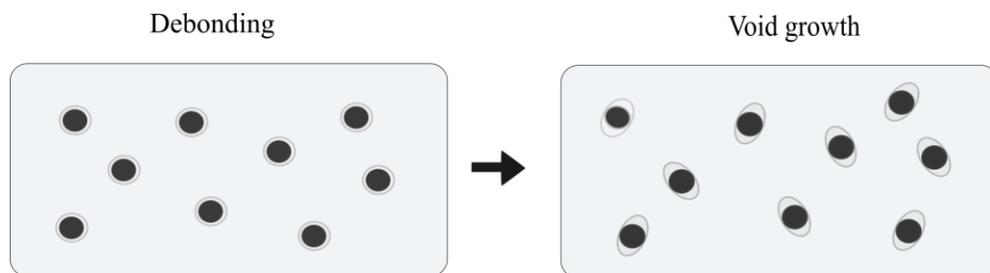
Figure 3.7: a) Debonding and b) Void growth.

Void growth might also enable the particle bridging mechanism during which the particles are stretched between the edges of the propagating crack resulting to greater energy absorption prior to failure (Figure 3.8).
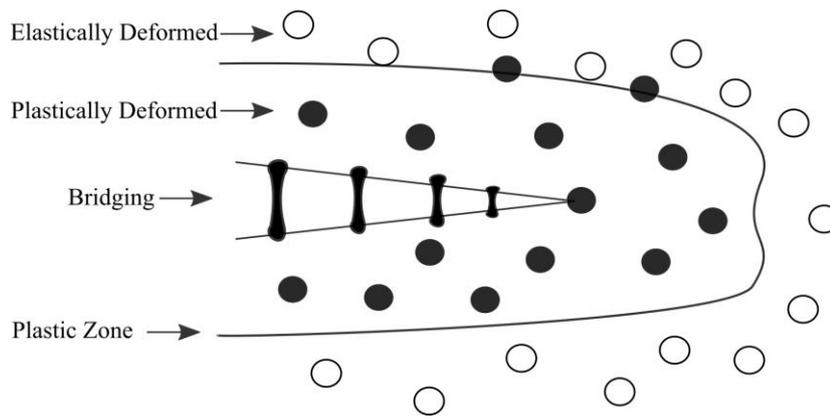
Figure 3.8: Crack bridging.

Finally, microcracks, which can be created close to the crack tip, are able to reduce the stress concentration, because they allow for residual stress release, which results in fracture toughness increase. Certain size and spatial distributions of microcracks in the vicinity of the main crack tip act as a hindrance to the crack and reduce the crack propagation rate.

3.6.4 Crack Blunting

During crack propagation, macromolecular chains in the vicinity of the crack tip are stretched and broken (crack blunting). Therefore, the initial sharp crack becomes more and more blunted as a result of the formation of a plastic zone and the decohesion of particles. The stress concentration effect at the crack tip becomes lower and the crack is slowed down (Figure 3.9).
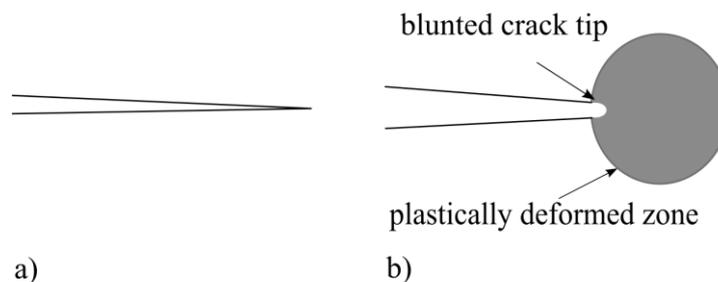
Figure 3.9: Crack blunting: a) the crack at the beginning and b) the blunted crack.

3.6.5 Matrix Plastic Deformation

Particles can also cause localised plastic deformation of the polymer matrix (i.e. shear banding and crazing) and as a result, enhance the fracture toughness [128]. Shear banding is a narrow zone of intense shear strain, usually of plastic nature, developed during severe deformation of a glassy polymer and results in partial orientation of the polymer chains [131].

Crazes are microscopic regions of highly localised plastic deformation similar to those developed on a macroscopic scale in glassy polymers. Crazing occurs in regions of high hydrostatic tension or in regions of high localised yielding, which leads to the formation of microvoids oriented parallel to the tensile direction. If an applied tensile load is sufficient, these crazed regions elongate and break causing the microvoids to grow and coalesce, so that cracks begin to form. The inclusion of rigid particles induces stress concentration and alters the local stress state, which favours local plastic deformation. Because of the large number of particles in nanocomposites, more plastic deformation might exist in these systems than in the unfilled polymers, which will then lead to higher fracture toughness values.

Despite the various toughening mechanisms proposed by different researchers, it is difficult to interpret an experimental result using only one theory. Fracture is a complex phenomenon and more than one of the aforementioned mechanisms might occur at the same time. In [127], fracture toughness was found to increase by 45% when 0.3 wt.% of amino-functionalised DWCNTs were used instead of non-functionalised for the composite fabrication. The improved performance was caused by increased interfacial strength due to functionalisation that gave rise to toughening mechanisms, such as pull-out and fibre bridging. Hsieh et al. [119] reported 40% increase of fracture energy with the addition of 0.5 wt.% of MWCNTs. Electron microscopy of the fracture surfaces showed clear evidence of nanotube debonding and pull-out mechanisms which contributed to this toughening effect. Finally, Fidelus et al. [120] demonstrated 70% increase of the tensile impact strength for 0.5 wt.% MWCNT epoxy/nanocomposites. This significant increase was explained by the presence of cavities bridged by nanotube ropes that led to energy dissipation by pull-out.

3.7 Adverse Effect of CNTs

Minor improvement or even decrease in mechanical properties of nanocomposites after small additions of CNTs into the matrix has been also reported in many studies. Such low reinforcing ability can be due to two reasons:

- Lack of interfacial adhesion, which is critical for the load transfer in composites.
- Poor dispersion of nanotubes in the matrix, which results in aggregation.

In [7, 132] only marginal improvement or reduction of tensile modulus was observed after the addition of CNTs into epoxy resin. Lau et al. [133] showed decrease in the flexural strength of CNT/epoxy composites, probably a result of weak CNT/matrix interface. Neither the addition of amino-functionalised MWCNTs in epoxy resin enhanced the tensile strength. This was due

to the absence of stress transfer to the internal layers of MWCNTs. Thus, only the outer layers contributed to the mechanical reinforcement. At higher filler concentrations, poor dispersion led to the increase of agglomerates, which acted as imperfections in the composite inducing premature failure [134].

Lachman et al. [130] demonstrated that the creation of defects and aggregates, associated with the difficulties of specimen preparation due to the high viscosity of the CNT/epoxy mixture induced by the very high area/volume ratio of nanotubes, decreased the tensile strength of the composites. In [135], significant decrease in fracture toughness of MWCNT/epoxy composites prepared by sonication was reported. Fracture toughness decreased for 0.25 wt.% CNT loading and then, increased for loadings up to 0.75 wt.%. However, further addition of MWCNTs dramatically reduced fracture toughness due to aggregation. The initial decrease of toughness at 0.25 wt.% CNT loading occurred, because the energy dissipation mechanisms were not activated as a result of good dispersion and interfacial bonding between the matrix and the fillers.

Chapter 4. Characterisation of MWCNT Reinforced Epoxy Resin

4.1 Overview

In order to obtain MWCNT reinforced epoxy composites with good mechanical performance, sufficient interfacial bonding between the matrix and the filler and homogeneous dispersion must be realised. This chapter is focused on the effect of the incorporation of multi-wall carbon nanotubes in epoxy resin. Various CNT loadings and different dispersion routes are assessed via a series of mechanical tests: tensile, flexural and single edge notched beam tests. Transmission electron microscopy and scanning electron microscopy are also utilised to characterise the fracture behaviour of the nanocomposites as well as the dispersion state achieved. Finally, the impact of CNT addition on the cure kinetics and glass transition temperature of the epoxy resin and its relationship with the nanoparticle distribution is investigated.

4.2 Materials

4.2.1 Epoxy Resin System

Two epoxy resin systems, one of low and one of high viscosity, were used for the nanocomposite fabrication. The properties and characteristics of each thermosetting resin are shown in Table 4.1.

Epoxy Resin System	Chemical Name	Relative Density (g/cm^3)	Viscosity (mPa s)	T_g (^{o}C)
RS-L135/RS-H136	Bisphenol A	1.14 – 1.18	500-1000	60-65
Technowrap 2K L.T.	Bisphenol A	1.16	3750	70

Table 4.1: Properties of the epoxy resin systems.

The RS-L135/ RS-H136 (RS) epoxy resin was supplied by PRF Composites and Technowrap 2K L.T. (TW) epoxy resin was supplied by Walker Technical. Both resins were mixed with the corresponding amine based hardener at weight ratios of 100:35 and 100:20 respectively. The pot life of the two epoxy resin systems was from 90 to 120min for the RS resin, whereas it was only 15min for the TW. The noteworthy difference in viscosity and pot life between the resins used is also reflected in their applications. The high viscosity TW epoxy resin is mostly utilised for on-site composite repairs where fast curing is required, while the RS epoxy resin

allows for a variety of laminating processing methods, such as pressure and vacuum bag moulding.

4.2.2 Multi-wall Carbon Nanotubes

Industrial grade NC7000™ thin multi-wall CNTs with 90% purity, supplied by Nanocyl SA, were incorporated in the epoxy resin systems (Figure 4.1).
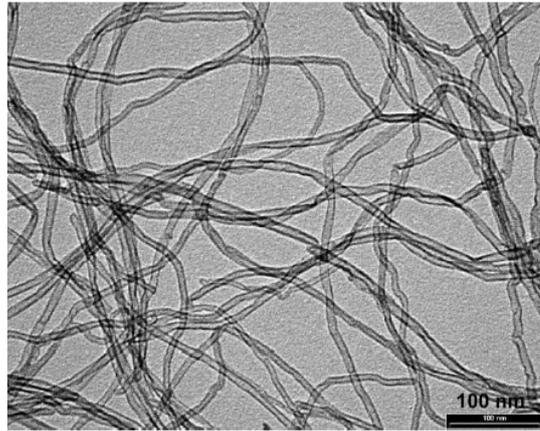
Figure 4.1: Multi-wall carbon nanotubes (TEM).

NC7000™ CNTs, which were synthesised via catalytic chemical vapour deposition (CCVD) method, have a diameter in the range of 9.5nm, average tube length equal to 1.5μm and surface area of around 250-300m^2/g. Some of their properties are shown in Table 4.2.

E (TPa)	1	Strain to Failure (%)	10
Strength (GPa)	10-60	Specific Density	1.3-2

Table 4.2: Mechanical properties of MWCNTs.

4.3 Dispersion Methods

One of the major challenges that researchers encounter during the incorporation of CNTs in the matrix is the phenomenon of aggregation according to which CNTs are clustered together and form bundles. Due to the fact that aggregates usually lead to significant deterioration of the mechanical, thermal and electrical properties of nanocomposites, many ways aiming to enhance the CNT dispersion in the matrix have been investigated. Such methods are mechanical dispersion techniques and non-covalent and covalent chemical treatments. In this study, three mechanical dispersion methods and one physical surface modification treatment were employed.

4.3.1 *Mechanical Dispersion Methods*

The mixing process involves the delivery of mechanical energy into the solution in order to break or reduce the size of agglomerates and then, disperse the individual CNTs and the remaining agglomerates homogeneously. The dispersion routes explored are described below.

- Method 1: Sonication

The ultrasonic tip sonicator UP200S (200 watts, 24 kHz) was used with a probe of 90mm length and 7mm diameter (Figure 4.2). During sonication process, the probe causes cavitation and a series of microscopic bubbles are formed and collapse generating powerful waves of vibration that cycle into the solution and break the aggregates.

Figure 4.2: Tip sonicator.

Ultrasonication depends on the: a) probe diameter, b) immersion depth of the probe, c) frequency, d) amplitude and d) sonication time. The probe was always fixed at the centre of the beaker and 5mm from its bottom. Due to the fact that local heating of the mixture was generated during this process, sonication was performed in pulse mode, i.e. 0.6sec on, 0.4sec off to allow for better temperature control. The amplitude, which affects the intensity of the cavitation effect and increases with increased amplitude values and the sonication time, which determines the total energy input, were the two parameters investigated (Table 4.3).

RS			TW	
Time (min)	Amplitude (%)		Time (min)	Amplitude (%)
15 20 30 60	40% 65%		15 30	65%

Table 4.3: Sonication and amplitude values for each epoxy resin system.

An important characteristic of sonication process is that it becomes more effective when low viscosity media are used. Therefore, both epoxy resins were heated at 40°C prior to the mixing in order to reduce the viscosity and promote dispersion.

- Method 2: Mechanical stirring and sonication

Considering the viscosity of the CNT/epoxy mixture and the fact that the energy of the tip sonicator is focused on a small, concentrated area [7], it cannot be ensured that cavitation process occurs across the whole volume of the mixture. Therefore, high-speed mixing for 5 or 15min at 10000rpm was used prior to sonication.

- Method 3: Ball milling

Ball milling was the third dispersion method examined. The CNT/epoxy mixture was placed in a zirconium oxide grinding bowl with 5mm diameter grinding balls (Figure 4.3). Ball-milling was performed for 45min at 400rpm in the Fritsch Pulverisette 6 Planetary Mono Mill apparatus.

Figure 4.3: Grinding bowls for ball milling.

4.3.2 Physical Surface Modification

Even after the utilisation of various dispersion techniques, CNTs tend to cluster together again, if they are left in a solution for a period of time. A chemical compound is usually added to separate individual CNTs from agglomerates, stabilise them and avoid re-agglomeration. In this study, a commercial block copolymer (BCP) was added into the CNT/epoxy mixture to improve and stabilise dispersion. The block copolymer used was the Disperbyk 2150 (BYK Chemie Company), which is an alkylammonium salt of a low-molecular weight polycarboxylic acid polymer. The improvement of dispersion after the introduction of this BCP was verified in [113] and was attributed to the following mechanism. BCP, which acts as a dispersing agent, consists of a lyophobic (solvent-repelling) and a lyophilic (solvent-attracting) block (Figure 4.4). The lyophobic part adsorbs onto the surfaces of CNT, while the lyophilic part is swollen by the solution. The repulsion among the lyophilic blocks overcomes the van der Waals attractive forces between the CNTs and hence, they are kept separated.
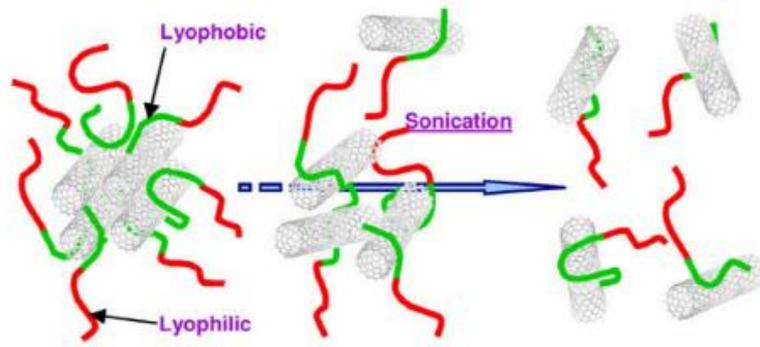
Figure 4.4: Suspension of CNTs in solution with block copolymer [114].

In this study, a small amount of BCP was mixed with the MWCNTs in acetone solution and was sonicated for 1min. The epoxy resin was then introduced ($\frac{re\sin+hardener}{BCP} = \frac{10}{0.15}$ by weight), following the manufacturing process described in Figure 4.5. Another important aspect that had to be taken into consideration was the removal of the acetone from the mixture. Although the CNT mixture (resin + CNTs) was placed in an oven to reach 60°C, which is acetone's boiling point and then, degassed in a vacuum chamber, acetone was still traceable in the nanocomposites (via DSC method). Solvents are usually used to facilitate dispersion, however, incomplete removal leads to formation of defects, because it evaporates during the curing process resulting in effect in lower mechanical and thermal properties [10].

4.4 Manufacturing Process

Pristine MWCNTs of 0.03, 0.1, 0.2, 0.3, 0.5 and 1 wt.% were added to the epoxy resin. Due to the different characteristics of the epoxy resin systems, the manufacturing process presented a few differences that will be thoroughly described below. However, the fundamental steps of the nanocomposite fabrication were kept constant and are shown in Figure 4.5.
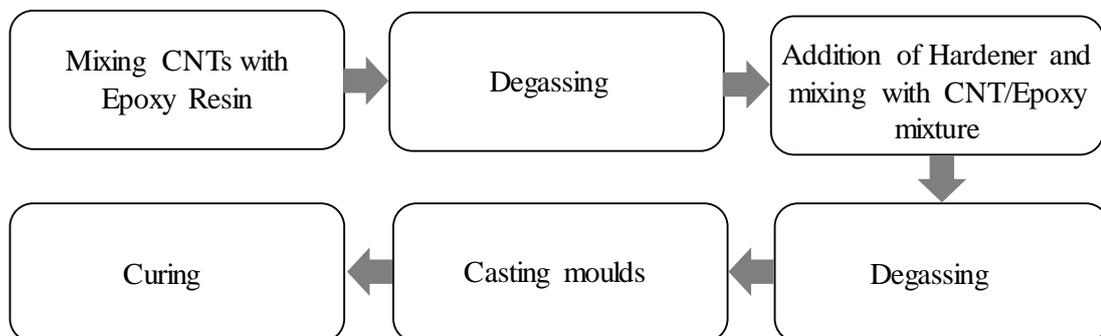
Figure 4.5: Manufacturing process of CNT nanocomposites.

A summary of the CNT loadings investigated for each epoxy resin system is given below (Table 4.4).

Resin System	CNT Weight Fraction (%)					
Technowrap	0.03	0.1	-	0.3	-	-
RS-L135	0.03	0.1	0.2	0.3	0.5	1

Table 4.4: MWCNT reinforced epoxy composites.

4.4.1 MWCNT/TW Epoxy Composites

MWCNTs were dispersed in TW epoxy resin via sonication method followed by degassing for 20min. Due to the increase of temperature during sonication process, the MWCNT/epoxy mixture was left to cool down to room temperature prior to the addition of the curing agent. Increased temperature in combination with the short pot life of TW epoxy resin would accelerate the curing process. Finally, the mixture was degassed again, but only for 5min because of the pot life time limitations.

4.4.2 MWCNT/RS Epoxy Composites

For the case of RS epoxy resin, all the aforementioned dispersion methods were investigated. After the dispersion of MWCNTs in the matrix, degassing of the MWCNT/epoxy mixture for 20min followed in order to reduce the entrapped air induced during mixing. The curing agent was then added and after 5min of hand stirring, the mixture (resin + MWCNTs + hardener) was degassed again for 20min to remove the remaining air.

The MWCNT/epoxy mixtures were finally cast in two different shaped moulds (Figure 4.6).

Figure 4.6: Casting process: tensile test mould (left) and flexural test mould (right).

The last step of the composite fabrication was the curing process at room temperature for 24h. The samples were then post-cured for 15h at 50°C and 10h at 80°C for the RS and TW epoxy resin systems respectively in order to reach the full strength of the materials.

4.5 Mechanical Test Methods

4.5.1 Tensile Test Method

The tensile properties of pure epoxy and MWCNT reinforced epoxy resin were evaluated by conducting tensile tests as described in ASTM D638-14 standard [136] at constant crosshead speed of 1mm/min. Standard dumbbell-shaped test specimens (Figure 4.7) were loaded to failure and an extensometer of 50mm gauge length was used to measure the axial displacement.
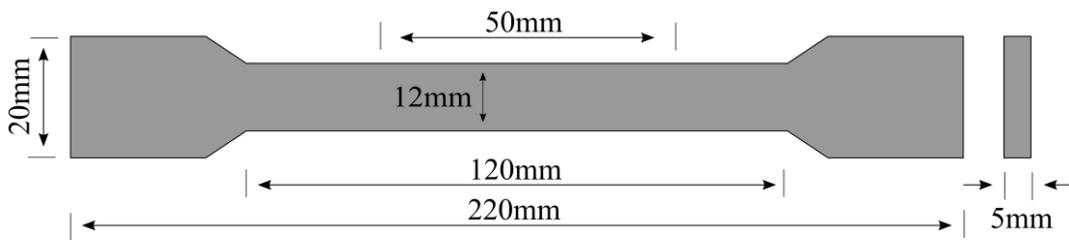
Figure 4.7: Dogbone specimen configuration.

4.5.2 Three-point Bend Test Method

Three-point bend tests were also performed in order to determine the variation of the flexural strength with the CNT weight content. According to ASTM D790-15 standard [137], a span-to-depth ratio of 16:1 was employed. Specimens of dimensions shown in Figure 4.8 were deflected at 1mm/min until rupture occurred in the outer surface of the test specimen or until maximum strain of 5% was reached. The span was kept constant and equal to 80mm throughout all the flexural tests.
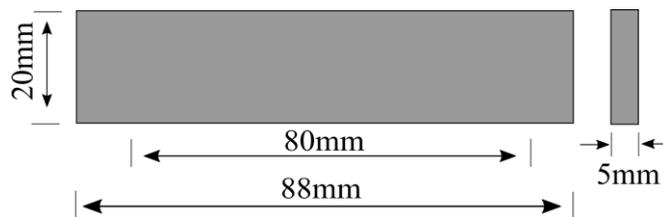
Figure 4.8: Three-point bend specimen configuration.

4.5.3 Single Edge Notched Beam Test Method

The single edge notched beam (SENB) test method was used to assess the toughness of the nanocomposite materials in terms of the critical stress intensity factor, K_{IC}, a parameter indicative of the resistance to fracture of the material. The tests were carried out in accordance with the ASTM D5045-99 standard [138]. A sharp notch was generated using a disc band saw (disc thickness= 0.3mm) and then, a natural crack was initiated by a razor blade (Figure 4.9).

For tough adhesives, it was recommended that the razor blade was drawn across the notch tip to create the precrack. The sliding action of the blade minimises the introduction of compressive residual stresses, which are introduced by tapping and lead to false K_{Ic} values. After the specimen preparation was complete, the test was conducted at 10mm/min.
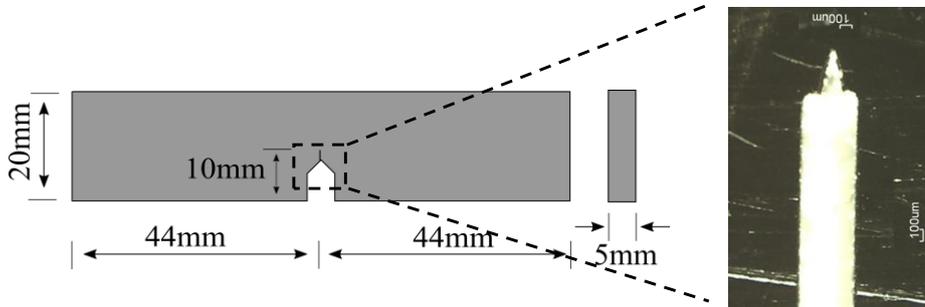
Figure 4.9: Single edge notched beam specimen configuration and the notch profile.

For this type of specimen, the critical stress intensity factor was calculated according to Equations (4) and (5), as described in the standard:

$$K_{Ic} = \left(\frac{P}{BW^{1/2}} \right) f(x) \quad (4)$$

Where, $f(x)$ is the geometric calibration factor given by:

$$f(x) = 6x^{1/2} \frac{\left[1.99 - x(1-x)(2.15 - 3.93x + 2.7x^2) \right]}{(1+2x)(1-x)^{3/2}} \quad (5)$$

and P is the load, B is the specimen thickness, W is the specimen width, a is the crack length and $x=a/W$.

In all tests, four specimens per case were tested.

4.6 Test Results - MWCNT/TW Epoxy Composites

The results obtained for the MWCNT/TW epoxy composites are shown in the next figures. Sonication at 65% amplitude was the method used for the CNT dispersion. The sonication time durations investigated were:

- 15min
- 30min

4.6.1 Tensile Tests

A slight increase of the Young's modulus is observed when either 0.03 wt.% or 0.1 wt.% of CNTs is added in the epoxy resin irrespective of the sonication time (Figure 4.10). This indicates better matrix/CNT adhesion than the case of 0.3 wt.% for which the modulus remains constant or moderately decreases.
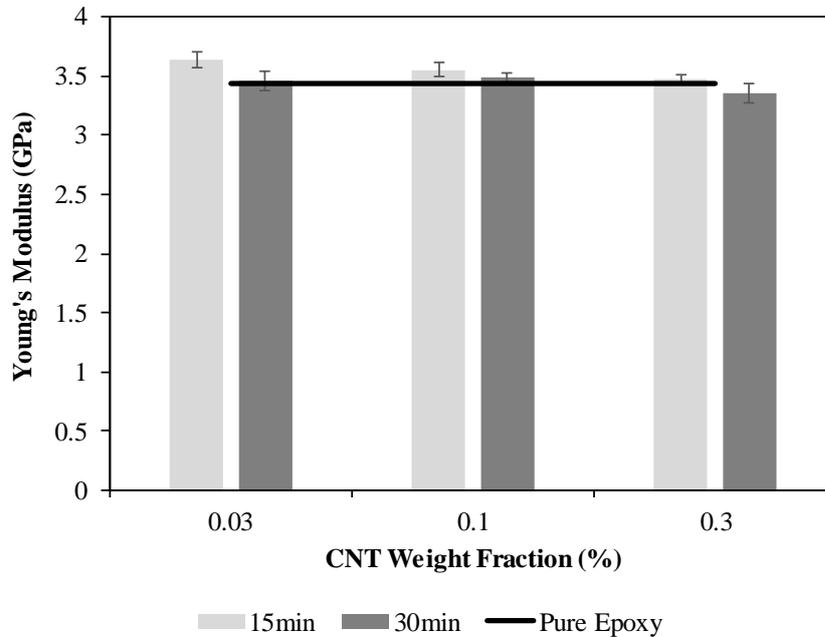
Figure 4.10: Young's Modulus versus CNT weight fraction for various sonication time durations.

On the other hand, the addition of CNTs in TW epoxy resin significantly decreases the tensile strength for all sonication time durations (Figure 4.11). When sonication time is 15min, tensile strength exhibits very low values, which almost remain unchanged with the CNT content.

The decrease of the tensile strength can be explained by the poor dispersion of CNTs in the matrix, which agglomerate and act as failure initiation sites. The sonication time is therefore doubled aiming to enhance dispersion. For the case of 0.03 wt.% and 30min sonication time, tensile strength increases by 18.6% compared to the one obtained for 15min, however, in both cases tensile strength is much lower than that of pure epoxy. For 0.1 and 0.3 wt.% and increased sonication time, tensile strength decreases, which might be attributed to the damage of the CNT structure.
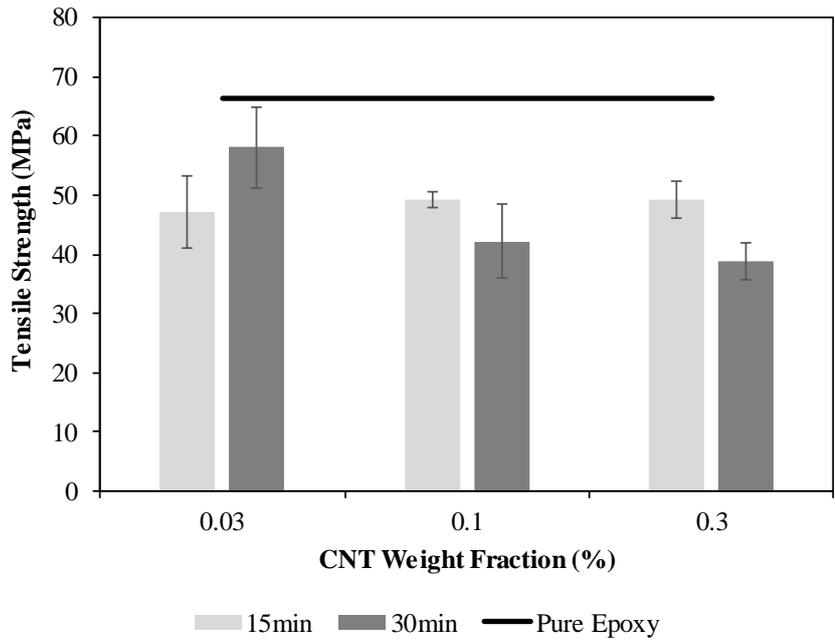
Figure 4.11: Tensile Strength versus CNT weight fraction for various sonication time durations.

Strain to failure also shows a noteworthy decrease after the incorporation of CNTs into TW epoxy resin indicating that nanocomposites are much more brittle than pure epoxy specimens (Figure 4.12). With regard to the effect of sonication time, similar conclusions as for the tensile strength can be drawn.
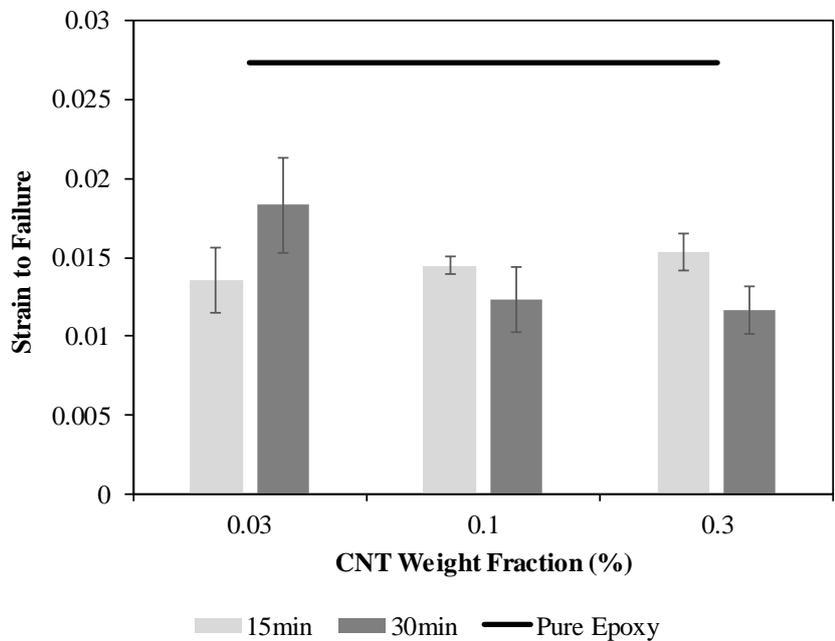
Figure 4.12: Strain to Failure versus CNT weight fraction for various sonication time durations.

4.6.2 Three-Point Bend Tests

Tensile tests are followed by three-point bend tests for which the flexural modulus and strength are plotted against the CNT weight fraction and are illustrated below. For the case of 15min sonication time, flexural modulus does not show any variation with the CNT loading in comparison to pure epoxy resin except for the case of 0.3 wt.%, where the modulus decreases (Figure 4.13). This is probably due to the phenomenon of aggregation, which is more noticeable for higher CNT contents and results to insufficient load transfer between the matrix and the filler.

 A similar drop is also obtained for 0.1 wt.% and for 30min of sonication. This can be explained by the fact that increased sonication time might have damaged the CNTs affecting negatively the matrix/filler load transfer.
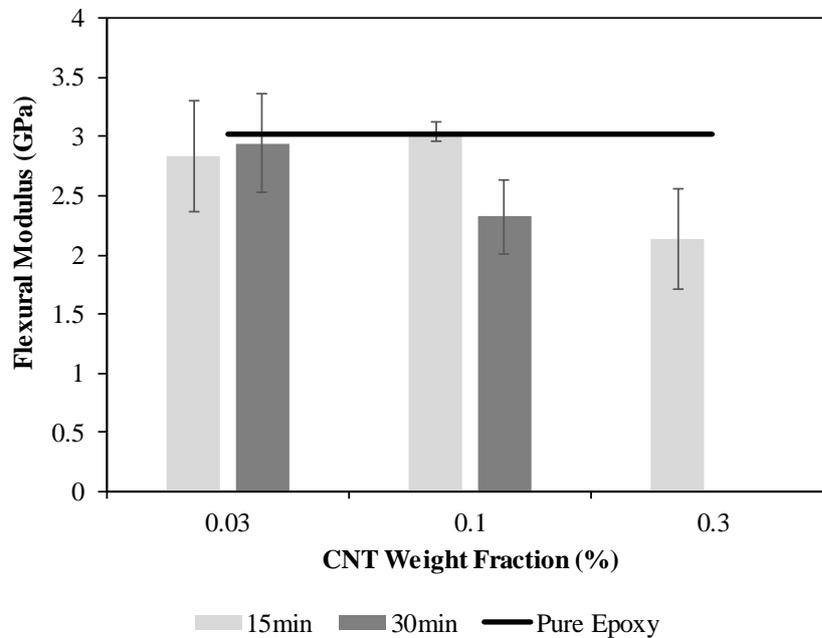
Figure 4.13: Flexural Modulus versus CNT weight fraction for various sonication time durations.

The addition of CNTs to TW epoxy resin is proved to be detrimental for the flexural strength decreasing its values by a factor of two when compared to those for pure epoxy irrespective of the CNT weight fraction and sonication time (Figure 4.14).
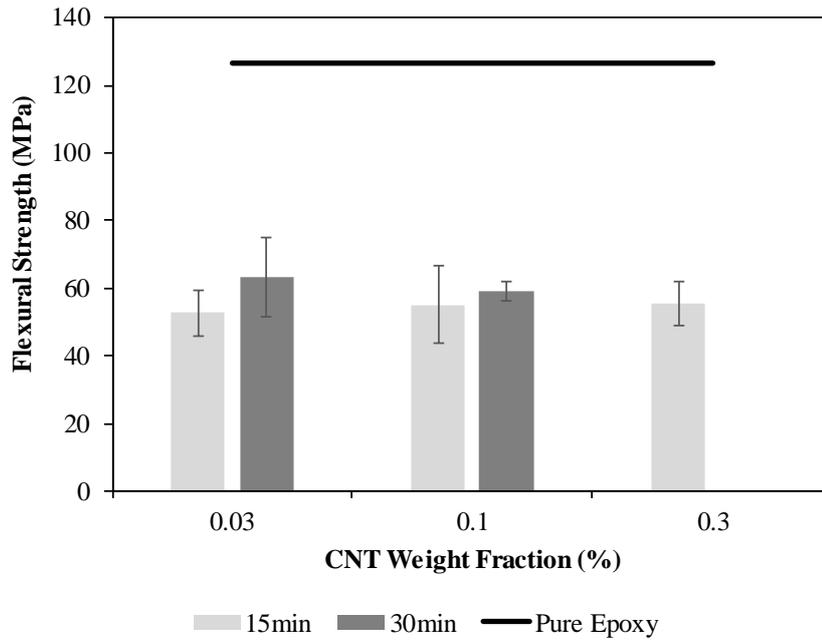
Figure 4.14: Flexural Strength versus CNT weight fraction for various sonication time durations.

4.6.3 Single Edge Notched Beam Tests

Fracture toughness remains almost unaffected when a small quantity of CNTs, i.e. 0.03 wt.%, is added in the epoxy resin. However, it increases by approximately 15% for the case of 0.1 wt.% and when sonication time is 30min, highlighting the beneficial effect of the increase of sonication time (Figure 4.15).
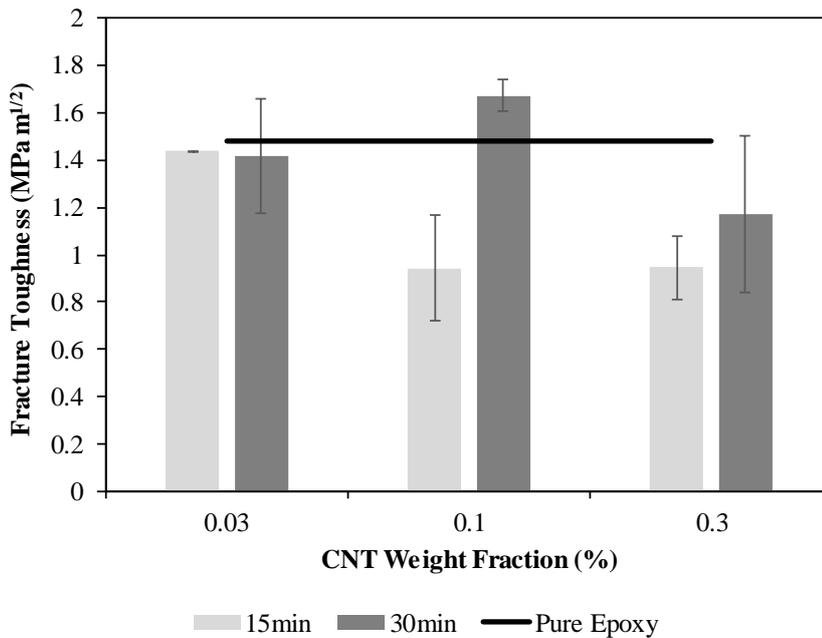
Figure 4.15: Fracture Toughness versus CNT weight fraction for different sonication time durations.

Hence, fracture toughness seems to be affected more by the decrease of the aggregates rather than the decrease of the CNT length in contrast to what was shown for the aforementioned mechanical properties. In order for the energy dissipation mechanisms to take place, composites with uniformly dispersed fillers are required. Therefore, further increase of the CNT content leads to the decrease of fracture toughness for both sonication time durations due to the increase of agglomerates.

4.6.4 MWCNT/TW Epoxy Composites Test Summary

To sum up, the addition of 0.03 wt.% CNT to TW epoxy resin results in mechanical properties almost equivalent to those of pure epoxy resin. Nonetheless, further increase of the CNT content leads to significant reduction of the properties despite the increase of sonication time from 15min to 30min. The poor mechanical performance of the nanocomposites is due to inhomogeneous dispersion that also leads to poor matrix/CNT adhesion, which can eliminate the beneficial effects of the CNT introduction. Another parameter that affects the mechanical performance is the entrapped air in the CNT mixture that is impossible to remove completely during degassing because of the high viscosity of TW epoxy resin. Thus, the remaining air turns into voids, which act as crack initiation sites.

The complexity of the manufacturing process of MWCNT/TW epoxy composites owing to the short pot life and the high viscosity of this epoxy resin system did not allow for the utilisation of the other two dispersion techniques. A second epoxy resin system was therefore investigated and the results are shown in the next section.

4.7 Test Results - MWCNT/RS Epoxy Composites

Ultrasonication is the first dispersion method assessed. Firstly, the effect of the dispersing agent (BYK) for two sonication time durations at 65% amplitude and different CNT loadings on the tensile properties is examined. After the sonication parameters, namely time and amplitude are optimised, ultrasonication is compared to the other two dispersion techniques.

4.7.1 Effect of BYK Dispersant on Tensile Properties

Young's modulus shows a marginal improvement, which is almost constant for all CNT loadings and both sonication time durations (Figure 4.16). The use of BYK does not further enhance the modulus apart from the cases of 0.1 wt.% CNT (15min sonication) and 0.3 wt.% CNT (30min of sonication).
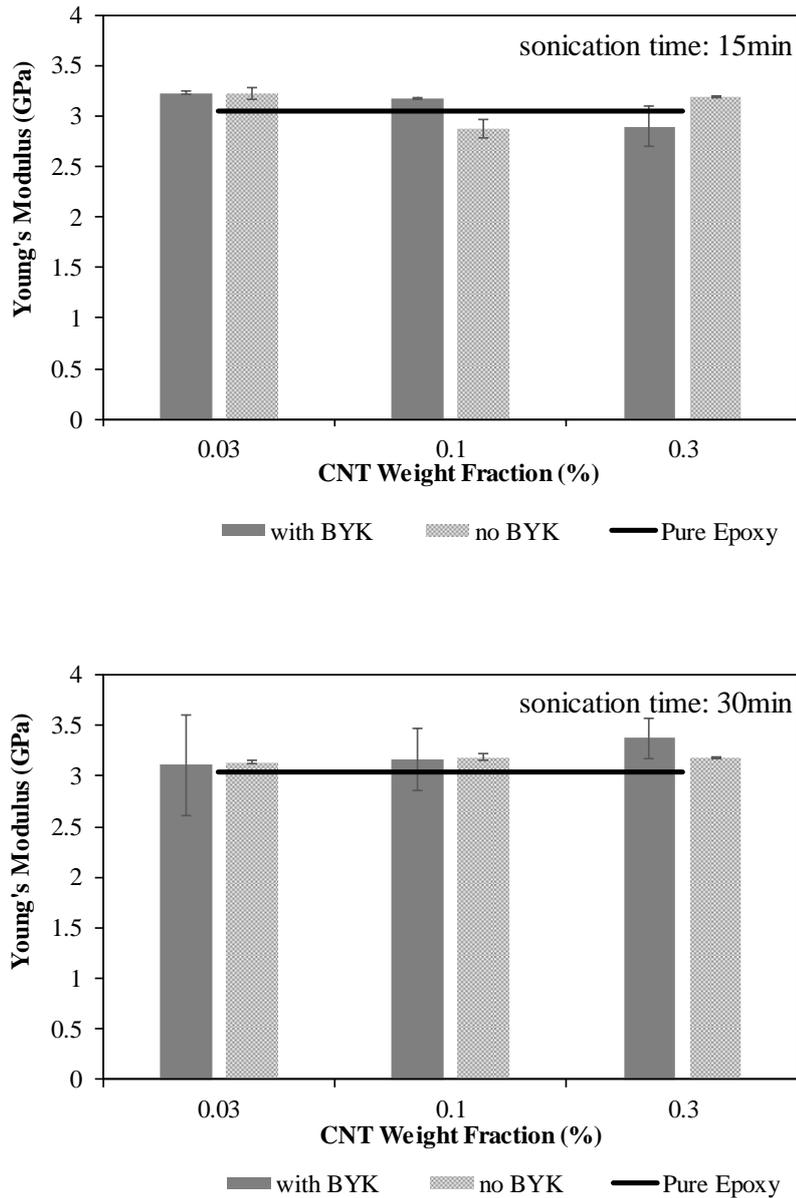
Figure 4.16: Young's Modulus versus CNT weight fraction when BYK is used for 15min (top) and 30min (bottom) of sonication.

Tensile strength exhibits no significant variation for both sonication time durations employed up to 0.1 wt.% CNT after which it drops (Figure 4.17). The addition of BYK in the CNT/epoxy mixture only enhances the tensile strength of 0.3% CNT filled epoxy composites, which are sonicated for 30min, achieving similar values to that of pure epoxy.
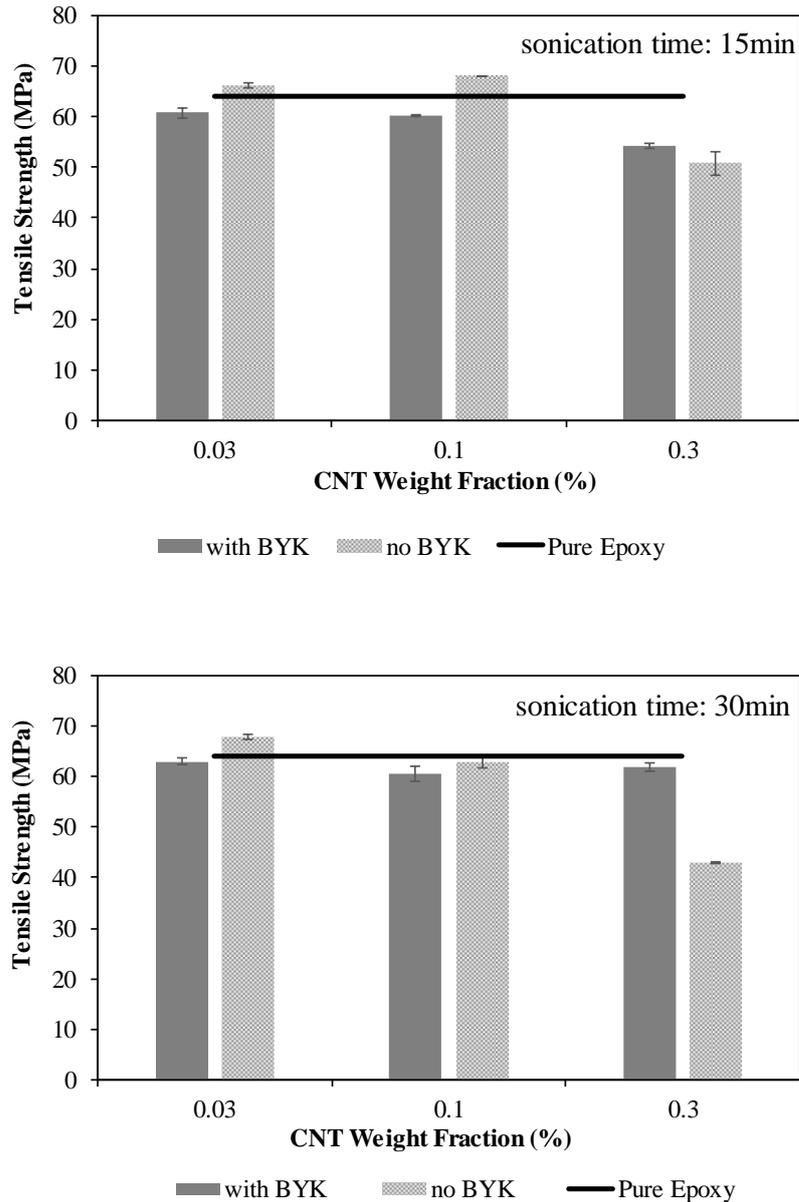
Figure 4.17: Tensile Strength versus CNT weight fraction when BYK is used for 15min (top) and 30min (bottom) of sonication.

Extended sonication up to 30min in combination with the addition of BYK dispersant is more beneficial for the highest CNT loading (0.3 wt.%) in comparison with the case when no BYK is used. This suggests that BYK can improve the CNT dispersion and decrease the number of aggregates accumulated due to the increase of the CNT content, but only for prolonged sonication, i.e. greater than 15min.

The strain to failure for both cases of sonication time (as also seen in Figure 4.12) decreases after the addition of CNTs, because the epoxy resin samples become more brittle (Figure

4.18). On the other hand, the specimens for which the BYK dispersant is used attain higher strain to failure values than the specimens with no dispersant.
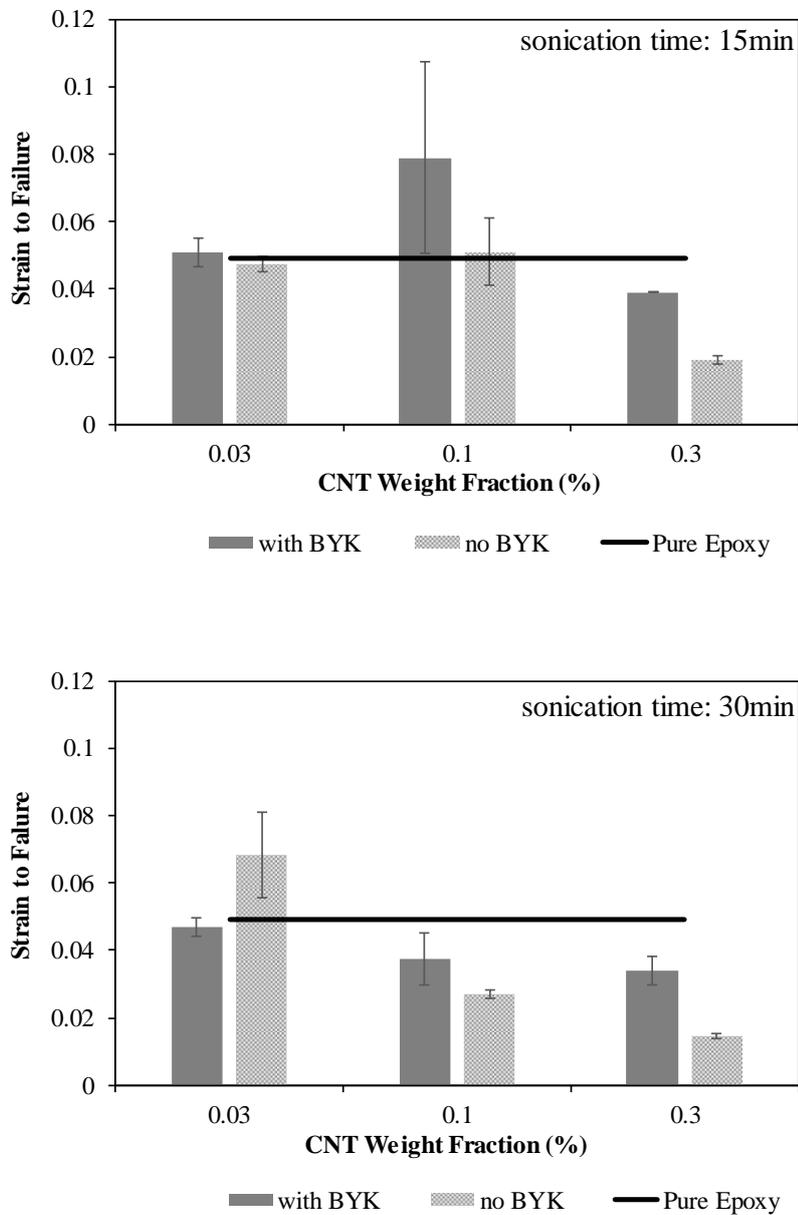
Figure 4.18: Strain to Failure versus CNT weight fraction when BYK is used for 15min (top) and 30min (bottom) of sonication.

The use of dispersing agent does not improve the tensile properties of the nanocomposites, as also shown in [139]. It is only found to be favourable for 0.3% CNT loading, where it does not allow the aggregates to impair the tensile properties of the epoxy matrix. Therefore, because of the little influence of BYK dispersant on the mechanical properties, no dispersant is used for the rest of the cases studied.

4.7.2 Effect of Different Sonication Times on Tensile Properties

Sonication time is one of the parameters that have been studied the most in the literature. By employing too short sonication, CNTs might not be efficiently dispersed in the matrix, whereas prolonged sonication can damage the CNT structure. Therefore, in this study, different sonication time durations are investigated in order to achieve good mechanical properties and homogeneous dispersion.

In Figure 4.19, Young's modulus is plotted against the CNT weight fraction, while varying the sonication time. The modulus shows a moderate increase with the CNT content for all cases of sonication time. However, when CNT weight fraction increases to 1%, the modulus reduces, probably due to the formation of aggregates that weaken the interfacial adhesion between the matrix and the filler.
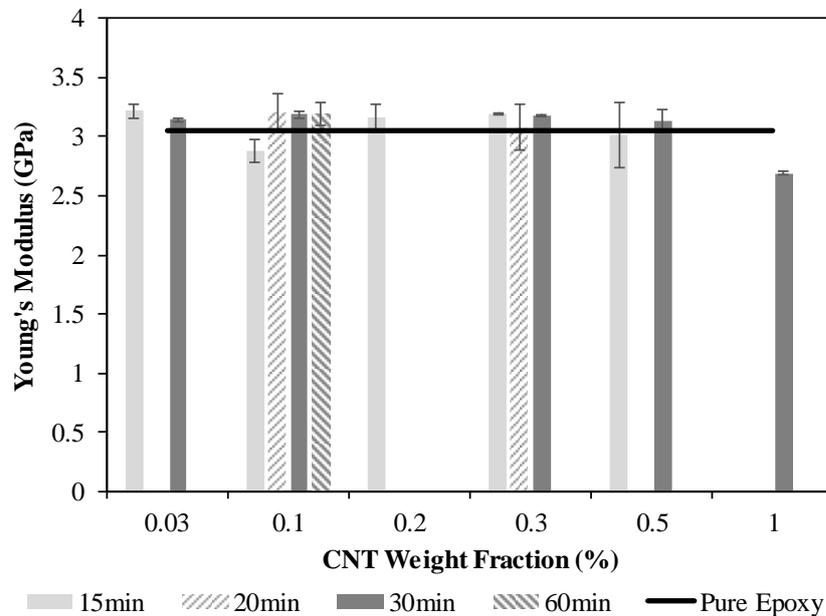
Figure 4.19: Young's Modulus versus CNT weight fraction for different sonication time durations.

At low loadings, i.e. 0.03 wt.%, the dispersed CNTs restrict the mobility of the polymer chains [4] and hence, improve the strength for both 15min and 30min of sonication. When the CNT content increases to 0.1 wt.%, tensile strength exhibits almost equal values to the ones of pure epoxy for all sonication time durations examined (Figure 4.20).
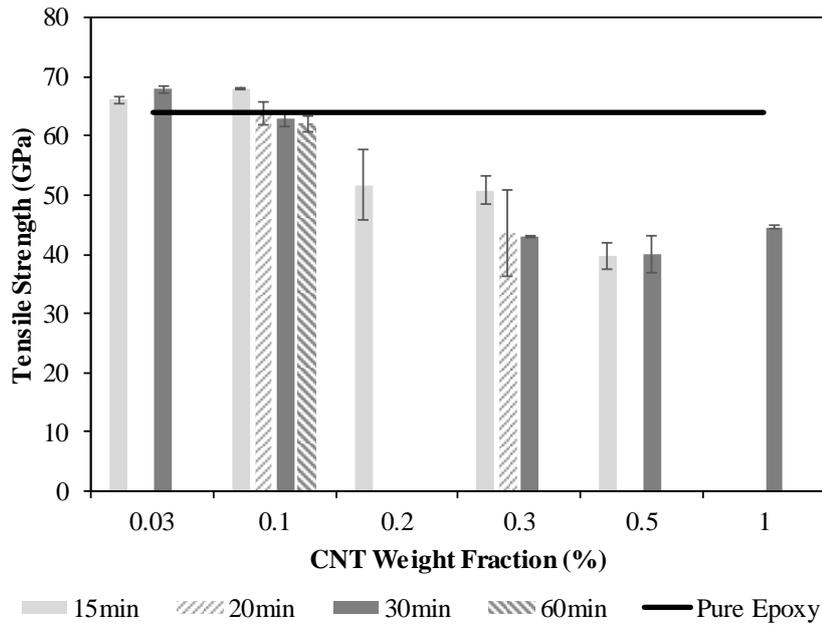
Figure 4.20: Tensile Strength versus CNT weight fraction for different sonication time durations.

However, further increase of the CNT weight fraction leads to the reduction of the tensile strength even with prolonged sonication until it reaches a plateau. This indicates that sonication process does not manage to break all the agglomerates, which increase with the increase of the nanotube content and result in premature failure.

In Figure 4.21, the embrittlement of the CNT nanocomposites is observed for all sonication time durations employed, which becomes more intense with the increase of the filler content.
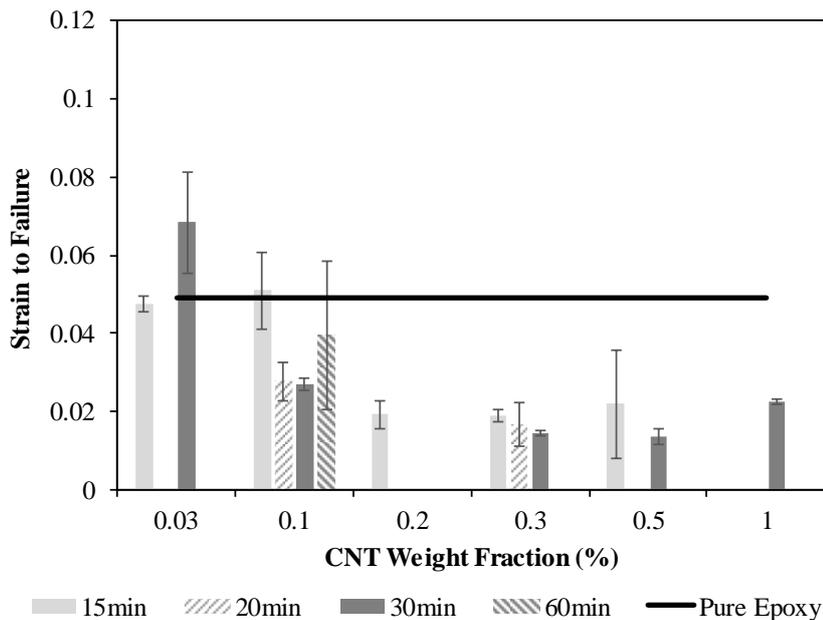
Figure 4.21: Strain to Failure versus CNT weight fraction for different sonication time durations.

4.7.3 Effect of Sonication Amplitude and Mechanical Stirring on Tensile Properties

The optimal loading so far is 0.1 wt.% CNT and hence, it is the one used as benchmark in order to evaluate the amplitude effect on the tensile properties. The amplitude, which is the power output of the ultrasonic processor, can vary from 20% to 100%. However, very high values of amplitude can increase the intensity of sonication process and thus, damage the CNT structure, whereas very low amplitude values might be insufficient to disperse the CNTs in the matrix. Therefore, two average amplitude values, i.e. 40% and 65% are studied for the cases of 15min and 30min sonication time.

A much more aggressive dispersion method is also investigated and compared to sonication. According to this method, the epoxy resin and CNTs were mechanically stirred at 10,000 rpm for either 5min or 15min and then, sonicated for 30min (i.e. 5+30min and 15+30min respectively). Mechanical stirring could not be used for longer periods of time, because the temperature of the mixture increased significantly even when the mixing lasted for less than 5min. An additional side effect of such intense method was the big amount of air that was introduced during mixing (foam-like mixture), which was impossible to remove completely via degassing. Therefore, sonication was employed after mechanical stirring in order to further enhance the CNT dispersion and also act as additional measure of removing the air bubbles [104].

It can be seen in Figure 4.22 that Young's modulus exhibits a marginal increase for both dispersion methods and amplitudes employed suggesting improvement in the interfacial bond between the matrix and the CNTs and therefore, efficient load transfer.

The tensile strength obtained for both amplitudes is similar to the tensile strength of pure epoxy resin (Figure 4.23). The comparison of sonication and mechanical stirring prior to sonication shows that the tensile strength almost remains unaffected by the two dispersion methods. However, when mechanical stirring lasts for 15min, a significant decrease in tensile strength is observed. This drop can be attributed to the air bubbles induced during mechanical stirring that lead to the introduction of imperfections, which degrade the nanocomposites.
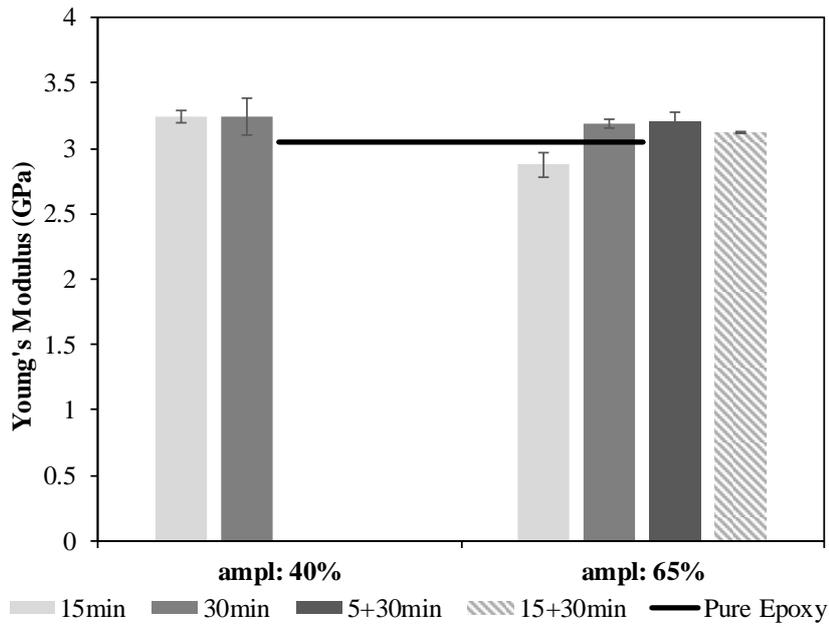
Figure 4.22: Young's Modulus versus sonication amplitude for 0.1 wt.% CNT.
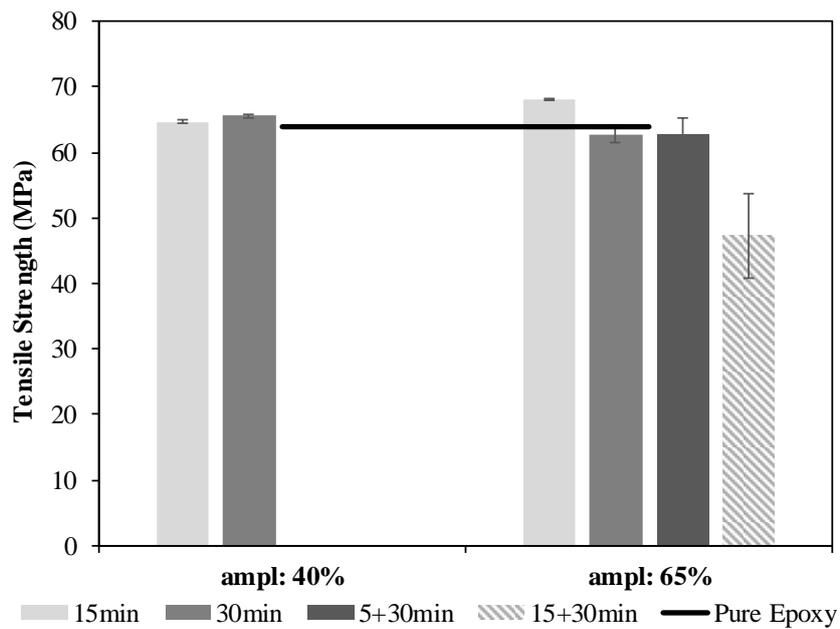
Figure 4.23: Tensile Strength versus sonication amplitude for 0.1 wt.% CNT.

In Figure 4.24, strain to failure decreases after the incorporation of CNTs in the epoxy resin when either sonication or 5min of mechanical stirring prior to sonication is employed. The lowest value though is obtained for the 15+30min case.
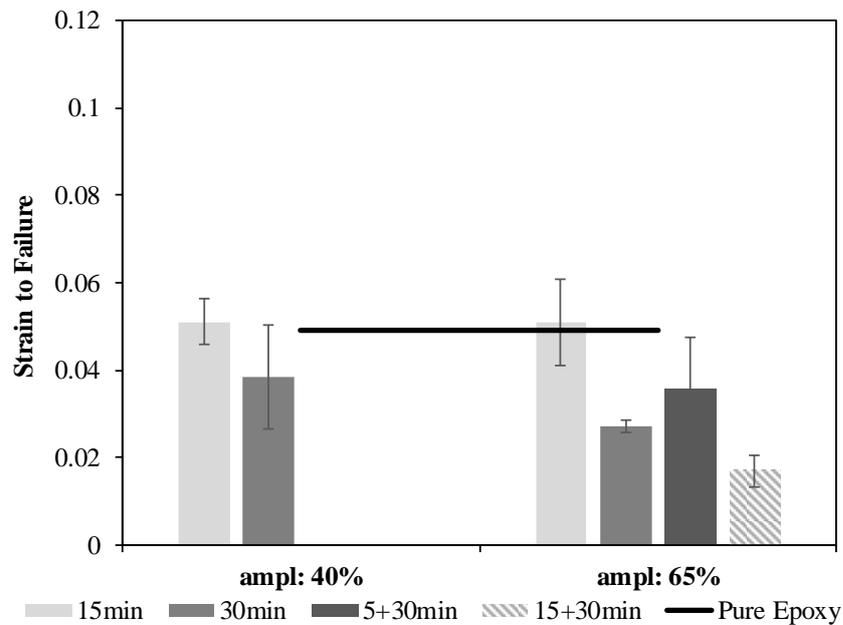
Figure 4.24: Strain to Failure versus sonication amplitude for 0.1 wt.% CNT.

It is therefore concluded that 5min is the maximum mixing time that can be achieved for mechanical stirring without diminishing the mechanical properties. Although similar test results have been obtained for both amplitudes, 40% is the amplitude selected in order to minimise the risk of CNT rupture and aspect ratio decrease that may occur during sonication process [108-110].

4.7.4 Effect of Dispersion Methods on Tensile Properties

The last part of the MWCNT/epoxy characterisation is the comparison of all dispersion methods. CNT nanocomposites of weight fractions up to 1% were manufactured using the following dispersion techniques:

a. Method 1: Sonication
b. Method 2: Mechanical stirring and sonication
c. Method 3: Ball milling

Tensile, three-point bend and single edge notched beam tests were conducted to assess the mechanical behaviour of CNT reinforced epoxy. The results obtained are presented in the following figures.

In Figure 4.25, Young's modulus exhibits a marginal increase with the increase of the CNT loading suggesting sufficient load transfer between the matrix and the CNTs for all dispersion

methods employed. Sonication is found to be effective for weight fractions up to 0.5%, whereas mechanical stirring in combination with sonication up to 0.3%.
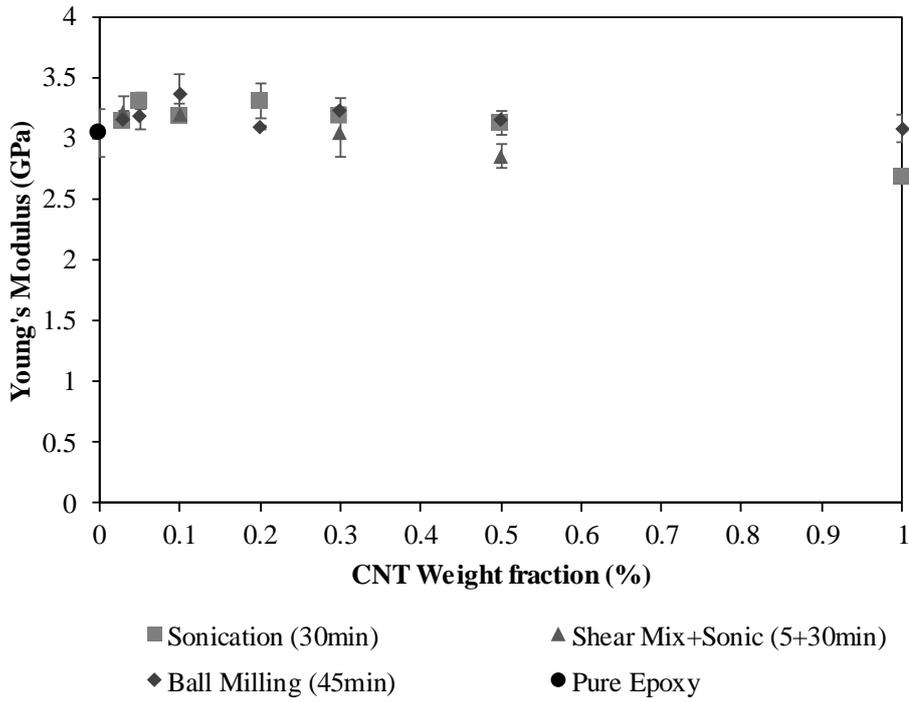
Figure 4.25: Young's Modulus versus CNT weight fraction for different dispersion methods.

Figure 4.26 summarises the tensile strength results of CNT/epoxy composites using different dispersion techniques.
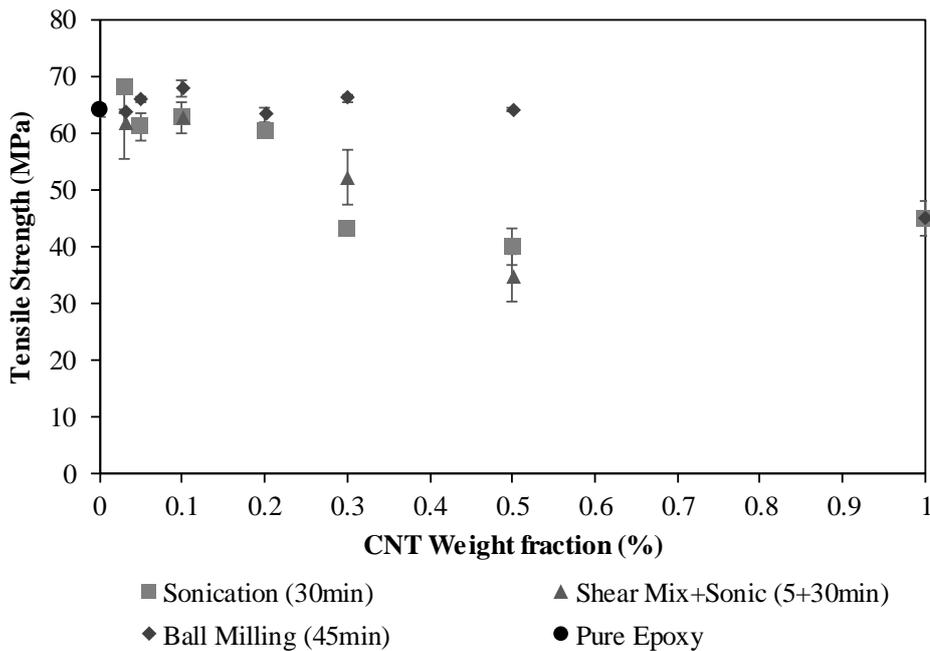
Figure 4.26: Tensile Strength versus CNT weight fraction for different dispersion methods.

Tensile strength remains unaffected up to 0.2 wt.% irrespective of the dispersion method. Further increase of the CNT content reduces considerably the tensile strength leading to a plateau with 30% lower values when compared to those of pure epoxy. Mechanical stirring prior to sonication does not influence the tensile strength for CNT weight fractions lower than 0.1%, whereas for 0.3 wt.%, it assists the CNT dispersion leading to enhanced tensile strength when compared to the case where only sonication is utilised. However, this does not apply to the case of 0.5 wt.%, where the tensile strength drops for both dispersion methods because of the increase of aggregated areas and creation of bubbles during mixing.

Ball milling seems to be the most efficient dispersion method for CNT loadings greater than 0.2 wt.%, for which the tensile strength values almost remain constant and equal to the tensile strength of pure epoxy in contrast to the other two techniques. Nevertheless, for the case of 1 wt.% CNT content, tensile strength reduces significantly for all dispersion methods including ball milling, suggesting that 0.5% is the maximum CNT weight fraction that can be achieved without degrading the tensile strength.

In Figure 4.27, strain to failure is plotted against the CNT weight fractions for all dispersion methods.
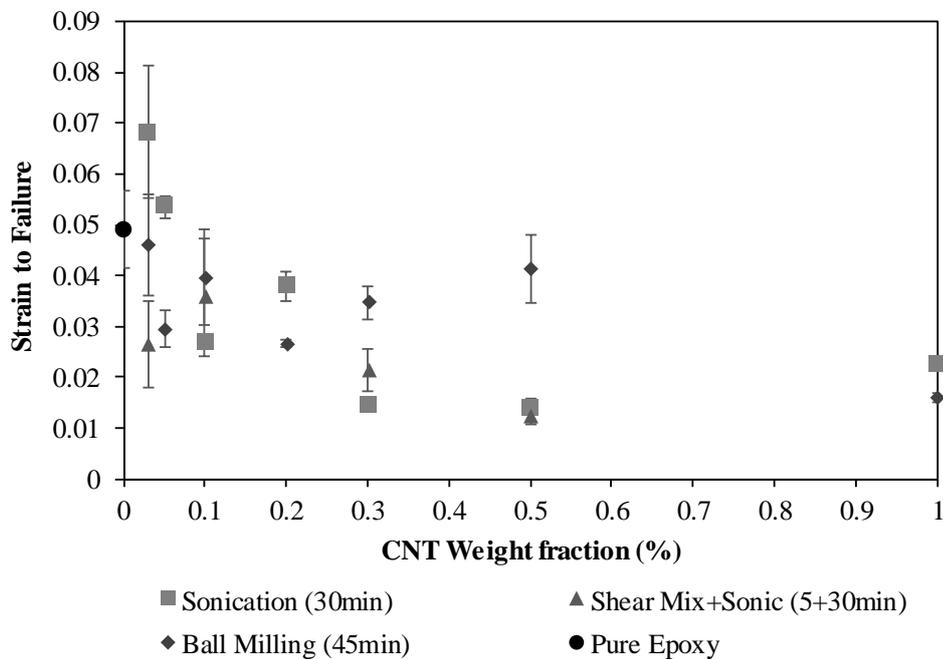
Figure 4.27: Strain to Failure versus CNT weight fraction for different dispersion methods.

A moderate increase of the strain to failure is observed for low CNT weight fractions, i.e. 0.03 and 0.05%, because it is more feasible to achieve uniform dispersion in such loadings.

However, this increase only occurs when sonication is employed and it is probably due to the fact that during sonication the minimum amount of air is introduced in the mixture in comparison to ball milling and mechanical stirring. Nonetheless, the higher the CNT content, the more brittle the specimen.

4.7.5 Effect of Dispersion Methods on Flexural Properties

Similar observations to those made for the tensile test results can be made for the flexural modulus and strength. In Figure 4.28, the flexural modulus is plotted against the CNT weight fraction. For all dispersion methods, the flexural modulus exhibits a slight increase with the CNT content, but only up to 0.5 wt.% after which it decreases. The slight reduction of the flexural modulus is associated with the CNT agglomeration and inhomogeneous dispersion. The comparison between the different dispersion techniques utilised does not show any noteworthy superiority of one method over another with regard to flexural modulus.
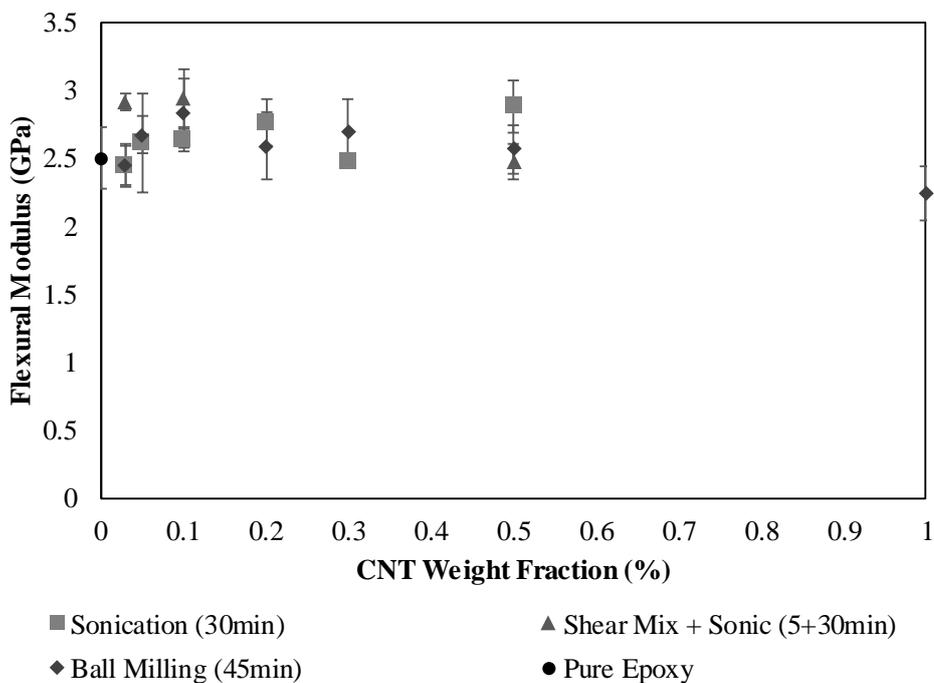
Figure 4.28: Flexural Modulus versus CNT weight fraction for different dispersion methods.

Flexural strength shows a similar trend to that of the tensile strength by almost remaining constant up to 0.3 wt.% [89] and then, decreasing when either sonication or mechanical stirring prior to sonication is employed (Figure 4.29). On the other hand, when ball milling is used to disperse the CNTs, flexural strength almost shows no variation for weight fractions up to 0.5%.
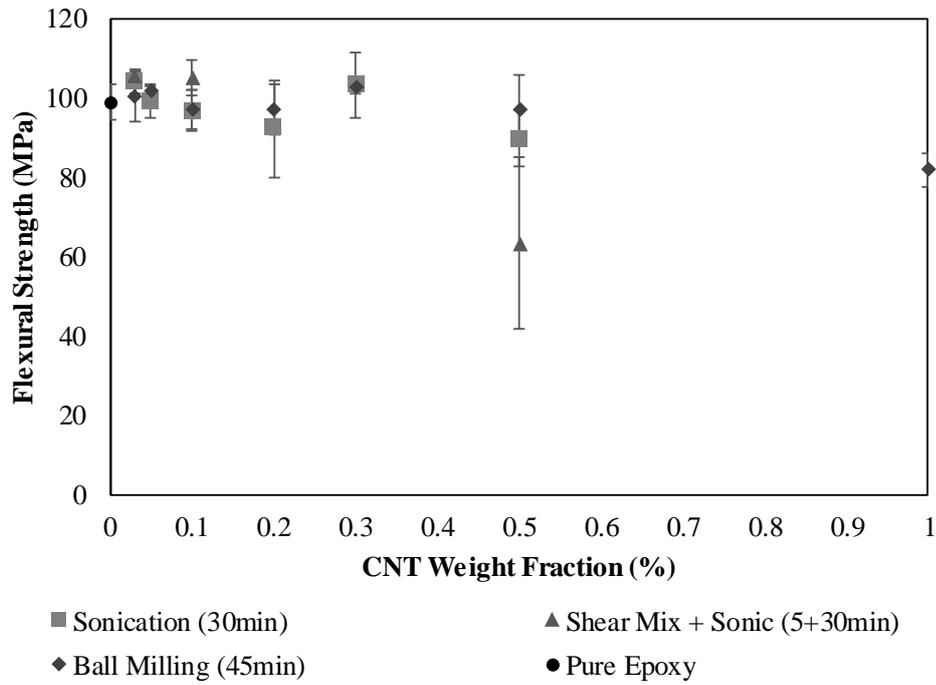
Figure 4.29: Flexural Strength versus CNT weight fraction for different dispersion methods.

4.7.6 Effect of Dispersion Methods on Fracture Toughness

The fracture toughness results obtained after the CNT reinforcement of the RS epoxy resin are shown in Figure 4.30.
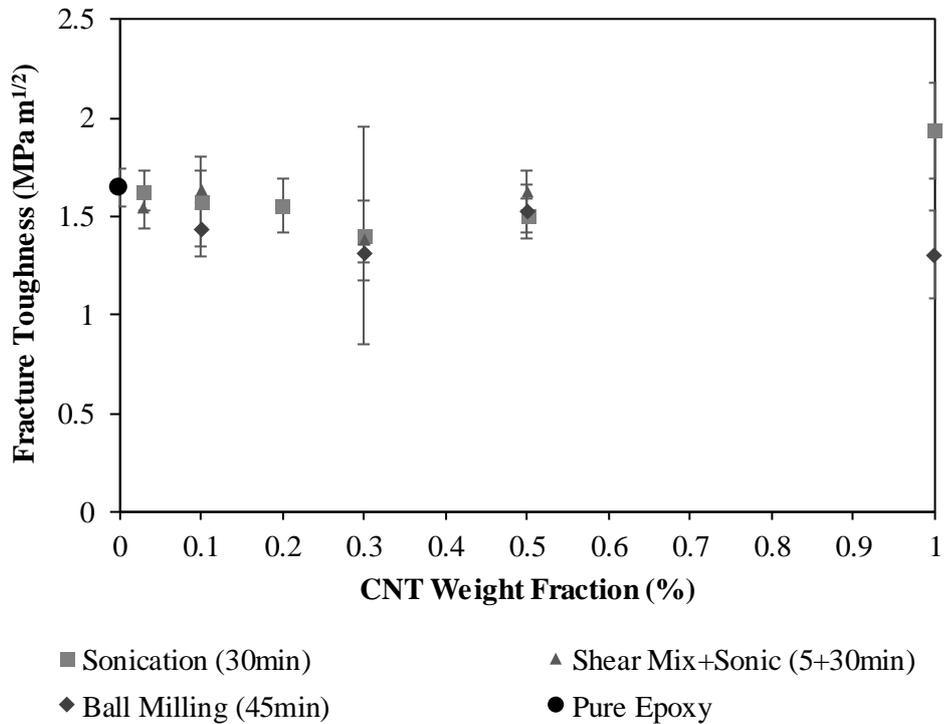
Figure 4.30: Fracture toughness versus CNT weight fraction for different dispersion methods.

Fracture toughness decreases slightly after the CNT addition compared to pure epoxy. The formation of MWCNT bundles and voids in the nanocomposites has an adverse effect on the toughening mechanisms [5]. Despite that 1 wt.% CNT reinforced epoxy contains the highest number of voids and agglomerates, which result in significant deterioration of the tensile and flexural properties (see Figure 4.26, Figure 4.27 and Figure 4.29), it shows improvement in fracture toughness. This can be explained by the fact that the due to the phenomenon of aggregation, CNT bundles of different sizes compensate for the imperfections and give rise to toughening mechanisms, such as pull-out, crack deflection and void nucleation.

4.7.7 MWCNT/RS Epoxy Composites Test Summary

The experimental results show that the increase of the CNT content beyond a critical loading, which is 0.3 wt.% CNT in this study, results in the reduction of the tensile and flexural properties. At high CNT loadings, the viscosity of the CNT/epoxy mixture increases considerably and has a negative impact on the sample preparation leading to the introduction of defects, e.g. voids and the formation of aggregates and thus, to poor dispersion.

To conclude, no significant variation of the mechanical properties is observed when either of the three dispersion routes is utilised.

4.8 Transmission Electron Microscopy

Transmission electron microscopy (TEM) was used to determine dispersion qualitatively by comparing the three dispersion methods: a) sonication, b) mechanical stirring/sonication and c) ball milling. The TEM micrographs of the samples were obtained using the Philips CM100 instrument and recorded at 100kV. Thin slices of about 70nm were cut from each specimen using an ultramicrotome.
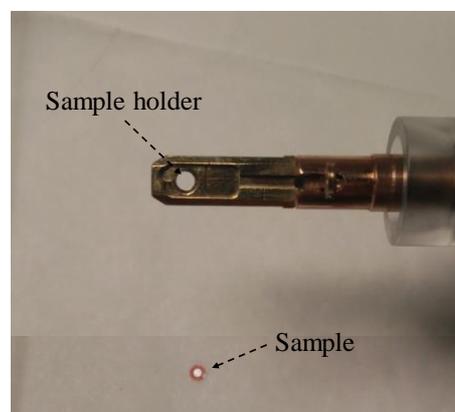
Figure 4.31: Sample and sample holder of the electron microscope.

The sample was then placed on the sample holder (Figure 4.31) and inserted into the electron microscope. The TEM micrographs of the nanocomposites for different CNT loadings are shown at 7900x magnification. The sample surfaces were scanned along the circumference and across the centre of each specimen in order to check the dispersion in as many areas as possible, so as to obtain representative images for each case.

4.8.1 Dispersion Assessment

For 0.03 wt. % CNT, mechanical stirring/sonication (method 2) and ball milling (method 3) are compared. It is shown that for both dispersion methods, there are many areas free from CNTs due to the small amount of CNT loading added in the epoxy resin (Figure 4.32a). Moreover, when ball milling is used, more CNT agglomerates are found in the samples suggesting poor dispersion (Figure 4.32b).
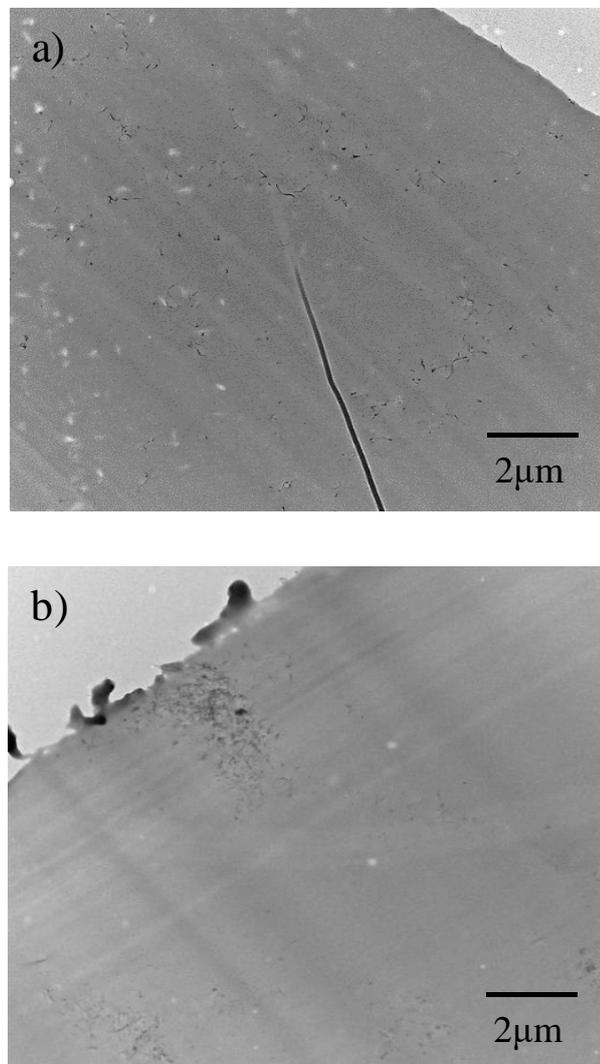
Figure 4.32: TEM micrographs of 0.03 wt.% CNT/epoxy specimens: a) mechanical stirring/sonication and b) ball milling.

Despite the increase of the CNT content to 0.1 wt.%, there are still areas free of CNT reinforcement across the specimen. When sonication is used as either a standalone dispersion method or in combination with mechanical stirring, dispersion seems relatively uniform (Figure 4.33a and b). On the contrary, a few aggregates are observed for the case of ball milling, indicating inhomogeneous dispersion (Figure 4.33c).
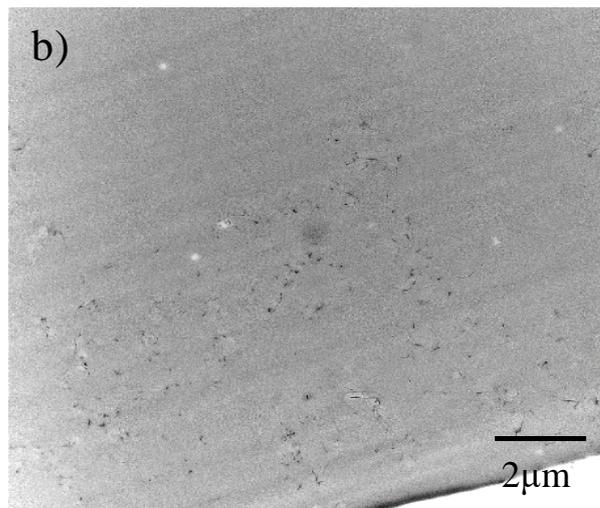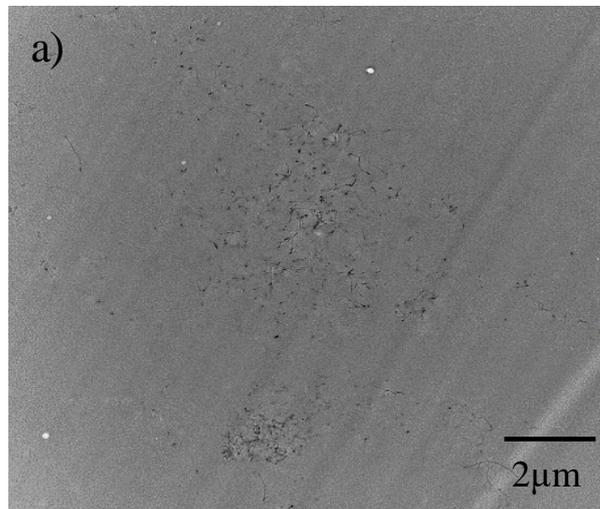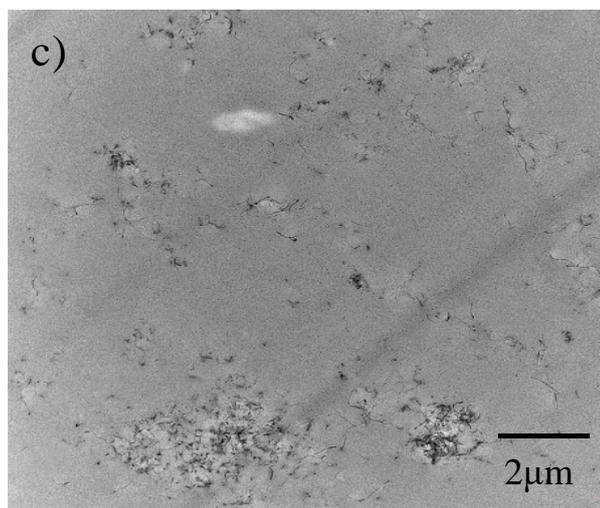
Figure 4.33: TEM micrographs of 0.1 wt.% CNT/epoxy specimens: a) sonication, b) mechanical stirring/sonication and c) ball milling.

The TEM micrographs for 0.3 wt.% CNT/epoxy composites are shown in the following figures. For the case of sonication (Figure 4.34a), CNTs are distributed quite uniformly however, few CNT clusters are also formed. Similar observations are made for the other two cases (Figure 4.34b and c). Another common characteristic of these three images is the existence of CNT free areas in spite of the increased amount of CNTs added to the epoxy resin. In Figure 4.34c, a big bubble surrounded by CNT aggregates can be seen. This is also observed for greater CNT loadings and it is due to the large number of air bubbles created during ball milling. The degassing process revealed that a very large amount of air was introduced to the CNT/epoxy mixture, which was foaming profoundly after ball milling process.
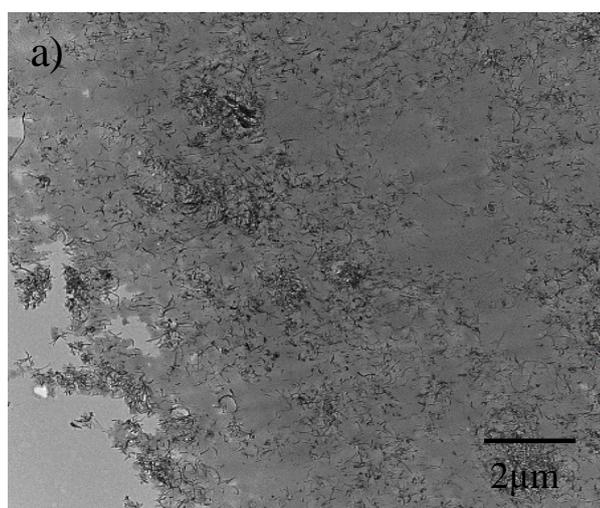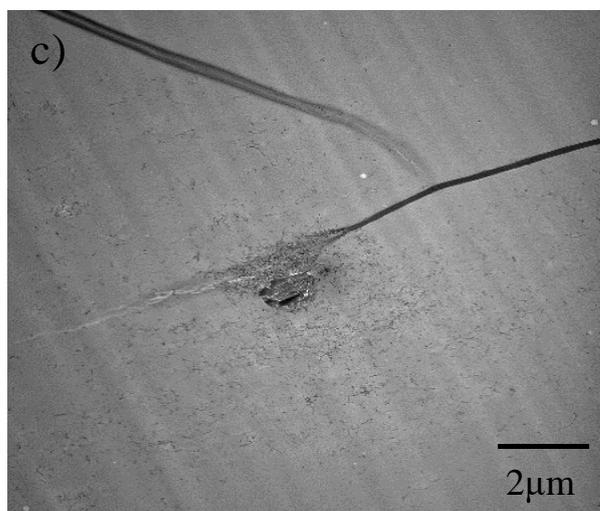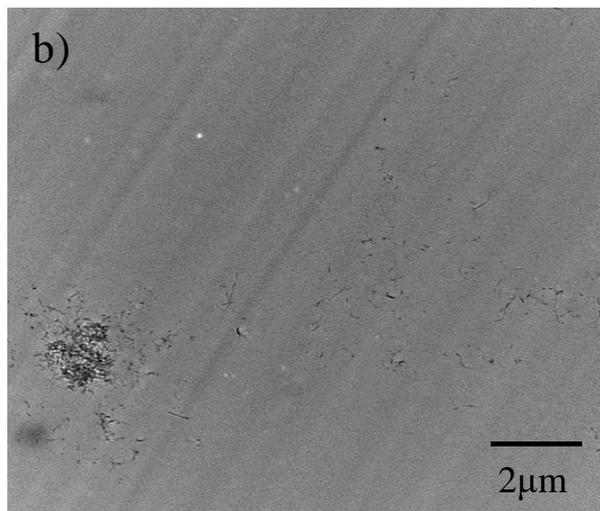
Figure 4.34: TEM micrographs of 0.3 wt.% CNT/epoxy specimens: a) sonication, b) mechanical stirring/sonication and c) ball milling.

The following figures show that the severity of agglomeration increases with the CNT weight fraction. The smallest amount of aggregates is observed for the case of sonication (Figure 4.35a). When mechanical stirring prior to sonication is used, the number of agglomerates increases, but CNTs cover almost the entire surface of the sample (Figure 4.35b). Although CNTs are dispersed quite uniformly, there are still areas free of CNTs, a phenomenon that is more apparent when ball milling is utilised. Large areas of CNT bundles can be seen in Figure 4.35c.
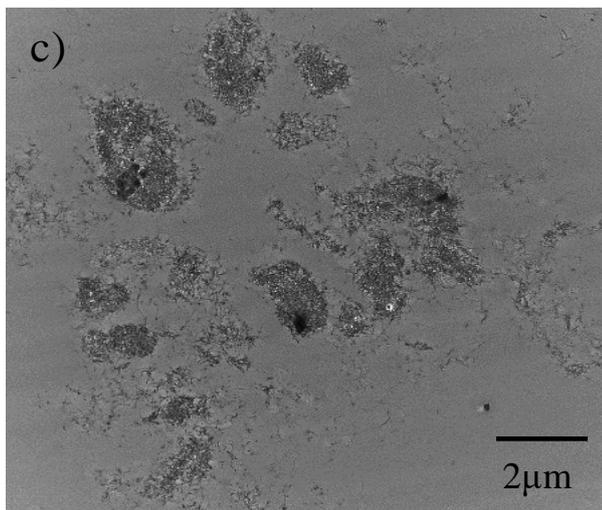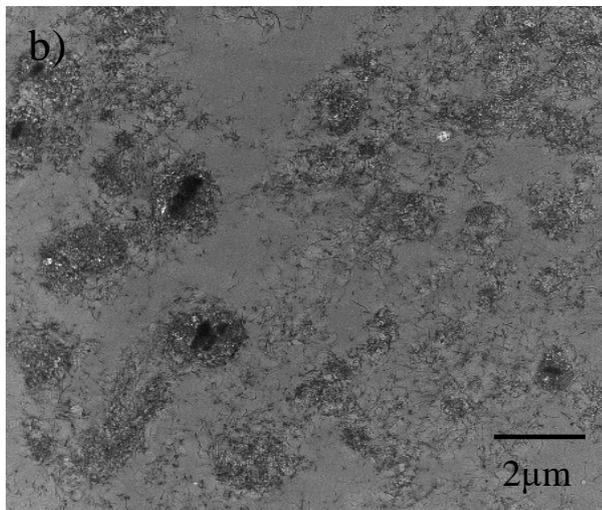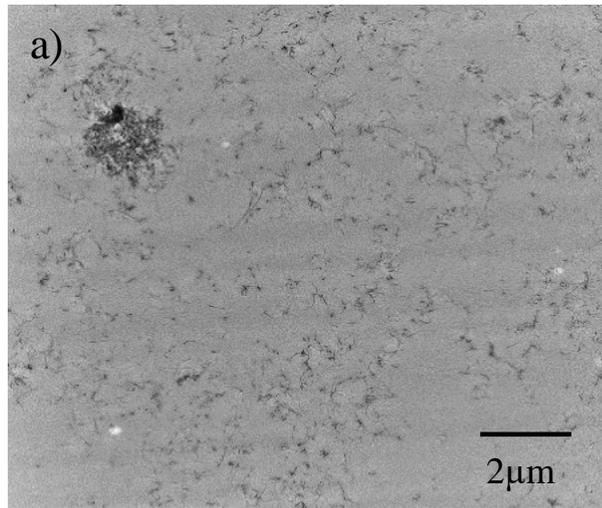
Figure 4.35: TEM micrographs of 0.5 wt.% CNT specimens: a) sonication, b) mechanical stirring/sonication and c) ball milling.

The maximum CNT weight fraction under investigation is 1% and due to the increased amount of CNTs added to the epoxy resin, there is a noteworthy increase of the size of the

agglomerates whose diameter is up to 2μm. However, sonication seems to have an advantage over ball milling, since the CNTs are more uniformly distributed along the length and width of the samples leaving very few areas free of nanofillers (Figure 4.36a and b).
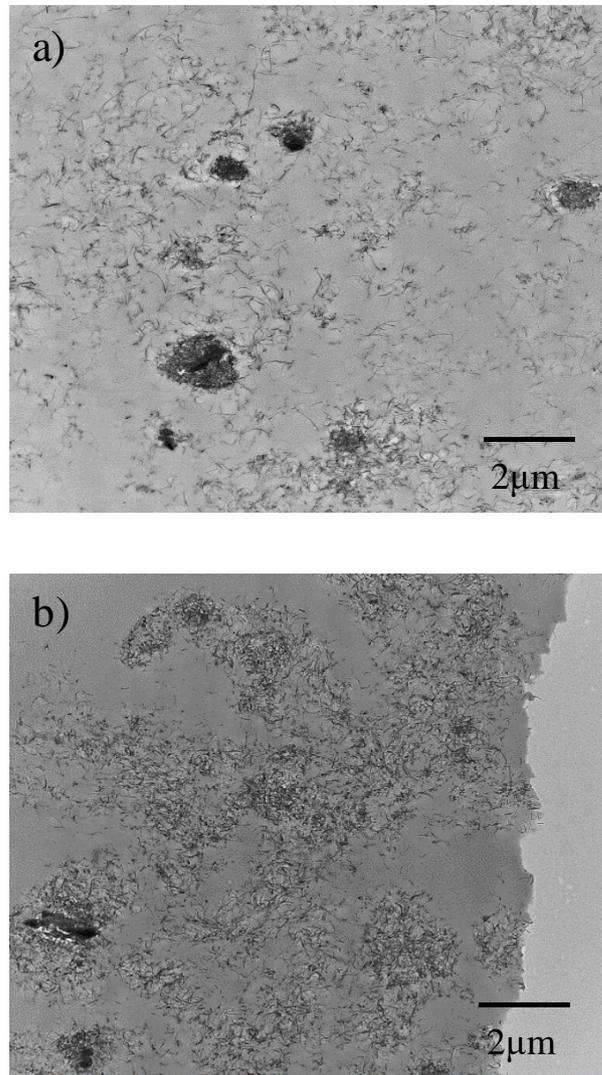
Figure 4.36: TEM micrographs of 1 wt.% CNT/epoxy specimens: a) sonication and b) ball milling.

4.8.2 Fracture Behaviour Assessment

TEM was also employed in order to investigate the fracture behaviour of the nanocomposites. By observing the cross section of the fracture surfaces of the samples, it is found that some of the CNTs, are protruding out of the plane corroborating the pull-out toughening mechanism, as illustrated in Figure 4.37.
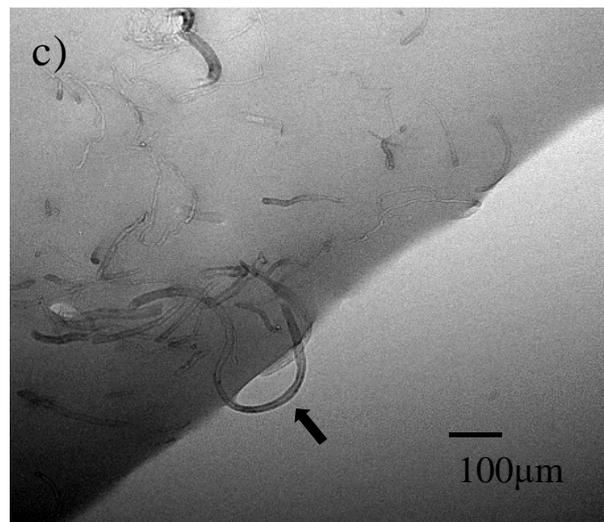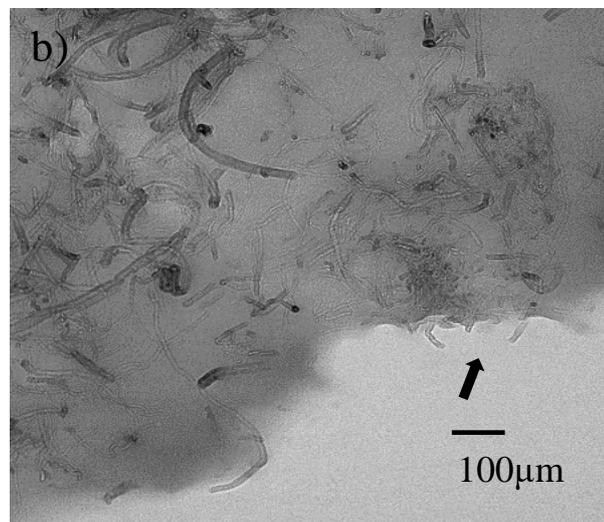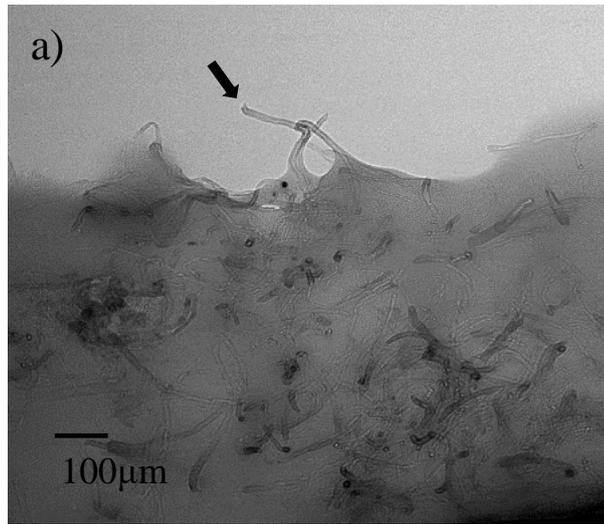
Figure 4.37: TEM on the fracture surfaces of CNT/epoxy specimens: a) 0.03 wt.%, b) 0.3 wt.% and c) 0.5 wt.% (sonication time=15 min).

The failure surfaces of the nanocomposites, also observed via SEM (Figure 4.38), are found to be rougher when CNTs are added into the epoxy matrix, whereas the areas free of CNTs are relatively smooth.
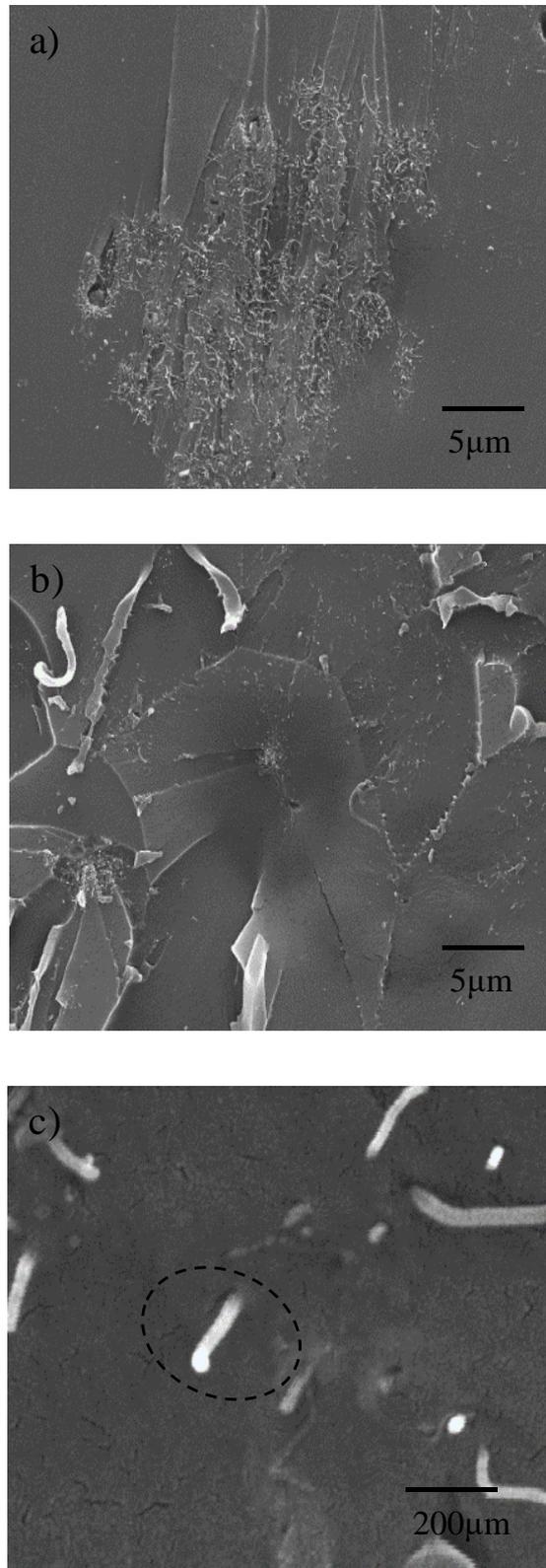
Figure 4.38: SEM image of the fracture surface of: a) 0.3 wt.%, b) 0.5 wt.% and c) 0.5 wt.% (pull-out) CNT/epoxy specimens after sonication.

The difference in the surface roughness suggests different fracture pathways (Figure 4.38a and b). As in the TEM microphotographs, the pull-out of CNTs is also verified from the SEM images. A close up view of this toughening mechanism is given Figure 4.38c and suggests weak interfacial bonding between the CNTs and the epoxy resin.

In spite of the agglomerated areas found in all samples, the energy dissipation mechanisms observed after the close examination of the fracture surfaces can explain the enhancement of fracture toughness for the case of 1wt.%. However, the phenomenon of agglomeration has an adverse effect on the tensile and flexural strength preventing CNTs from transferring their exceptional properties to the reinforced epoxy.

4.9 Differential Scanning Calorimetry

Electron microscopy methods can only provide information on the sample surface and in effect they are only representative for the selected fields of view [100]. Therefore, the overall dispersion along the whole specimen cannot be evaluated.

Differential scanning calorimetry (DSC) is the most widely used technique to monitor the cure kinetics of CNT reinforced epoxy composites. In the literature, it has been reported that CNTs can alter the cure reaction and hence, affect the total heat of reaction. Due to the correlation of the total heat of reaction with the state of CNT dispersion in the matrix, this method was also used in this study as an additional dispersion assessment technique. The main advantage of this method is that it takes the whole volume of the specimen into account.

The Perkin Elmer simultaneous thermal analyser (STA6000), which can acquire both DSC (differential scanning calorimetry) and TGA (thermogravimetric analysis) results in a single run, was used. The effect of the CNT addition on the kinetic transition (e.g. total heat of reaction and peak temperature) and glass transition temperature (T_g) of epoxy resin was studied by dynamic DSC scans.

After the fabrication of the nanocomposites, uncured specimens of an average mass of 15mg were tested using the STA6000 in nitrogen environment with a purge rate of 40mL/min. The cure reaction of the samples occurred in a crucible during the analysis. Due the fact that the DSC apparatus consisted of only one furnace, the empty crucible had to be tested first in order to obtain the baseline and then, subtract it from the values acquired after the MWCNT/epoxy sample had been tested. The experimental method used for the uncured specimens is the following:

1. Heat from 30ºC to 200ºC at 10ºC/min
2. Cool down to room temperature

The specimens were heated up to an elevated temperature and scanned at a slow rate in order to attain better resolution of the transition, i.e. cross-linking. Finally, the cured samples were re-tested under the same conditions in order to verify maximum cure and determine the glass transition temperature.

4.9.1 Cure Kinetics Assessment

The evaluation of the effect of CNTs, dispersed using sonication, on the cure kinetics of epoxy resin was performed via a non-isothermal DSC scan. The heat changes that occur during the cross-linking of uncured MWCNT/epoxy samples of different CNT loadings are shown in Figure 4.39. The curing process of all samples irrespective of the CNT content is represented by an exothermic event (large peak) during which energy is expelled by the material in order to polymerise. The initial T_g cannot be observed in this graph, because the tests start at 30ºC. At the completion of curing, the DSC heat flow returns to a quasilinear response. The area under the exothermic peak is integrated to give the total heat of cure using the Pyris software.
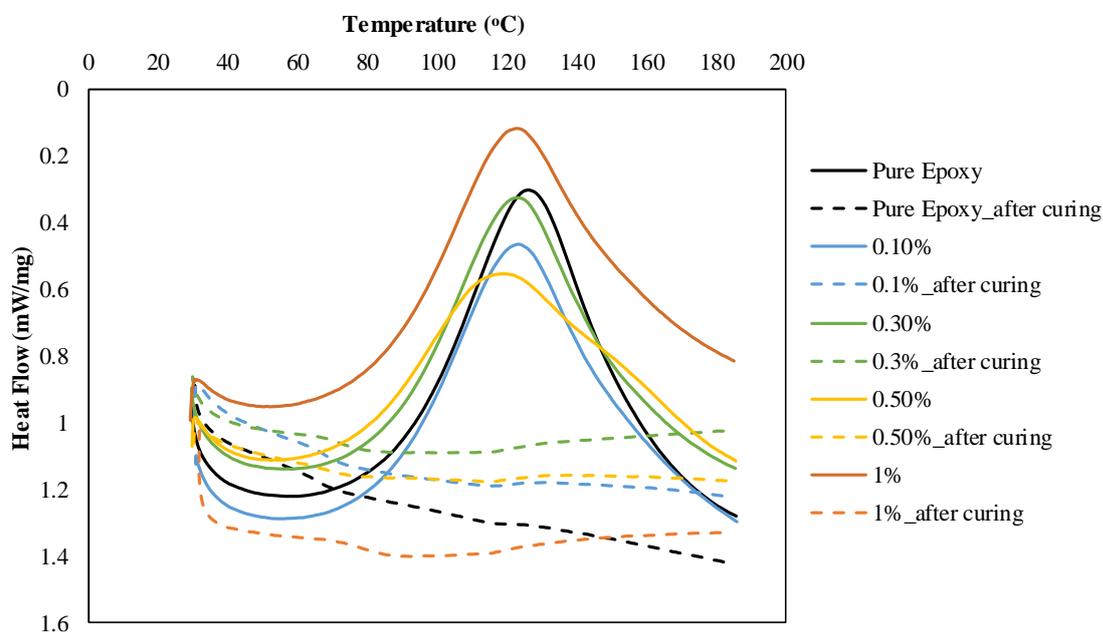
Figure 4.39: Cure profile of CNT reinforced epoxy and pure epoxy resin samples.

Table 4.5 shows the total heat of reaction and the peak cure temperature for all MWCNT/epoxy composites, which apart from the cure behaviour; they provide additional insight to the degree of dispersion of the samples.

CNT Concentration (wt.%)	Total Heat of Cure (J/g)	Peak Cure Temperature (ºC)
0	233.103	126.36
0.1	216.901	124.81
0.3	202.365	122.91
0.5	212.964	126.27
1	219.600	125.97

Table 4.5: Heat of cure and peak cure temperature.

The total heat of cure and peak cure temperature are also plotted in Figure 4.40. The decrease of the total heat of reaction for 0.1 and 0.3 wt.% CNT loadings can be attributed to the individual CNTs that act as hindrance to the cross-linking reaction. The higher the CNT loading the lower the heat of reaction [123].
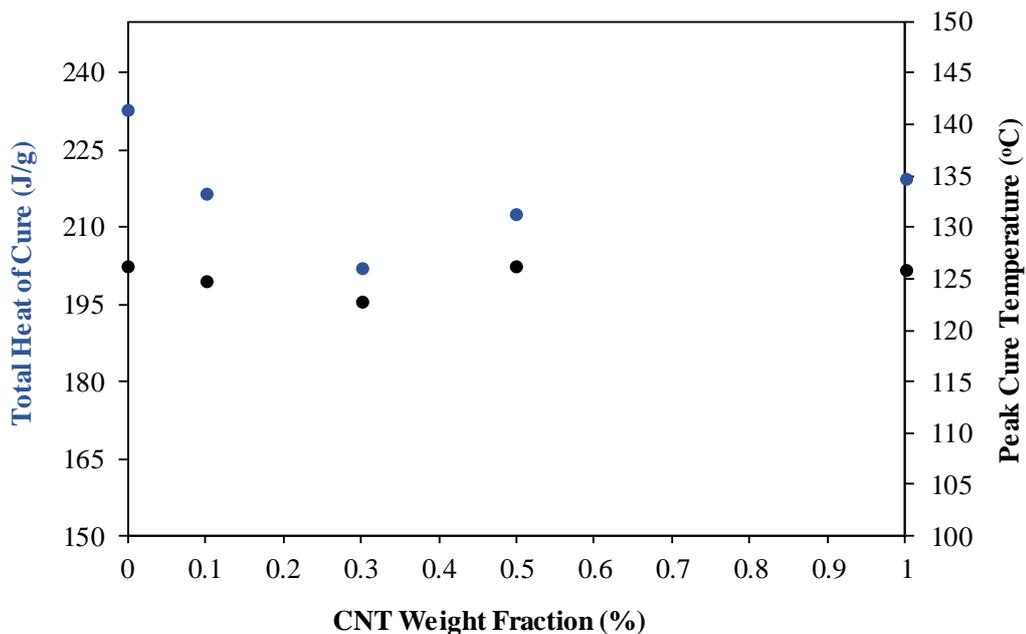
Figure 4.40: Heat of cure and peak cure temperature versus temperature.

Further increase of the CNT content to 0.5 and 1 wt.% has an adverse effect on the total heat of cure. Aggregated CNTs are much less efficient in blocking the chemical reactions, so higher values for the total heat of reaction are obtained. It can be therefore concluded that the most homogeneous dispersion is achieved for 0.3 wt.% CNT content, whereas the addition of 1 wt.% of CNTs in the matrix leads to the increase of agglomerates and hence, poor dispersion.

A shift of the exothermic reaction peak to lower temperatures is also observed after the incorporation of CNTs in the epoxy resin (Figure 4.39). This suggests that MWCNTs act as catalysts and accelerate the cure reaction [121]. The dotted lines in Figure 4.39 stand for the second scan that was performed for all samples in order to verify maximum cure. As the thermosetting resin cures, the heat of cure decreases. Therefore, the absence of exothermic peaks denotes that the samples are fully cured. In reality, the resin may still have some lingering residual cure [140].

Finally, the T_g values are found to be in the range of 60°C to 65°C for all nanocomposites and the pure epoxy resin samples, indicating that the samples are equally cured [125]. The addition of nanotubes does not affect significantly the glass transition temperature suggesting that although CNTs accelerate the cure reaction, they do not alter the overall degree of cure [119].

4.10 Conclusions

Two epoxy resin systems were investigated, namely TW and RS. For the case of TW epoxy resin, increase of the CNT content beyond 0.03 wt.% leads to significant reduction of the properties in spite of the increase of sonication time from 15min to 30min. On the other hand, the critical loading shifts from 0.03 wt.% to 0.3 wt.% when CNTs are added in the RS epoxy resin, after which the tensile and flexural strengths decrease. This is due to inhomogeneous dispersion and air bubbles acting as crack initiation sites.

In summary, none of the properties studied improve with the addition of MWCNTs to either epoxy resin system used. On the contrary, for specific dispersion methods and high MWCNT weight fractions (> 0.3%), the mechanical properties degrade.

Marginal improvement [7, 132] or even decrease [133] in the mechanical properties of nanocomposites after small additions of CNTs into the matrix has been also reported in the literature. The main reasons for the unsuccessful transfer of the exceptional properties of the CNTs to the matrix are poor: a) dispersion of the nanofillers and b) filler/matrix interfacial adhesion. In order to tackle the dispersion issue, calendering could be used as an alternative, since better results have been reported when this method is utilised [7]. The CNT/matrix interfacial adhesion can be addressed through functionalisation, i.e. oxidative treatment of the CNTs, which has been seen to result in stronger CNT/matrix interface [90].

Chapter 5. Metal-to-Metal Joints

5.1 Introduction

In the previous chapter, MWCNT/epoxy composites were characterised in order to gain in depth understanding of how parameters, such as CNT loading and dispersion method affect their mechanical performance. In this chapter, the MWCNT reinforced epoxy resin is used as adhesive in order to bond metal-to-metal, namely Steel/Steel and Aluminium/Aluminium single lap joints aiming at the improvement of the joint strength. Different substrate surface preparation methods are also investigated in order to optimise the adhesion between the substrates and the epoxy resin.

5.2 Materials

Steel and aluminium substrates are used for the joint fabrication. The metal substrates, which are machined from steel (mild) and aluminium plates, are initially tested under tension and 3-point bending, so as to obtain their mechanical properties (Table 5.1).

Metal Substrates	Young's Modulus (GPa)	Yield Stress (MPa)	Tensile Strength (MPa)	Flexural Strength (MPa)
Steel (for rail industry)	201	300	357	625
Aluminium (alloy 5061)	70	265	308	522

Table 5.1: Mechanical properties of metal substrates.

5.3 Substrate Surface Preparation Methods

Substrate surface preparation is one of the most critical steps for the manufacturing of adhesively bonded joints. The existing oxide layer of the metal specimens must be removed and replaced by a stable oxide layer, which is chemically compatible with the adhesive and free of corrosion products and other surface contaminants, such as grease. In this way, good interfacial strength between the metal substrates and the adhesive is achieved resulting in the realisation of durable joints.

The substrate surface preparation methods can be classified in three general categories:
- mechanical abrasion
- use of solvents
- chemical treatments

In this study, abrasion with sandpaper, linishing (belt sanding), sand blasting and grit blasting are the methods utilised for the steel substrates, whereas the aluminium substrates are roughened using either sandpaper or grit blasting. The aluminium substrates are also subjected to chemical and electrochemical treatments, i.e. forest products laboratory etching (FPL) and phosphoric acid anodising (PAA).

Prior to the application of the chemical treatments, a series of tests were required in order to determine the sufficient duration of each process that would modify the oxide layer and provide a certain degree of texturing of the surfaces for mechanical interlocking between the adhesive and the adherend.

5.3.1 FPL/PAA Characterisation

The surface preparation of the aluminium samples involves the pre-treatment via the forest products laboratory (FPL) process, which consists of two steps: a) degreasing with the use of an alkaline cleaner and b) etching in a $K_2Cr_2O_7$: H_2SO_4 solution. After thorough rinse, the aluminium specimens are anodised in an aqueous solution of H_3PO_4. The FPL/PAA process is described in Figure 5.1.
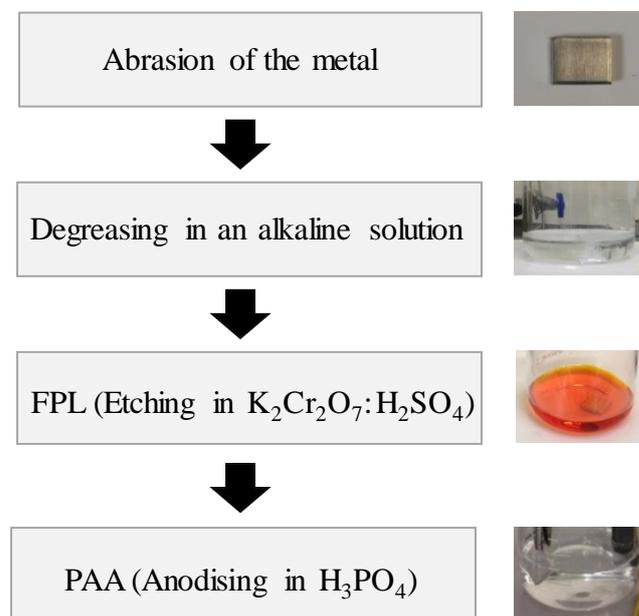
Figure 5.1: Chemical treatment of aluminium substrates.

For the first part of the chemical treatment characterisation, both processes are used as standalone methods in order to establish the optimal duration for each one. The substrate surface preparation, i.e. mechanical abrasion and alkaline degreasing is performed according to the cleaning and surface preparation standard (method O) [141] and is always applied prior to either of the chemical treatments. All methods employed are described below:

1. *Mechanical abrasion*: Firstly, the aluminium substrate is abraded using sandpaper of fine grit; 220 and then, 400. The coarse debris is removed with water jet followed by the application of acetone-impregnated wipes to remove fine debris.

2. *Alkaline degreasing*: Pre-treated as in 1 and then, the aluminium surface is dried and degreased using an alkaline solution to remove the existing oxide layer. The immersion of the sample in 40g/L NaOH solution lasts for 2min at 60°C. It is subsequently removed and rinsed in de-ionised water.

3. *FPL treatment*: Pre-treated as in 2 and the sample is then submerged in de-ionised water solution with 330ml/l sulphuric acid (95-98% v/v) and 50g/l potassium dichromate. The duration of FPL process is in the range of 15min to 40min at 60°C. The samples are finally rinsed thoroughly in de-ionised water and left to dry.

4. *PAA treatment*: Pre-treated as in 2 and followed by the PAA process [142]. The aluminium sample, which is one of the two electrodes, is anodised in a water solution with phosphoric acid (85% v/v) at 10V under direct current (current≈ 2A) using a graphite rod as the second electrode. During anodising (Figure 5.2), the electrical current causes oxygen to be released at the anode, which reacts with the aluminium to form the aluminium oxide, the so-called anodic film. The immersion time in the anodising tank determines the thickness of the anodic film.
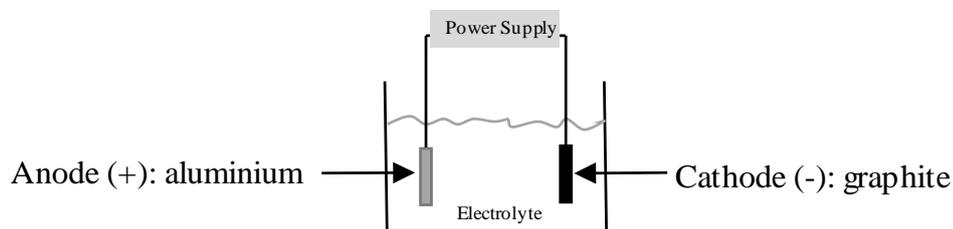
Figure 5.2: Anodising process.

In our study, the electrical current is passing from the anode to the cathode for 15min to 30min at room temperature. At the end of the anodising process the aluminium sample is removed from the tank and rinsed thoroughly in tap water. Finally, it is placed in an oven at 40-60°C to dry.

A summary of the immersion time durations investigated for each process is shown in Table 5.2.

Treatment	Immersion Time (min)			
FPL	15	25	30	40
PAA	15	25	30	-

Table 5.2: Immersion time for etching and anodising processes.

Optical microscopy (OM) and scanning electron microscopy (SEM) have been used to examine the aluminium surfaces after the application of the aforementioned methods. The images obtained are shown below.

FPL Etching

After 15min of etching, the oxide layer formed on the aluminium surface exhibits very low porosity (Figure 5.3a and Figure 5.4a). There are also many areas free of pores on the sample surface in contrast to the case of 25min, for which the most homogeneous porosity distribution is achieved (Figure 5.3b and Figure 5.4b).
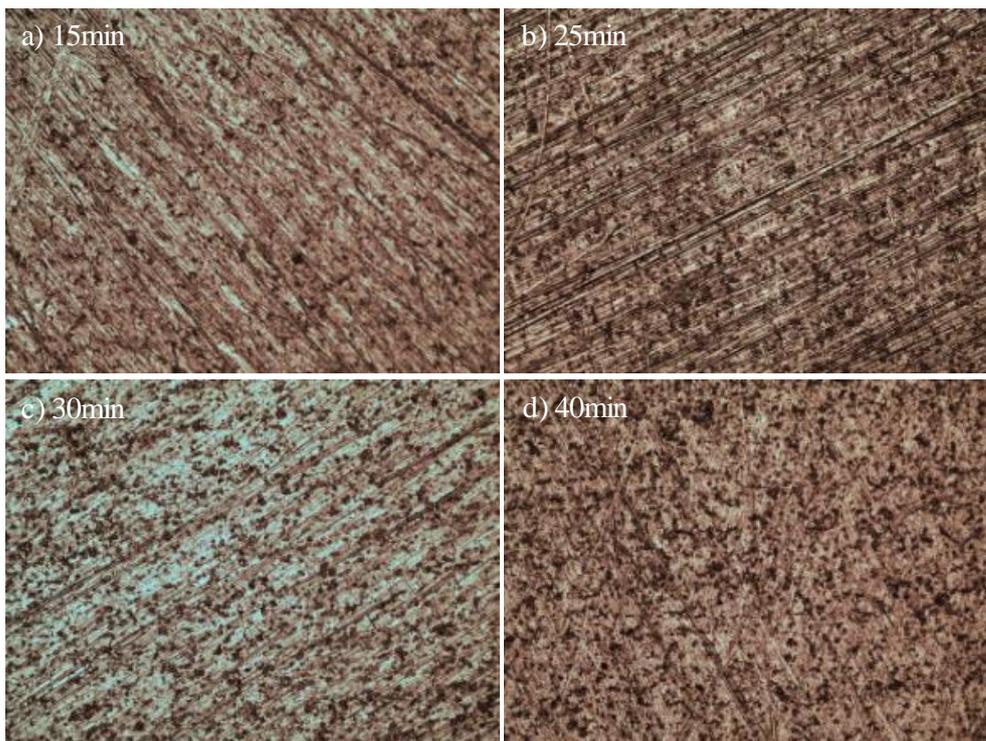
Figure 5.3: Aluminium surfaces after: a) 15min, b) 25min, c) 30min and d) 40min of etching (OM - 10x).

After 30min and 40min of etching, the pore diameter increases and the porosity formation becomes denser (Figure 5.3c & d and Figure 5.4c & d).
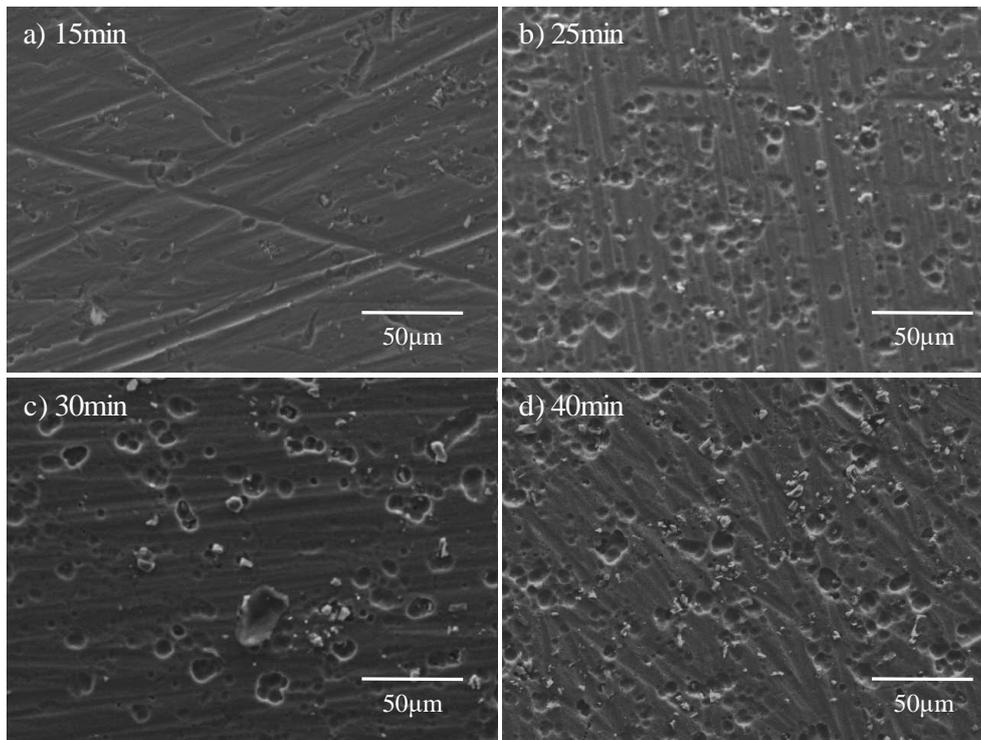
Figure 5.4: Aluminium surfaces after: a) 15min, b) 25min, c) 30min and d) 40min of etching (SEM - 500x).

PAA

The oxide layer formed after 15min of anodising is of low porosity (Figure 5.5a and Figure 5.6a), which increases after the anodising time is extended to 25min (Figure 5.5b and Figure 5.6b). However, the porosity of the oxide layer becomes much denser for the case of 30min with a pore diameter greater than in the other two cases (Figure 5.5c).

Figure 5.5: Aluminium surfaces after: a) 15min, b) 25min and c) 30min of anodising (OM - 10x).
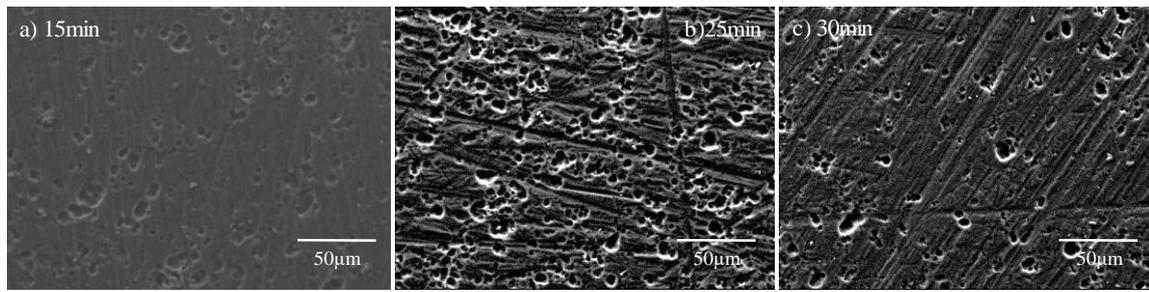
Figure 5.6: Aluminium surfaces after: a) 15min, b) 25min and c) 30min of anodising (SEM - 500x).

Etching (FPL)-Anodising (PAA)

The two treatments are superimposed in order to deposit a porous and stable oxide layer on the substrate (anodising) on top of the oxide layer formed after etching. After close examination of the images obtained from OM and SEM, four case studies have been investigated aiming to identify the effect of PAA process on the aluminium surfaces while keeping the etching time constant (Table 5.3).

Process	Sample 1	Sample 2	Sample 3	Sample 4
Etching	25 min	25 min	40 min	40 min
Anodising	15 min	30 min	15 min	30 min

Table 5.3: Time durations for etching and anodising.

According to the immersion time selected for each pre-treatment, the aluminium samples are firstly immersed in an alkaline cleaner and then, the FPL and PAA processes follow.

When FPL is 25min and PAA is 30min, the pore distribution on the oxide layer is relatively uniform (Figure 5.7b and Figure 5.8b). However, when PAA reduces to 15min, the pore formation is less intense with many areas of minimal porosity (Figure 5.7a and Figure 5.8a).
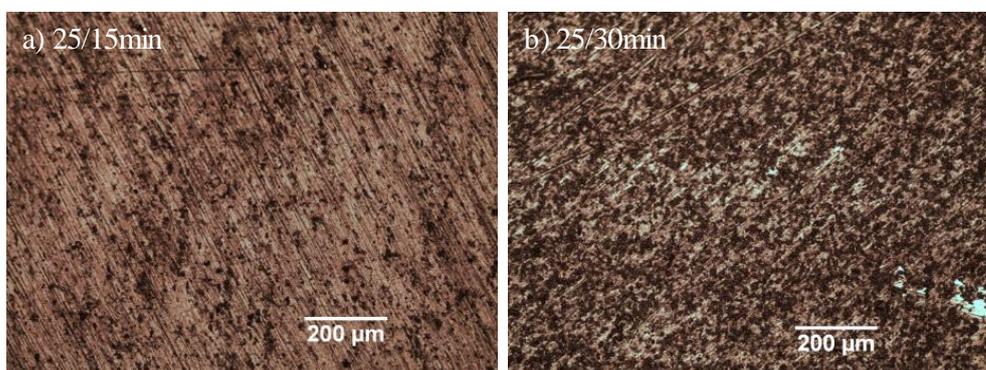
Figure 5.7: Aluminium surfaces after etching and anodising: a) 25min/15min and b) 25min/30min (OM - 10x).
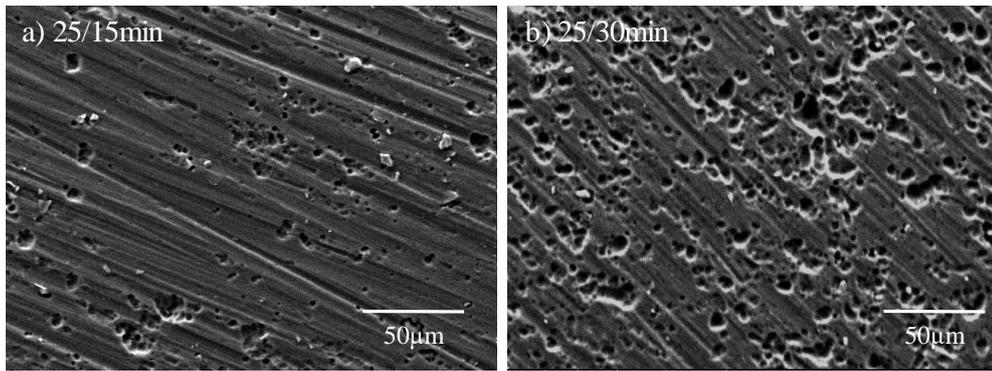
Figure 5.8: Aluminium surfaces after etching and anodising: a) 25min/15min and b) 25min/30min (SEM - 500x).

After 40min of etching and irrespective of the immersion time of PAA process, both oxide layers look quite similar suggesting that the duration of etching process is the one that determines the degree of porosity of the oxide layer (Figure 5.9 and Figure 5.10).
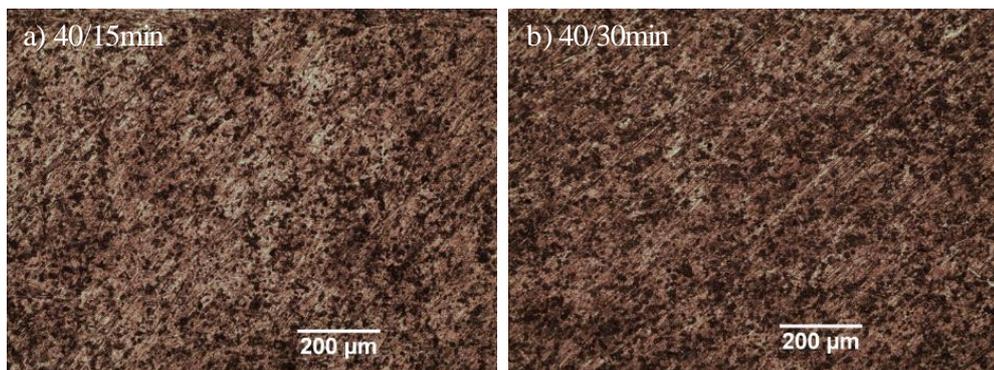
Figure 5.9: Aluminium surfaces after etching and anodising: a) 40min/15min and b) 40min/30min (OM - 10x).
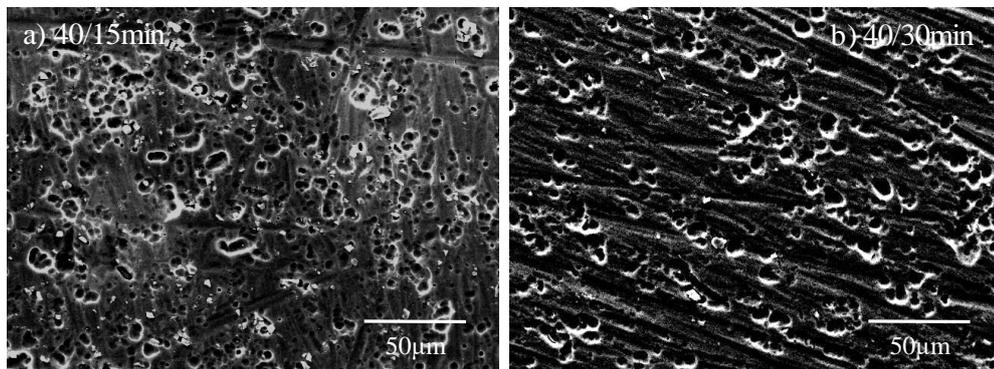
Figure 5.10: Aluminium surfaces after etching and anodising: a) 40min/15min and b) 40min/30min (SEM - 500x).

The characterisation of the aluminium surfaces described above aimed to determine the immersion time for each process, so as to obtain surfaces with homogeneous and porous oxide layers suitable for mechanical interlocking. Therefore, 25min of etching followed by 25min of anodising are the selected immersion time durations, which have been employed for the surface preparation of the aluminium substrates immediately prior to bonding.

5.3.2 Surface Roughness Measurements

The Mitutoyo surface roughness measuring tester SJ-210 is used to measure the surface roughness of the metal substrates obtained after surface preparation (Figure 5.11).
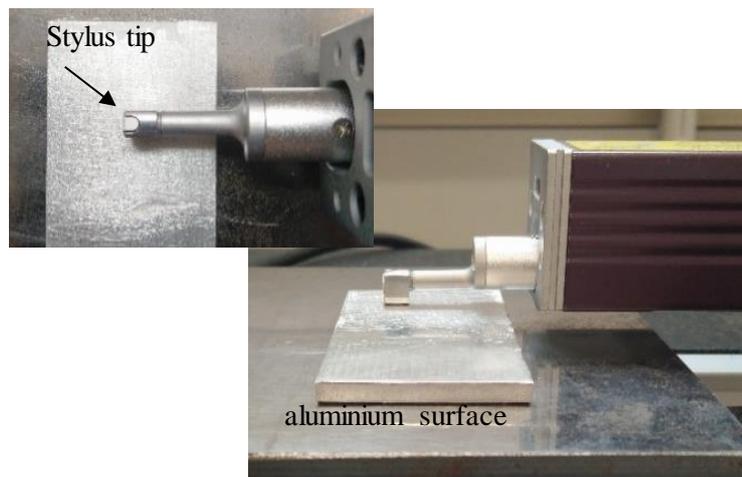
Figure 5.11: Surface roughness measurement.

Three measurements are taken per sample using the stylus tip of the tester and the average surface roughness is calculated in *μm* (Table 5.4).

Preparation Method	Steel	Aluminium
Sandpaper	1.113	1.302
Linishing	1.345	-
Sand blasting	0.932	2.781
Grit blasting	5.884	7.877
Etching/Anodising	-	0.969

Table 5.4: Surface roughness of metal substrates.

5.4 Single Lap Joint Manufacturing

The surface preparation of the metal substrates is followed by acetone degreasing in order to remove any contamination that could deteriorate the quality of the bond. The adhesive is then applied on one substrate and the other substrate is placed on top. A simple mould and weight configuration is used for each single lap joint in order to maintain alignment and control the adhesive thickness within the range of 0.3mm and 0.5mm (Figure 5.12).
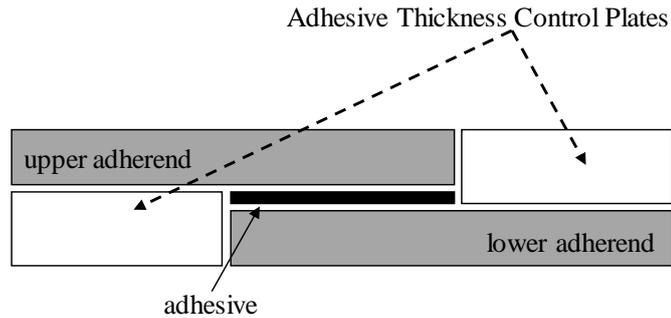
Figure 5.12: SLJ mould configuration.

The adhesive used for the joint manufacturing is MWCNT reinforced epoxy of 0.1, 0.3 and 0.5 wt.%, which has been manufactured as described in Chapter 4. Pure epoxy resin adhesive is also utilised in order to obtain the benchmark single lap joints. All specimens are cured at room temperature for 24h and post-cured at 50°C for 15h.

5.5 Lap Shear Tests

Lap shear tests are conducted at constant crosshead speed of 1mm/min [143]. A single lap joint with 25mm x 25mm overlap length is shown in Figure 5.13.
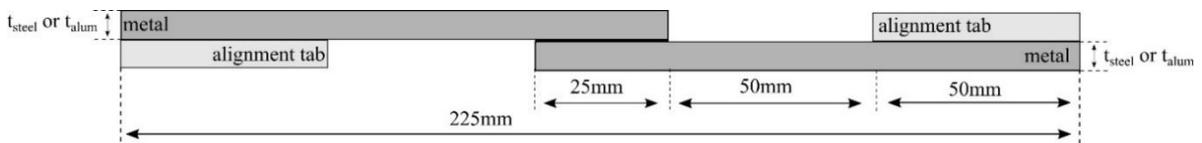
Figure 5.13: Metal-to-metal single lap joint configuration.

The dimensions of the metal substrates are shown in Table 5.5.

Metal Substrates	Width (mm)	Thickness (mm)	Length (mm)
Steel (thin)	25	2.37	125
Steel (thick)	25	6	125
Aluminium	25	3.5	125

Table 5.5: Dimensions of metal substrates.

Finally, in order to ensure symmetric loading, inserts with thickness equal to the sum of the adhesive and adherend thickness are used within the clamps (Figure 5.14).
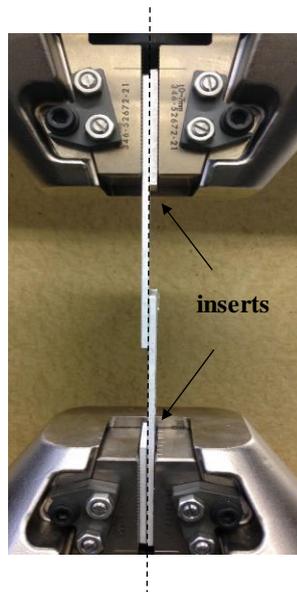
Figure 5.14: Lap shear test.

The reported test values in this work are an average of four measurements. The failure modes have been determined by visual inspection.

5.6 Results and Discussion

5.6.1 Steel-to-Steel Single Lap Joints

The single lap joint strengths for the different surface preparation methods applied to the steel substrates prior to bonding with pure epoxy resin are compared in Figure 5.15.
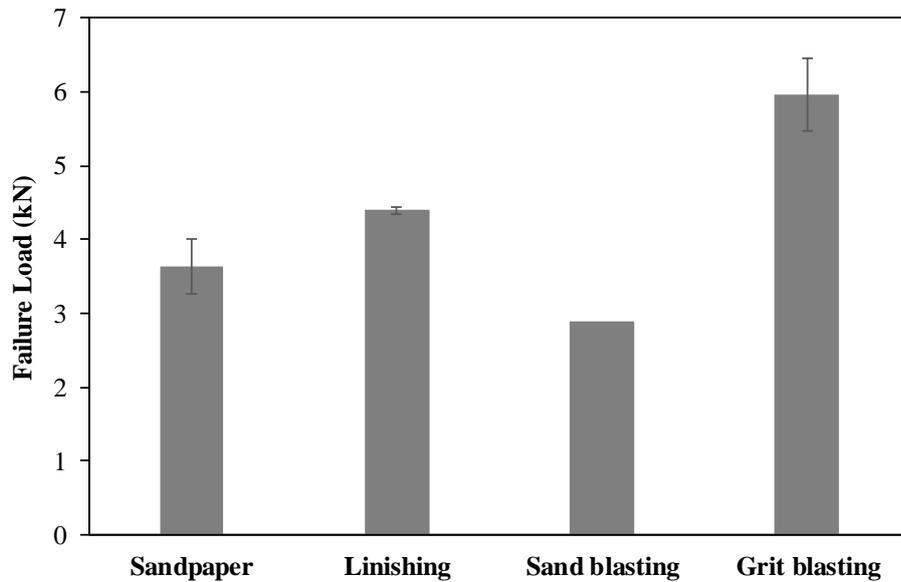
Figure 5.15: Failure load of Steel/Steel SLJs versus substrate surface preparation methods.

The maximum joint strength is obtained for the grit blasted single lap joints, whereas sand blasting gives the lowest strength. The adhesion between the substrate and the adhesive is therefore optimised when rough surface finish is achieved . The results are also in accordance with the surface roughness test measurements shown in Table 5.4.

Since the optimum adhesion between the adherend and the adhesive is obtained with grit blasting, this is the surface preparation method also utilised for the bonding of Steel/Steel joints with MWCNT reinforced epoxy adhesive. In Figure 5.16, the effect of the CNT addition in the epoxy resin adhesive in relation to the failure load is shown.
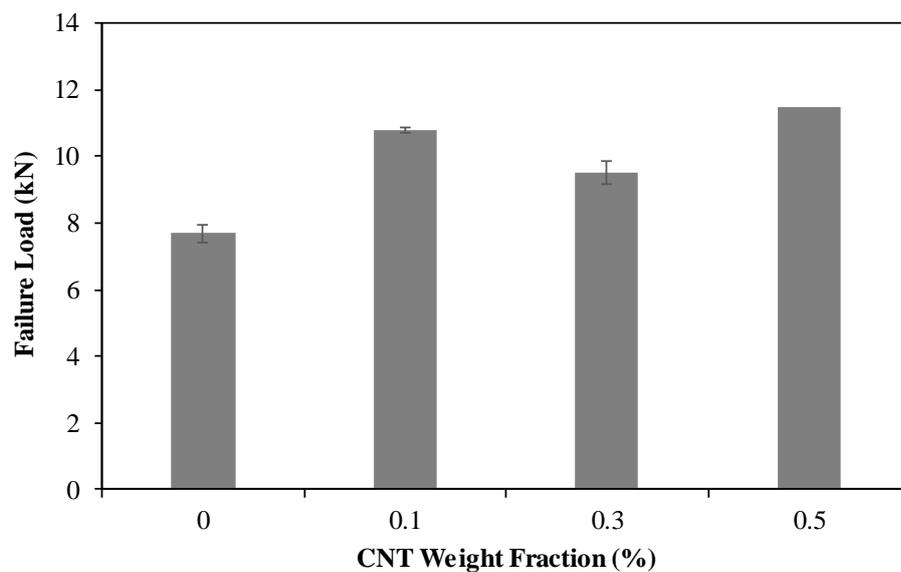
Figure 5.16: Failure load of Steel/Steel SLJs versus CNT weight fraction (grit blasting).

The joint strength significantly increases with the increase of the CNT loading of the epoxy adhesive. In order to further investigate the CNT effect and factor out the influence of possible non-linear deformation of the adherends, Steel/Steel single lap joints with 6mm thickness have been also tested (TAST). The thick metal adherends do not experience extended plastic deformation and therefore, the full capacity of the adhesive can be utilised[2].

The beneficial effect of MWCNTs on the joint performance of thick Steel/Steel single lap joints bonded with MWCNT reinforced epoxy adhesive is shown in Figure 5.17, where the joint strength is shown to increase by 20% for 0.1 and 0.3 wt.% and by 40% for 0.5 wt.%. For the 0.3 and 0.5 wt.% CNT loading cases, a similar increase of the joint strength to that shown in Figure 5.16 is obtained.
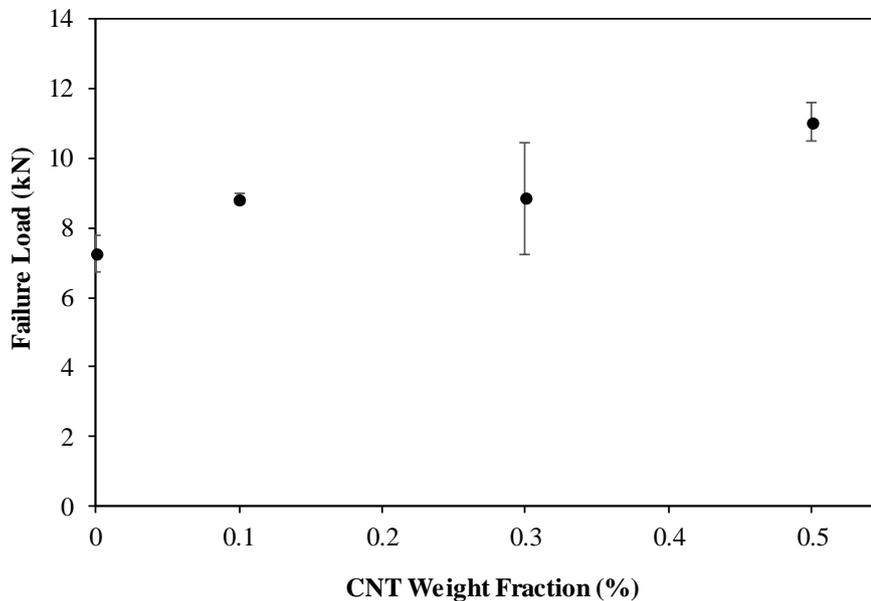
Figure 5.17: Failure load of thick Steel/Steel SLJs versus CNT weight fraction.

The large scatter shown for the case of 0.3 wt.% is attributed to problems encountered during the manufacturing of the joints.

5.6.2 Aluminium-to-Aluminium Single Lap Joints

Owing to the fact that the surface preparation of the substrates highly affects the joint strength, the impact of various surface preparation methods on the Aluminium/Aluminium single lap joints is also investigated. The aluminium surfaces have been subjected to grit blasting and etching/anodising. Aluminium/Aluminium joints with no surface preparation

---

[2] It has been shown [11, 14] that SLJs with metal adherends fail when their adherends start to deform plastically.

apart from simple surface roughening with sandpaper have been also manufactured and tested in order to obtain the control samples.

The failure load of Aluminium/Aluminium joints is plotted against the different surface preparation methods (Figure 5.18). When the only surface preparation method used is roughening with sandpaper, the joint strength is quite low and increases by 126% and 170% when either etching/anodising or grit blasting is used respectively.
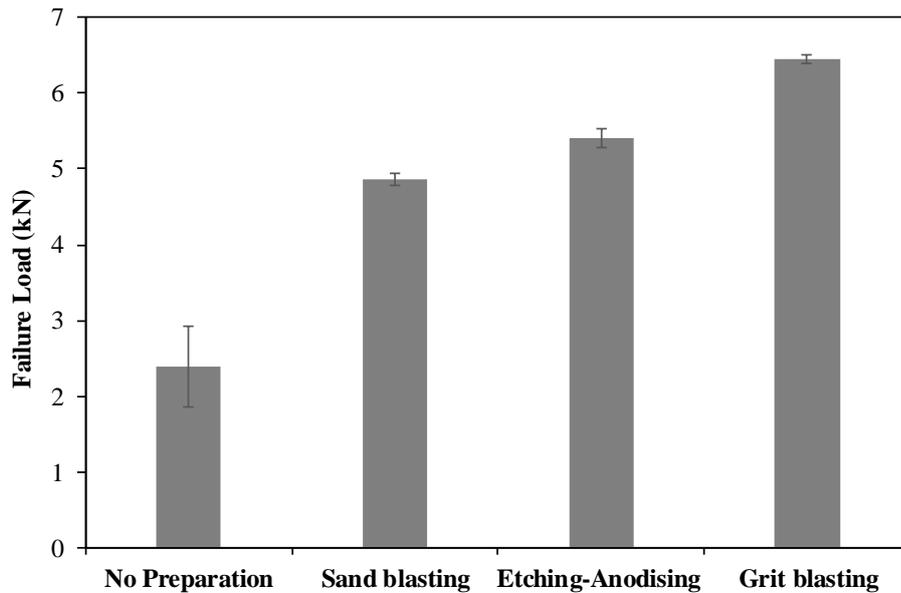
Figure 5.18: Failure load of Aluminium/Aluminium SLJs versus different substrate surface preparation methods.

The fracture surfaces of the Aluminium/Aluminium single lap joints subjected to chemical treatment and those with no surface preparation show an irregular pattern (Figure 5.19a and c). On the contrary, the fracture pattern is symmetric for the case of grit blasting (Figure 5.19b) indicating that there are no weak points along the overlap length and width with the crack initiating and propagating from both ends of the overlap.

Figure 5.19: Bonding area of Aluminium/Aluminium single lap joints after failure: a) no surface preparation, b) grit blasting and c) etching-anodising.

By employing the two aforementioned surface preparation methods, Aluminium/Aluminium single lap joints have been bonded with the MWCNT reinforced epoxy adhesive. The variation of the joint strength with the CNT content of the epoxy adhesive is plotted in Figure 5.20.
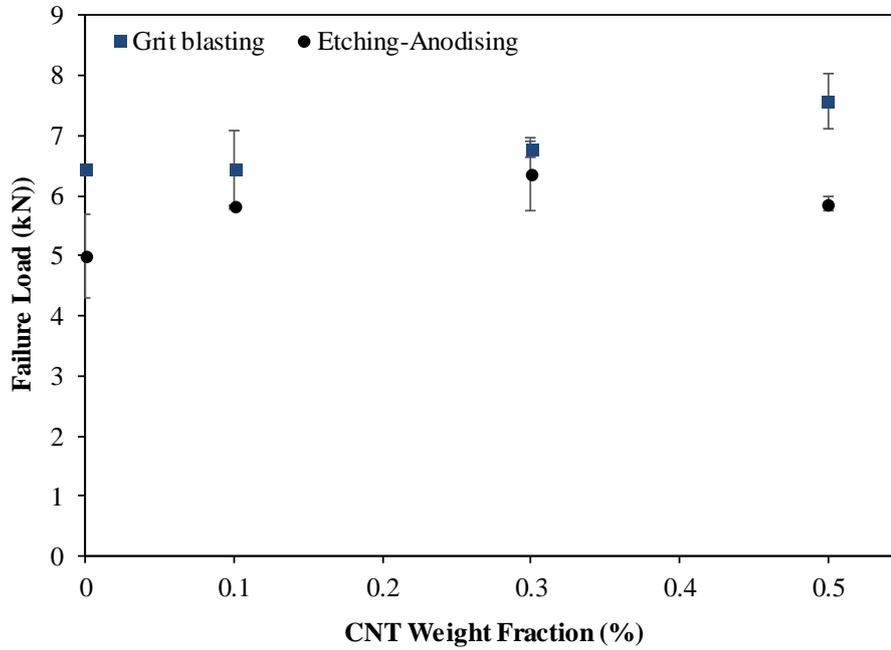
Figure 5.20: Failure load of Aluminium/Aluminium SLJs versus CNT weight fraction for two different substrate surface preparation methods.

It is evident that the dominating factor in defining the joint strength is the surface preparation method. Grit blasted single lap joints give up to 30% higher failure load values when compared to the chemically treated ones. The addition of CNTs in the epoxy resin adhesive has also a positive effect on the failure load of the Aluminium/Aluminium single joints for both surface preparation methods.

All joints fail close to the adhesive/adherend interface. The bonding area of the grit blasted single lap joints after failure is illustrated in Figure 5.21.
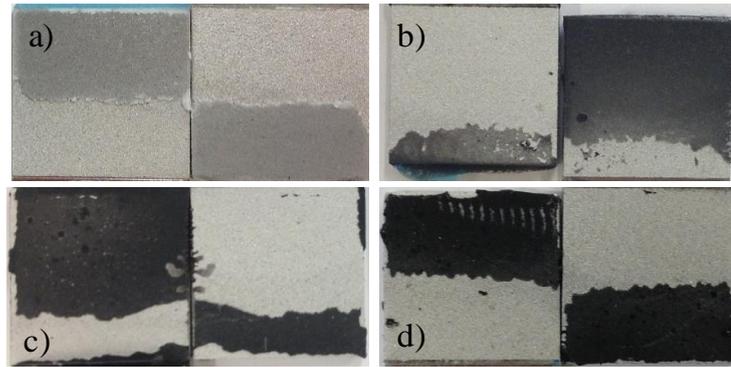
Figure 5.21: Bonding area of Aluminium/Aluminium single lap joints after failure: a) pure epoxy resin, b) 0.1 wt.%, c) 0.3 wt.% and 0.5 wt.% CNT epoxy adhesive (grit blasting).

5.7 Conclusions

The substrate surface preparation is found to be a significant parameter defining the joint strength. For both types of metal-to-metal joints, the highest load bearing capacity is obtained when grit blasting is utilised. Therefore, it is the method used for the next stage of our experimental work; the manufacturing of dissimilar material lap joints.

Despite the fact that the surface treatment is more prominent than the adhesive composition, the toughening effect of multi-wall carbon nanotubes has been also observed. For the grit blasted joints, the moderate increase of the joint strength with the increase of CNT weight fraction suggests that CNTs can positively affect the joint integrity via the increase in adhesive/adherend interfacial strength. However, this positive effect is only evident when the substrate surface preparation is optimised.

Chapter 6. Metal-to-Composite Joints

6.1 Introduction

The joint performance depends on a number of parameters, such as the overlap length, the adhesive and adherend properties, the adhesive and adherend thickness and the substrate surface preparation. This chapter is focused on the investigation of the first three parameters, namely the overlap length and the adhesive and adherend properties, while the rest remain constant. Four different materials are used as substrates: carbon fibre reinforced polymers (CFRP), glass fibre reinforced polymers (GFRP), aluminium and steel, which are bonded using the MWCNT reinforced epoxy of various weight fractions. The effect of the overlap length and CNT loading on the strength and fracture toughness of dissimilar material joints is evaluated.

6.2 Materials and Methods

Metal-to-composite single lap joints of three different overlap lengths, i.e. 25mm, 40mm and 60mm are bonded using the MWCNT reinforced epoxy adhesive. The metal substrates are cut from either 5061 aluminium alloy or mild steel (thin) plates. Woven glass and carbon fabric (290 gsm, plain weave) supplied by Easycomposites, are used for the fabrication of the composite substrates. The mechanical properties of both metal and composite substrates as obtained from mechanical testing are shown in Table 6.1.

Substrates	Young's Modulus (GPa)	Tensile Strength (MPa)	Yield Stress (MPa)	Flexural Strength (MPa)
Steel (for rail industry)	201	357	300	625
Aluminium (alloy 5061)	70	308	265	522
GFRP (V_f =45%)	21	432	-	162
CFRP (V_f =40%)	47	561	-	358

Table 6.1: Mechanical properties of substrates.

6.3 Manufacturing Process

6.3.1 Single Lap Joints

Prior to joint manufacturing, the nano-modified epoxy resin with CNT loadings ranging from 0.1 to 1 wt.% is prepared. As discussed in Chapter 4, the fabrication involves the combination of two dispersion methods: mechanical stirring and ultrasonication. More specifically, the epoxy resin and MWCNTs are mechanically stirred for 5min at 10,000rpm, followed by sonication (amplitude= 40% and cycle= 0.6) for 30min. The mixture is then placed in a vacuum chamber for 20min in order to eliminate the air introduced during mixing. The hardener is finally added and after 5min of hand stirring, the mixture (resin + CNTs + hardener) is degassed again for 20min.

After the completion of the adhesive manufacturing, the substrate surface preparation is carried out, a process vital for the successful implementation of the adhesive bonding technology. Grit blasting was found to be, as shown in Chapter 5, the most efficient surface preparation method promoting good adhesion between the substrates and the adhesive. Thus, the bonding area of all metal substrates is thoroughly prepared via this technique. Acetone degreasing of the surface is then adopted to remove any debris prior to the application of the adhesive.

The general fabrication process of the co-cured single lap joints includes the utilisation of a glass plate used as a mould and two metal plates of the same dimensions: a) the grit blasted plate, which is used as substrate and b) the auxiliary plate or spacer, which is used only during the manufacturing process. A release agent is applied on all plates to guarantee easy removal from the glass mould, while the overlap area is covered with polyester tape to avoid any contamination by the release agent. The grit blasted plate is then placed on the glass mould with the spacer next to it on top of which the composite layers are laminated (Figure 6.1).
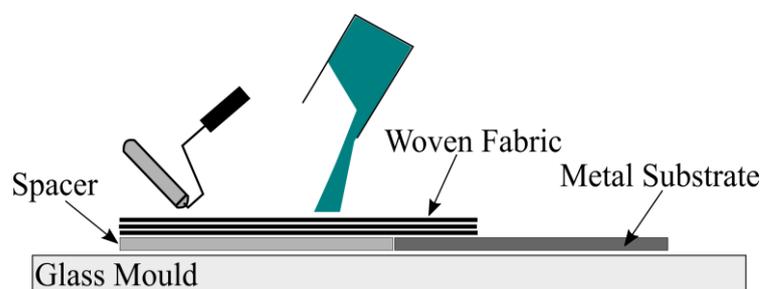
Figure 6.1: HLU process.

A MWCNT filled epoxy resin rich layer is applied on the bonding area of the grit blasted plate immediately after acetone degreasing. A ply of either woven glass or woven carbon cloth of

0.23mm and 0.27mm ply thickness respectively, is laid on top followed by the subsequent layers. In total, sixteen layers of glass cloth and twelve layers of carbon cloth impregnated with pure epoxy resin by simple HLU (hand lay-up) are laid up in order to achieve a laminate thickness of approximately 4mm and 3mm respectively. The composite laminated on the metal plate is then cured at room temperature for 24h and post-cured for 15h at 50°C under constant pressure loading. After the machining of the manufactured composite/metal plates, four specimens per plate are extracted.

Three different types of co-cured metal-to-composites joints have been manufactured and for each case MWCNT filled epoxy of various weight fractions is used for bonding (Table 6.2).

	Overlap Length (mm)												
SLJs	**25**					**40**			**60**		
CFRP/Steel	0%	0.1%	0.3%	0.5%	1%	0%	0.1%	0.3%	0%	0.1%	0.3%
GFRP/Aluminium	0%	0.1%	0.3%	0.5%	1%	0%	0.1%	0.3%	0%	0.1%	0.3%
GFRP/Steel	0%	0.1%	0.3%	0.5%	1%	0%	-	0.3%	0%	-	0.3%

Table 6.2: CNT loadings of nano-modified epoxy resin used for the manufacturing of metal-to-composite single lap joints.

6.3.2 Double Cantilever Beam Joints

A similar process to the one described above, is followed for the manufacturing of double cantilever beam (DCB) specimens. The grit blasted plate is cleaned with acetone to ensure that it is free of any contaminants and then, it is placed on the glass mould. A polyester film of 70μm thickness and 40mm length is placed at one end across the width of the plate to provide the crack initiator and then, it is covered with the MWCNT epoxy adhesive. Finally, the carbon and glass fabric layers are laid on top using pure epoxy resin and the obtained DCB plates are cured.

To reduce the possibility of any thermal shock or residual stresses accumulating within the adhesive layer, the entire assembly is left in the oven in order to cool down slowly to room temperature. After cutting the DCB plates into 25mm wide specimens, the load blocks are bonded onto them using a two-part Araldite epoxy resin. A thin layer of typewriter correction fluid is also applied on the edges of the specimens to facilitate the crack length measurements (Figure 6.4).

6.4 Mechanical Testing

6.4.1 Lap Shear Test

Lap shear test specimens are loaded until failure at constant crosshead speed (1mm/min) according to ASTM D D1002-10 [144]. The bonding area is: a) 25mm x 25mm, b) 25mm x 40mm and c) 25mm x 60mm corresponding to the three overlap lengths, i.e. 25mm, 40mm and 60mm that are used. The single lap joint configuration is shown in Figure 6.2.
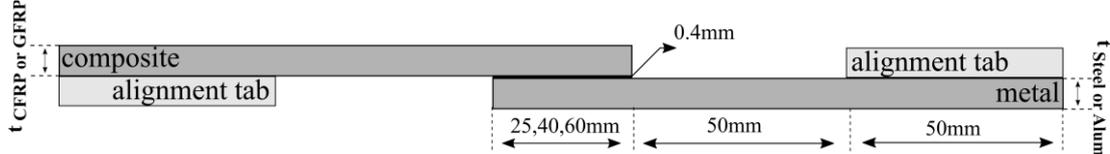
Figure 6.2: Single lap joint configuration.

Tabs are also used to eliminate misalignment during testing. Four specimens are tested per joint configuration and the failure modes are determined by visual inspection of the fracture surfaces.

6.4.2 DCB Test

Double cantilever beam (DCB) tests are performed to determine the mode-I adhesive fracture energy, G_{IC}, of the adhesive joints according to the BS ISO 25217:2009 standard [145]. The length and width of the adherends used are 125mm and 25mm respectively, whereas the thickness varies depending on the adherend type, as follows: t_{CFRP}= 3.2mm, t_{GFRP}= 4mm, t_{STEEL}= 2.37mm and t_{ALUM}= 3.5mm (Figure 6.3).
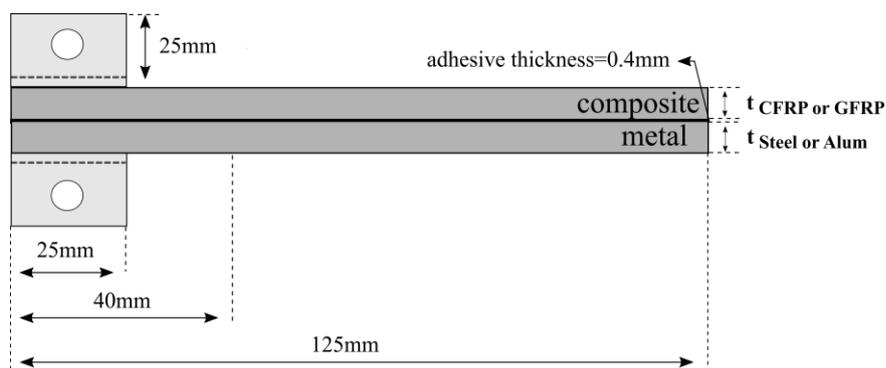
Figure 6.3: Double cantilever beam configuration.

The test consists of two stages: a) the pre-cracking stage (loading crosshead speed= 1mm/min and unloading crosshead speed= 10mm/min), which stops as soon as the crack is seen to

move on the edge of the specimen and b) the mode-I testing with the same loading and unloading testing speeds (Figure 6.4).

During the loading cycle, the crack is allowed to grow by approximately 5mm and then, the specimen is unloaded. This process is repeated until the crack has propagated for 65mm. A travelling microscope is used to determine the crack length at each loading cycle with high accuracy.
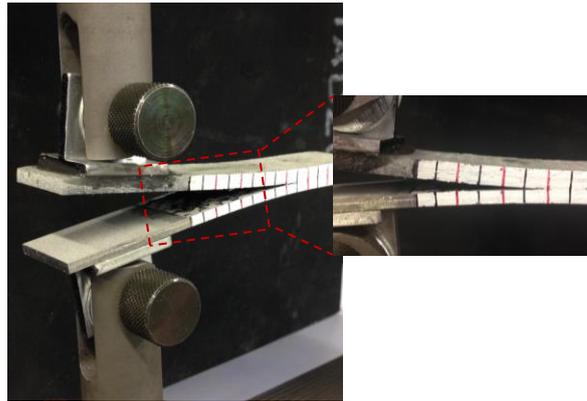
Figure 6.4: DCB test.

The load-displacement curves obtained from the test are finally used to calculate the total fracture energy.

6.5 Results and Discussion

The effect of the CNT loading of the adhesive on the bonding strength of dissimilar material co-cured joints with different overlap lengths is presented here. In all dissimilar material single lap joints, failure occurs along the adhesive/adherend interface due to stress concentrations in the vicinity of the wedges caused by the geometry and bi-material interface.

In all dissimilar material single lap joints, the crack path initiates at the top side of the overlap length and propagates through the metal/adhesive interface (Figure 6.5). This failure mode indicates that the metal/adhesive interface is weaker compared to the composite/adhesive one and/or that the stress concentrations at the metal/adhesive edge are higher due to the sharper geometry (270° re-entrant bi-material corner).
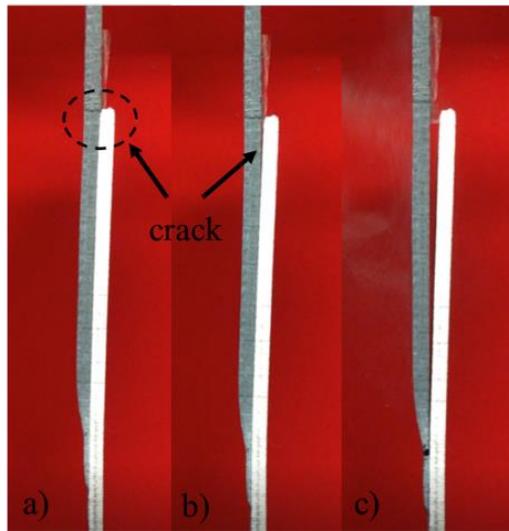
Figure 6.5: Failure process in dissimilar material single lap joints: a) crack initiation, b) crack growth and c) failure.

6.5.1 CFRP-to-Steel Single Lap Joints

The failure load of CFRP/Steel single lap joints increases with the increase of the overlap length for all MWCNT weight fractions achieving the highest improvement equal to 60% for the case of pure epoxy resin adhesive and for 60mm overlap length (Figure 6.6). This is something expected as the load carrying surface increases.
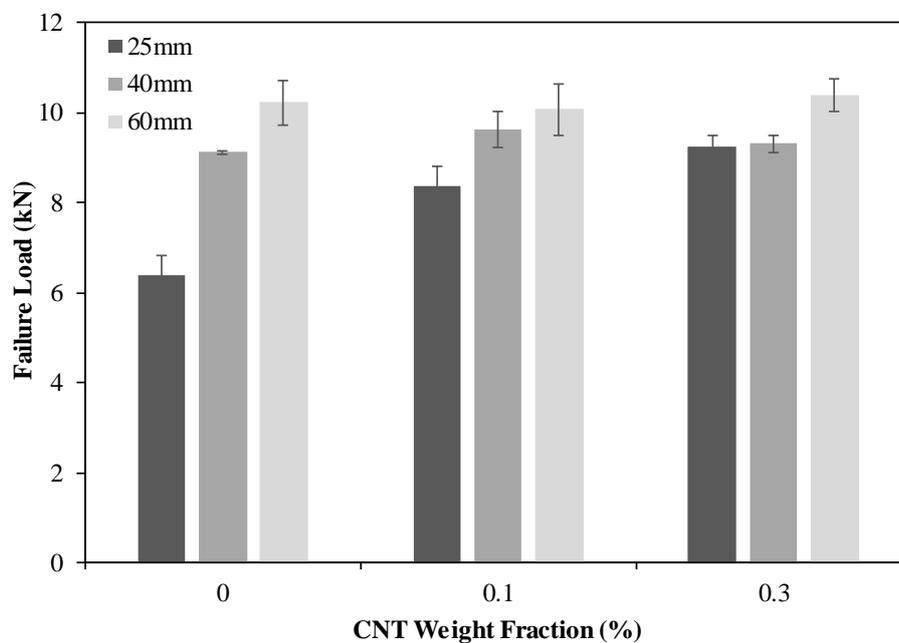
Figure 6.6: Failure load versus CNT weight fraction of CFRP/Steel joints for three overlap lengths.

However, the incorporation of MWCNTs in the epoxy resin seems to affect the joint strength values only when the overlap length is 25 mm. The highest loading capacity is obtained for

0.1 and 0.3 wt.% CNT loadings, where the failure load increases by 30% and 45% respectively. For greater overlap lengths, i.e. 40mm and 60mm, bonding strength shows a moderate increase or no increase at all after the MWCNT incorporation in the epoxy adhesive.

6.5.2 GFRP-to-Aluminium Single Lap Joints

In Figure 6.7, similar observations to section 6.5.1 can be made for the case of GFRP/Aluminium single lap joints. The failure load increases significantly with the increase of the overlap length for all CNT loadings. For the case of 25mm overlap length, the joint strength increases by 27% on average for both 0.1 and 0.3 wt.% CNT loadings, whereas for the case of 40mm overlap length the failure load remains unaffected. However, the highest loading capacity is achieved for the overlap length of 60mm and CNT loading equal to 0.3 wt.%.
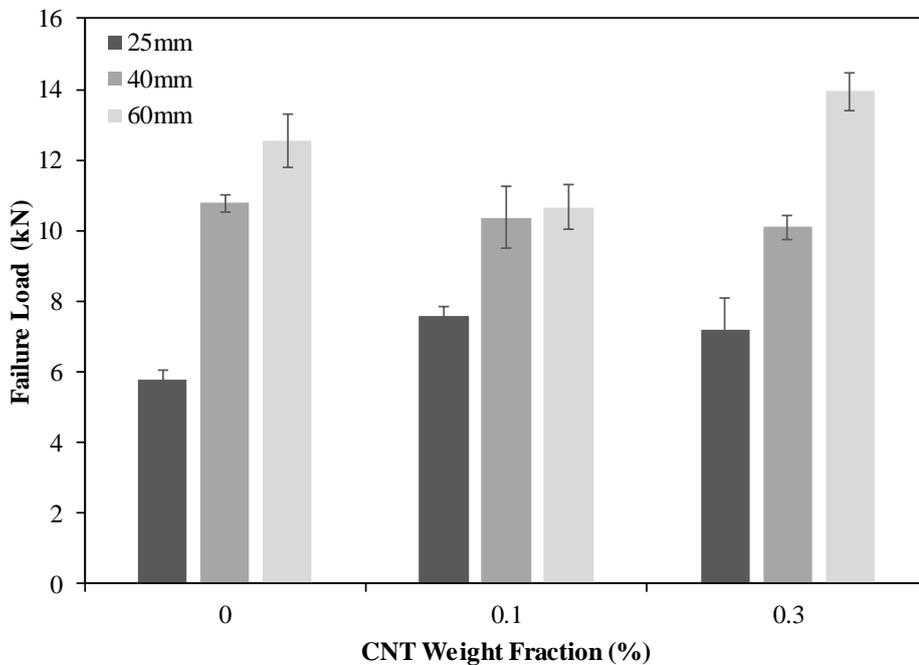
Figure 6.7: Failure load versus CNT weight fraction of GFRP/Aluminium joints for three overlap lengths.

6.5.3 GFRP-to-Steel Single Lap Joints

The failure load of GFRP/Steel single lap joints improves as the overlap length increases to either 40mm or 60mm (Figure 6.8). However, the utilisation of MWCNT filled epoxy adhesive does not enhance the joint strength for any of the overlap lengths and CNT weight contents studied here. This is most probably because these joints fail within the adhesive and hence, any enhancement in the adhesive/adherend interfacial strength through MWCNTs will not result in further improvement of the joint strength.
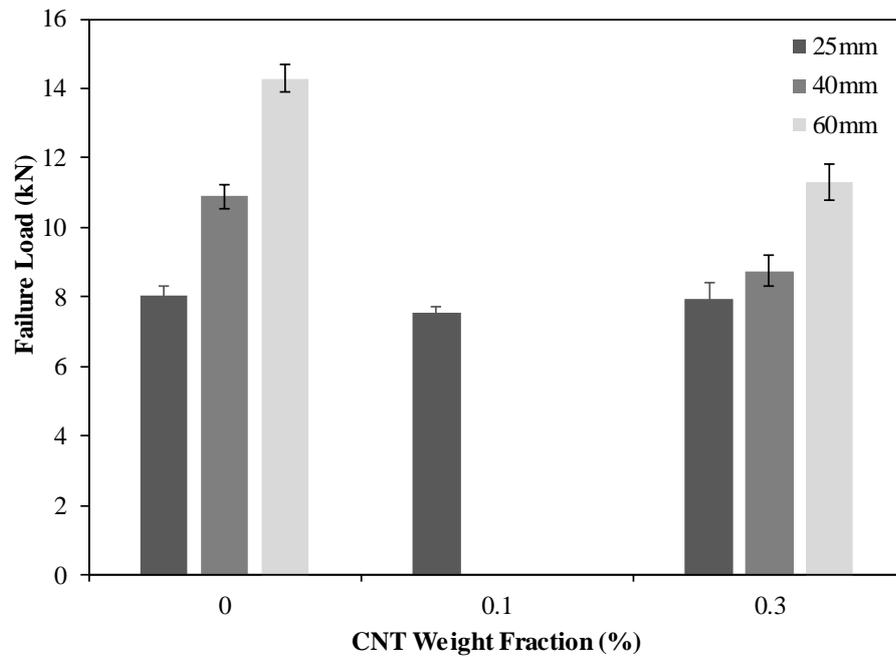
Figure 6.8: Failure load versus CNT weight fraction of GFRP/Steel joints for three overlap lengths.

We did not proceed with the manufacturing of joints with 40mm and 60mm overlap length bonded with 0.1 wt.% MWCNT reinforced adhesive, because the minimal effect of the MWCNTs on the joint strength has already been shown.

6.5.4 Dissimilar Material Single Lap Joints: Overlap Length and MWCNTs

The aforementioned results suggest that the increase of the overlap length is proved to be beneficial for all joint configurations leading to higher failure load level [24, 35, 146]. However, the utilisation of the MWCNT/epoxy adhesive in joints with either 40mm or 60mm overlap length does not increase the failure load. This is attributed to the fact that the maximum peel stresses of the joints are already close to the bulk adhesive tensile strength and further enhancement of the adhesive/adherend interface via the incorporation of MWCNTs does not increase the joint strength, as it will be shown from FEA in Chapter 7 (see Figure 7.16 and Figure 7.17).

6.5.5 Ball Milling vs. Sonication Method

The comparison between the different dispersion methods presented in Chapter 4 showed that ball milling does not decrease the mechanical properties of the nanocomposites for CNT weight fractions up to 0.5%. Therefore, ball milling is further investigated, so as to examine whether this advantage over mechanical stirring/sonication can be also reflected on the joint strength.

CFRP/Steel and GFRP/Aluminium single lap joints with 25mm overlap length are bonded using a nano-modified adhesive of 0.1 wt.%, which has been fabricated using: a) mechanical stirring/sonication and b) ball milling. The two dispersion methods are compared in Figure 6.9. The failure loads of the reference single lap joints, i.e. the joints bonded with pure epoxy resin are also presented.
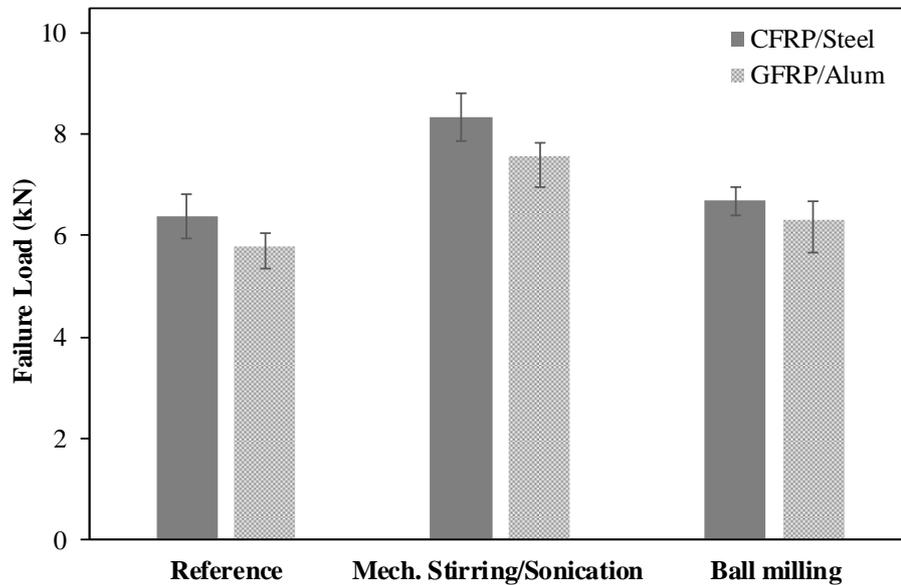
Figure 6.9: Failure load versus dispersion methods for 0.1 wt.% CNT (overlap length= 25mm).

After the addition of MWCNTs in the epoxy resin adhesive, the failure load of CFRP/Steel and GFRP/Aluminium joints is enhanced irrespective of the dispersion method employed. However, sonication method increases the joint strength by 30% for both joint configurations, whereas ball milling increases bonding strength only by 4% and 8% for CFRP/Steel and GFRP/Aluminium joints respectively. A possible explanation for the lower performance of the joints when ball milling is utilised is the introduction of big amount of air bubbles during mixing, which were not possible to remove completely during degassing and hence, acted as failure initiation points (see Chapter 4).

6.5.6 Dissimilar Material Joints with 25mm Overlap Length

The joint strength obtained from testing all dissimilar material single lap joints with 25mm overlap length is plotted against the CNT weight fractions of the nano-modified adhesives in Figure 6.10.

The failure load increases for CFRP/Steel and GFRP/Aluminium joint configurations, when MWCNT reinforced epoxy is used as adhesive instead of pure epoxy resin, in contrast to the

bonding strength of GFRP/Steel joints, which is almost unaffected by the addition of MWCNTs in the epoxy adhesive.
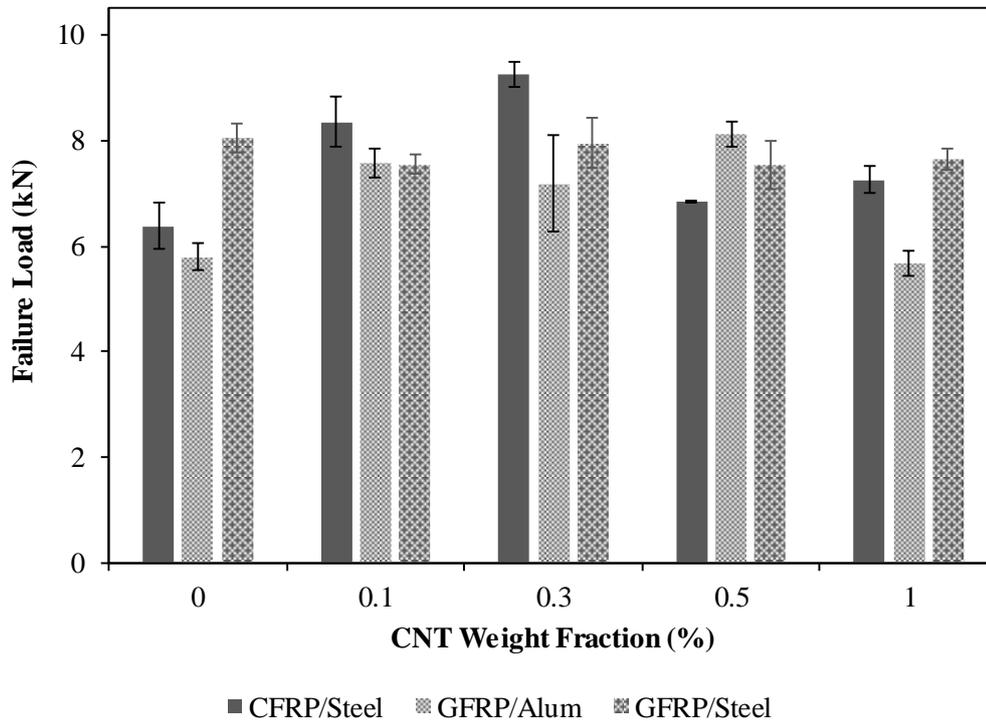
Figure 6.10: Failure load versus CNT weight fraction for 25mm overlap length.

The highest loading capacity is obtained for the CFRP/Steel single lap joints, which increases by 30% for 0.1 wt.% and 45% for 0.3 wt.%. The failure load of GFRP/Aluminium joints also exhibits a noteworthy improvement when the MWCNT filled epoxy resin is used to bond the substrates. In particular, for the case of 0.5 wt.% CNT loading, it increases by 40%. However, the failure load reaches a plateau after further increase of the CNT content to 1 wt.% obtaining values almost equal to that obtained when pure epoxy resin is used for bonding. This is attributed to the poor dispersion of the MWCNTs in the epoxy resin adhesive, as shown in Chapter 4, which results in the formation of aggregates that prevent the MWCNTs from enhancing the interfacial strength between the adherends and the adhesive.

The addition of MWCNTs in the epoxy adhesive not only affects the bonding strength of the joints, but it also alters the failure mode, which can be seen in the images of the fracture surfaces of the respective adherends after joint failure illustrated in Figure 6.11.

With the increase of the CNT weight fraction, the failure mode shifts from adhesive/adherend interfacial failure to adhesive failure.
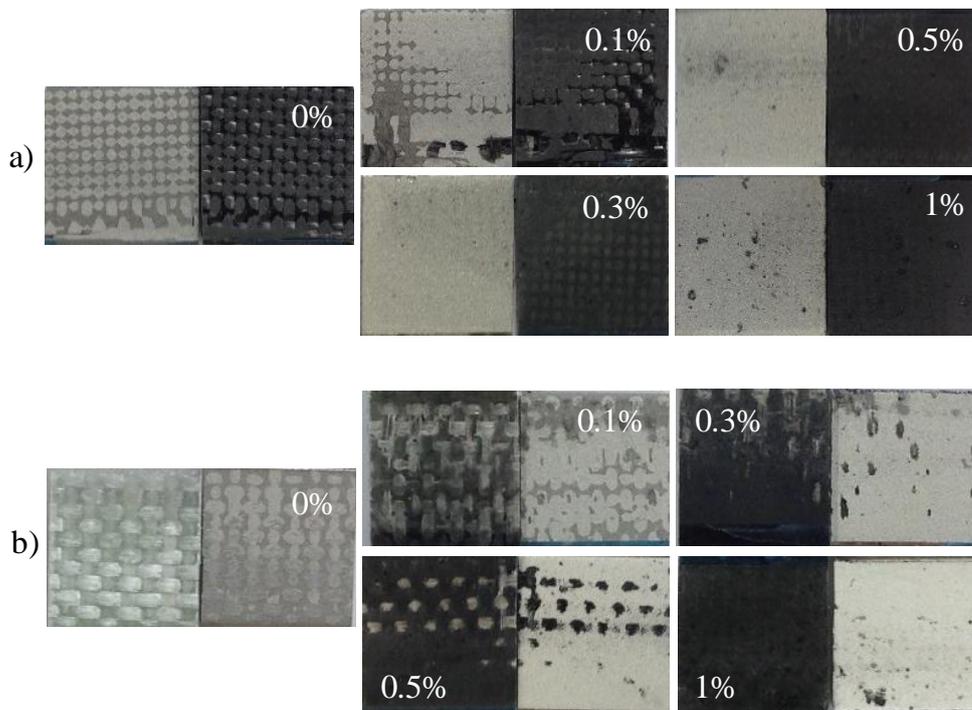
Figure 6.11: Bonding area of: a) CFRP/Steel and b) GFRP/Aluminium single lap joints bonded with pure epoxy resin, 0.1, 0.3, 0.5 and 1 wt.% CNT.

When pure epoxy resin is used to bond the CFRP and steel substrates, the adhesive is visible on both fracture surfaces. Whereas for the case of 0.1 wt.% CNT loading, the adhesive covers most of the CFRP surface and for the case of 0.3, 0.5 and 1 wt.%, the CFRP substrate is fully covered by the adhesive indicating a higher interfacial bond between the fibres and the MWCNT epoxy.

Although the failure mode of GFRP/Steel single joints is almost identical to the other two joint configurations (Figure 6.12), the joint strength remains almost constant irrespective of the CNT loading (Figure 6.10), as already shown in section 6.5.3.
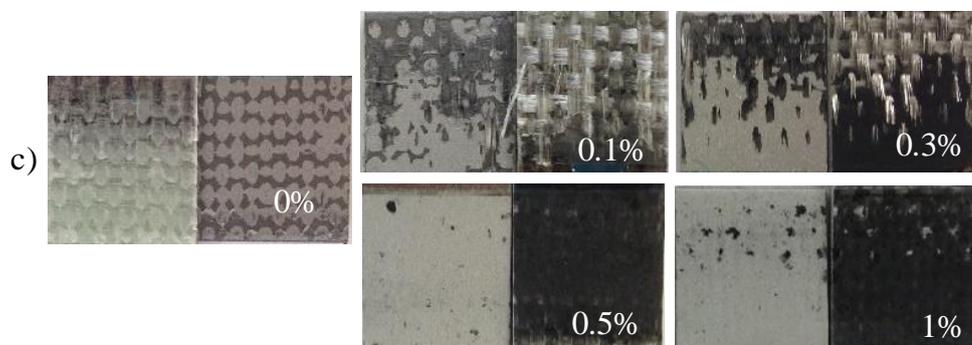
Figure 6.12: Bonding area of GFRP/Steel single lap joints bonded with pure epoxy resin, 0.1, 0.3, 0.5 and 1 wt.% CNT.

6.6 DCB Test Results

CFRP/Steel, GFRP/Aluminium and GFRP/Steel DCB specimens have been tested. In Figure 6.13, a typical load-displacement curve is shown.
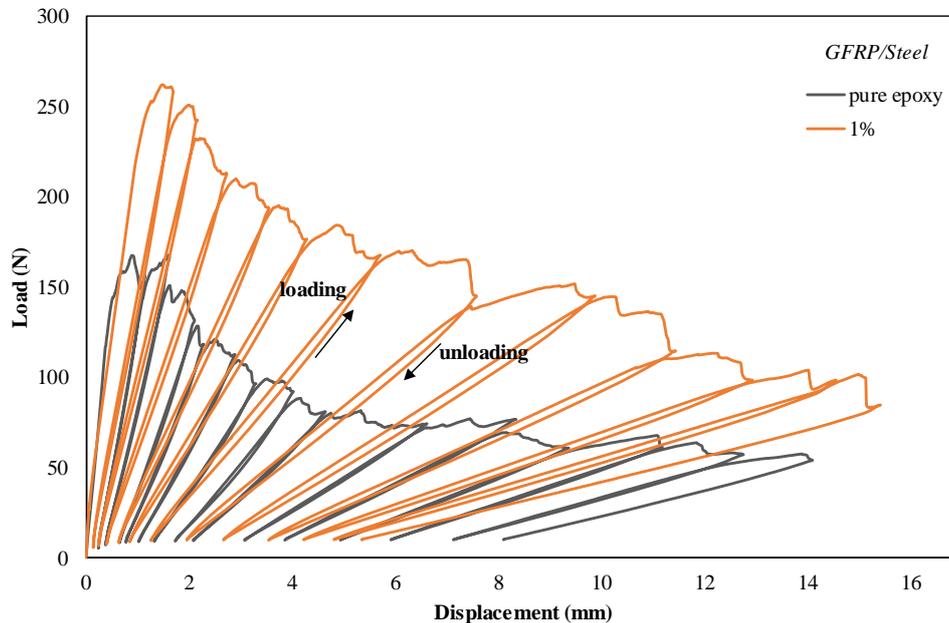
Figure 6.13: Load-displacement curve for GFRP/Steel specimens bonded with pure epoxy resin and MWCNT reinforced epoxy adhesive (1 wt.%).

The crack length and the respective load values obtained from the tests have been utilised for the calculation of the total strain energy release rate of all dissimilar material joints via the VCCT method (see Chapter 7, section 7.2).

6.7 Conclusions

The effect of the joint overlap length as well as the effect of various CNT weight fractions have been investigated for a wide variety of different metal-to-composite single lap joint configurations, namely CFRP/Steel, GFRP/Aluminium and GFRP/Steel.

The failure load of all joint configurations increases with the increase of the overlap length. The incorporation of MWCNTs in the epoxy resin adhesive is shown to increase the load bearing capacity of CFRP/Steel and GFRP/Aluminium single lap joints with 25mm overlap length. This is because for these joint configurations, the increase of CNT weight fraction results in a shift from adhesive/adherend interfacial failure to failure within the adhesive, as shown from the examination of the fracture surfaces. On the contrary, GFRP/Steel joints do not show any improvement after the addition of MWCNTs in the epoxy resin adhesive. This is most probably because these joints fail within the adhesive and hence, any enhancement in

the adhesive/adherend interfacial strength through MWCNTs will not result in further improvement of the joint strength.

Chapter 7. FEA Analyses

The single lap joint and DCB tests are simulated using the finite element package ANSYS 14.5. For the case of single lap joints, the stresses obtained are used in conjunction with simple stress based criteria in an attempt to better understand the failure modes of the different single lap joint configurations tested. For the case of DCB tests, Virtual Crack Closure Technique (VCCT) is employed in order to calculate the Strain Energy Release Rate (SERR).

7.1 Single Lap Joint Models

Since the adhesive and adherend thicknesses are much smaller than the joint width, plane strain conditions are assumed and the single lap joints are modelled as two-dimensional. Quadrilateral-shaped elements are used with the mesh density being refined at the wedges (Figure 7.1). The number of elements along the overlap length varies such that the element size remains the same between joints with different overlap lengths.
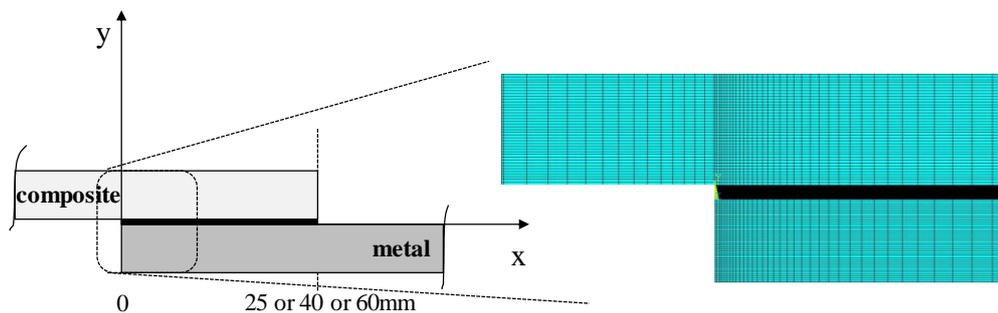
Figure 7.1: Mesh density at the wedges.

In order to obtain an accurate representation of the stress field within the adhesive, it is essential to model the adhesive layer with a finite element mesh size smaller than the adhesive layer thickness [59]. The overlap ends are singular regions therefore, a mesh density refinement along the overlap length was required in order to capture the singular stress field near the wedges.

The mesh density along the overlap length varied using different element sizes: a) 40, b) 80 and c) 120. An example of the different meshes obtained for Aluminium/Aluminium single lap joints while altering the element size is shown in Figure 7.2.
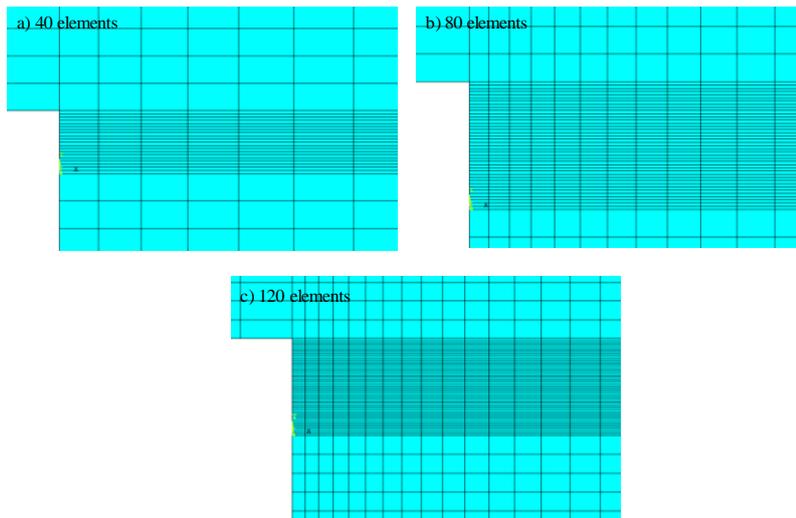
Figure 7.2: Different element sizes used to represent the adhesive layer of Aluminium/Aluminium single lap joints: a) 40 elements, b) 80 elements and c) 120 elements along the overlap length.

In Figure 7.3, it can been seen that after the increase of the element size from 80 to 120, the maximum peel stress values differ by only 1% suggesting that mesh convergence has been achieved. 80 elements have therefore been selected for the finite element analysis.
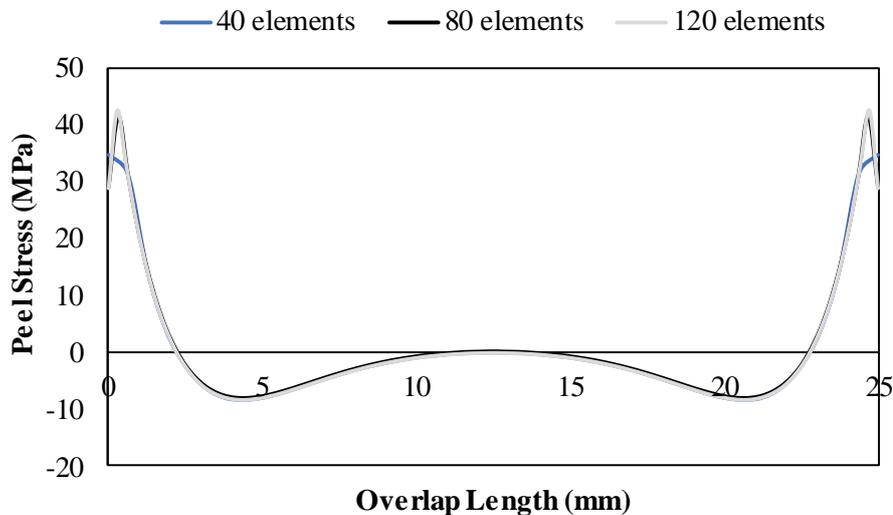
Figure 7.3: Peel stress distribution for Aluminium/Aluminium joints when three different element sizes are used along the overlap length.

The boundary conditions applied on the single lap joint models are shown in Figure 7.4. The joints are fixed in the x-direction on one end and the load is applied as distributed load on the other end. The tabbed areas are fixed in the y-direction to simulate the constraints imposed by the test jigs.
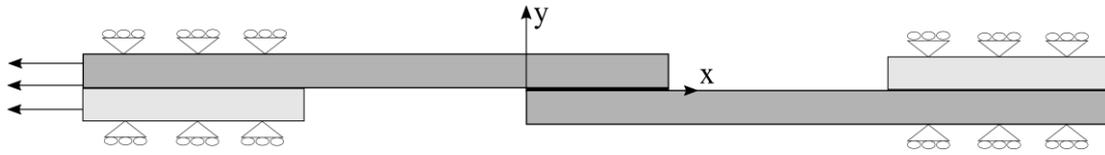
Figure 7.4: Loading and boundary conditions of single lap joint model.

The CFRP and GFRP adherends are modelled as linear orthotropic materials with their elastic properties given in Table 7.1.

	E_1 (GPa)	E_2 (GPa)	G_{12} (GPa)	G_{23} (GPa)	ν_{12}	ν_{23}
CFRP	47	5.96	3.26	2.1	0.33	0.41
GFRP	20	7	4.14	3.44	0.26	0.2

Table 7.1: Elastic properties of composite adherends.

The steel and aluminium adherends are modelled as isotropic exhibiting: a) linear elastic, or b) elastic-perfectly plastic behaviour with their properties given in Table 7.2.

	E (GPa)	ν	Yield Stress (MPa)
Steel (thin)	201	0.3	300
Steel (thick)	201	0.3	800
Aluminium	70	0.3	265

Table 7.2: Material properties of metal adherends.

As it was shown in Chapter 4, the small amount of CNT reinforcement does not significantly affect the elastic properties of the epoxy, which is used as adhesive for the manufacturing of the various joint configurations. Therefore, the elastic properties of the pure epoxy adhesive and the adhesive filled with MWCNTs of various weight fractions are assumed the same in the simulations (Table 7.3).

	E (GPa)	ν
Adhesive	3.04	0.36

Table 7.3: Elastic Properties of pure epoxy resin adhesive.

7.1.1 Stress Analysis of Metal-to-Metal Single Lap Joints

Two Steel/Steel and one Aluminium/Aluminium single lap joint configurations have been tested (see Chapter 5) and modelled here. The joint dimensions and failure loads are given in Table 7.4.

Lap Joints	Joint Width (mm)	Adherend Thickness (mm)	Free Adherend Span (mm)	Avg Failure Load (N)
Steel/Steel (thin)	25	2.37	50	7679
Steel/Steel (thick)	25	6	50	7241
Aluminium/Aluminium	25	3.5	50	6447

Table 7.4: Geometry and failure loads of the metal-to-metal joint configurations.

Linear FEA models and models where the adherends are simulated as elastic-perfectly plastic and geometric non-linearity, i.e. large deflections and rotations, is taken into account, have been run for every joint configuration in order to check how the adhesive shear and peel stresses vary along the overlap length. The applied load on all FEA models is the corresponding average experimental failure load shown in Table 7.4.

Figure 7.5a and Figure 7.5b show the variation of the shear and peel stresses for the cases where the Aluminium/Aluminium joints are assumed to have: a) linear material properties and small deflections and b) non-linear adherend properties and large deflections (denoted as non-linear).
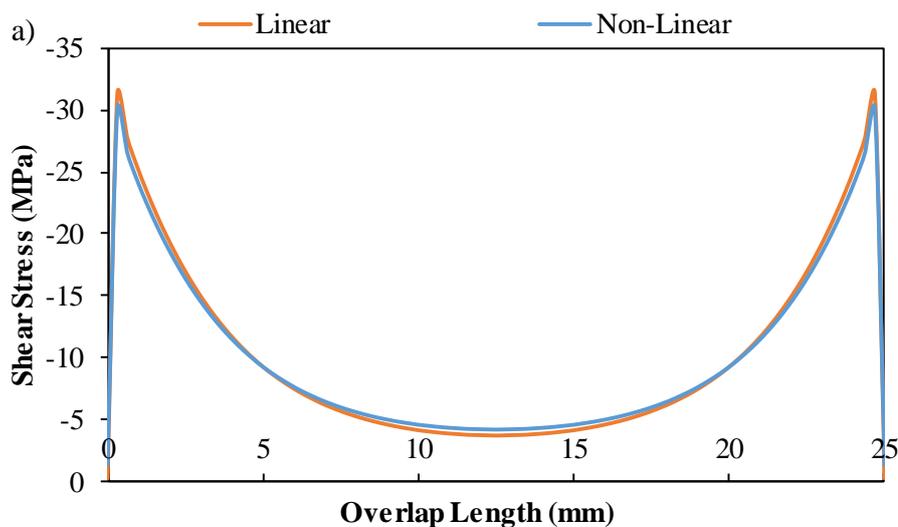
Figure 7.5: a) Shear stress and b) peel stress distributions from linear and non-linear Aluminium/Aluminium joint FEA models.

Figure 7.6a and Figure 7.6b show the variation of the corresponding shear and peel stresses for the thin Steel/Steel joints.

Figure 7.6: a) Shear stress and b) peel stress distributions from linear and non-linear thin Steel/Steel joint FEA models.

Figure 7.7a and Figure 7.7b show the variation of the corresponding shear and peel stresses for the thick Steel/Steel joints.

Figure 7.7: a) Shear stress and b) peel stress distributions from linear and non-linear thick Steel/Steel joint FEA models.

From the stress graphs above, it is shown that the results between linear and non-linear models are very similar for the Aluminium/Aluminium and thin Steel/Steel joint configurations. This can be explained by the fact that the failure loads of the 25mm overlap length joints are low enough, so as not to cause significant plasticity in the adherends or large deformations in the adhesive. The stress results from the linear models are therefore used for the failure criteria employed in section 7.1.2 for the assessment of the joint strengths.

However, for the case of the thick Steel/Steel joint configuration, the shear and peel stresses from linear and non-linear analyses are significantly different. This is because the eccentricity of the loading path is higher for these joints due to the higher thickness of the adherends. The stiff adherends do not deform much and thus, all the eccentricity of the load path has to be accommodated by the adhesive causing large deformations and rotations in the elements of the latter. The stress results from the non-linear models are hence used for the failure criteria employed in the next session for the assessment of the thick Steel/Steel joint strengths.

7.1.2 Failure Criteria for Metal-to-Metal Single Lap Joints

Metal-to-metal joints exhibit brittle failure initiating at the overlap ends within the adhesive or at the adhesive/adherend interface (see Chapter 5). This type of failure mode suggests that the maximum peel stress failure criterion is more suitable than the maximum shear or von-Mises stresses criteria, since the adhesive does not show signs of plastic deformation.

The maximum peel stresses as obtained from the different lap joint configurations for all MWCNT contents in the adhesive are shown in Table 7.5, where joint strength seems to increase with the increase in CNT loading for all joint configurations.

Lap Joints	CNT Weight Fraction of Adhesive	Bulk Adhesive Tensile Strength (MPa)	Avg. Failure Load (N)	Max. Peel Stress (MPa)
Aluminium/Aluminium	0 %	64.0	6447	41.3
	0.1%	62.8	6435	41.2
	0.3 %	52.2	6769	43.3
	0.5%	40.0	7576	48.5
Steel/Steel (thin)	0 %	64.0	7679	38.3
	0.1%	62.8	10804	53.9
	0.3 %	52.2	9533	47.6
	0.5%	40.0	11462	57.2
Steel/Steel (thick)	0 %	64.0	7241	26.1
	0.1%	62.8	8831	31.9
	0.3 %	52.2	8846	31.9
	0.5%	40.0	11049	39.9

Table 7.5: Average joint failure load and maximum peel stresses in the adhesive for all metal-to-metal joint configurations.

In Figure 7.8, the maximum peel stresses of the adhesive at joint failure for the three joint configurations (denoted as black points) and the tensile strength of the bulk adhesive (denoted as red points joined by straight line) are plotted against the various MWCNT loadings. For low CNT weight fractions, i.e. wt. %< 0.3, the maximum peel stress of the adhesive at joint failure is lower than the tensile strength of the corresponding bulk adhesive. This possibly suggests that the failure at the adhesive/adherend interface occurs prior to the full utilisation of the adhesive strength leading to adhesive/adherend interfacial failure (white area under red line).

However, as the CNT content increases, the adhesive/adherend interfacial strength increases and hence, the maximum peel stress of the adhesive at joint failure approaches the strength of the bulk adhesive.

Figure 7.8: Variation of maximum peel stress and bulk adhesive tensile strength for metal-to-metal joint configurations.

For the case of Aluminium/Aluminium and thin Steel/Steel joints with 0.5% CNT weight fraction, the adhesive peel stresses at failure are higher than the bulk adhesive strength, which is in theory not possible. This is because:

a. the failure mode is more complex and the maximum peel stress criterion is not valid in this case, or

b. due to the much higher volume of the 0.5 wt.% CNT bulk tensile test specimen (see Chapter 4) compared to the 0.5 wt.% CNT/epoxy adhesive used in the joint, as only a few milligrams are required for bonding, the former has higher chances of containing defects, such as voids and aggregates that result in lower strength.

7.1.3 Stress Analysis of Metal-to-Composite Single Lap Joints

CFRP/Steel, GFRP/Aluminium and GFRP/Steel single lap joint configurations have been tested (see Chapter 6) and are modelled here. The joint dimensions and failure loads are given in Table 7.6.

Lap Joints	Joint Width (mm)	Metal Thickness (mm)	Composite Thickness (mm)	Free Adherend Span (mm)	Avg. Failure Load (N)
CFRP/Steel	25	2.37	3.2	50	6380
GFRP/Aluminium	25	3.5	4	50	5793
GFRP/Steel	25	3.5	4	50	8053

Table 7.6: Geometry and failure loads of composite-to-metal joint configurations.

Linear FEA models and models where the metal adherends are simulated as elastic-perfectly plastic and geometric non-linearity, i.e. large deflections and rotations is taken into account, have been run for every joint configuration in order to check how the adhesive shear and peel stresses vary along the overlap. The applied load on all FEA models is the corresponding average experimental failure load shown in Table 7.6.

Figure 7.9a and Figure 7.9b show the variation of shear and peel stresses for the cases where the CFRP/Steel joints are assumed to have: a) linear material properties and small deflections and b) non-linear metal adherend properties and large deflections respectively (denoted as non-linear).
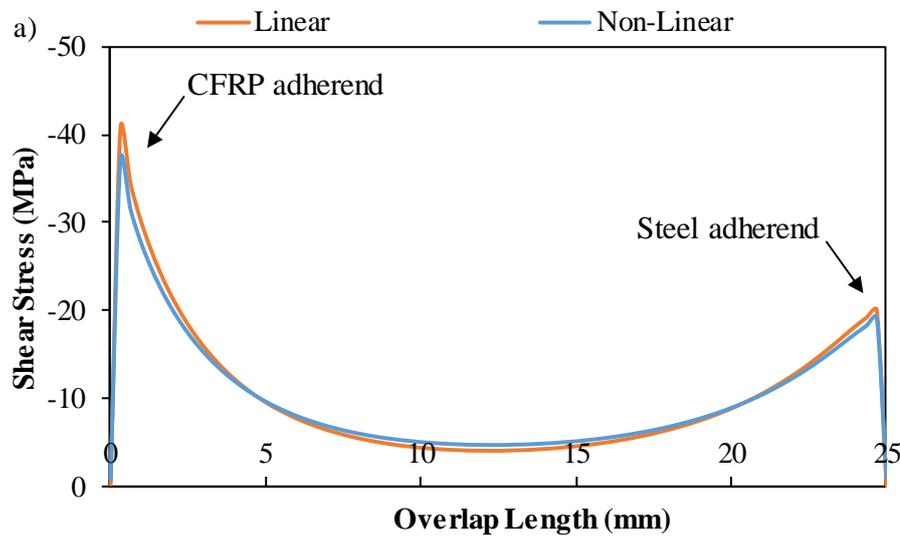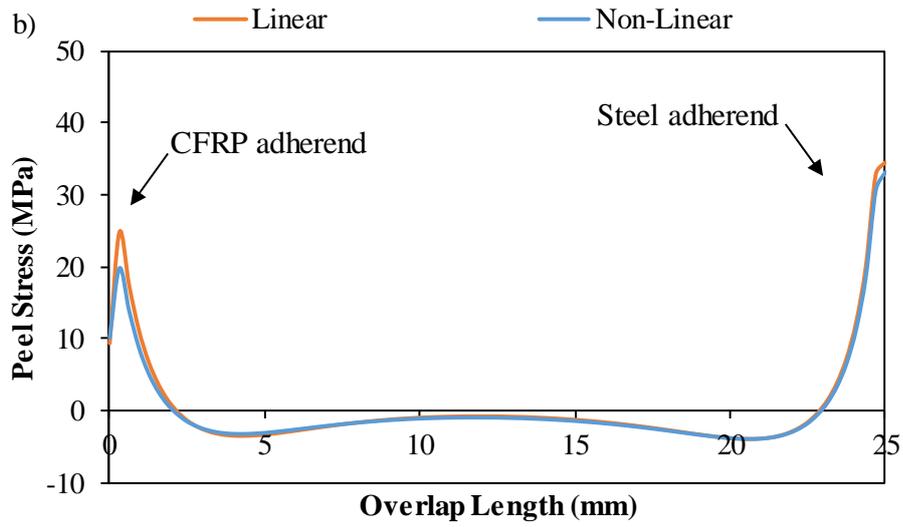
Figure 7.9: a) Shear stress and b) peel stress distributions from linear and non-linear CFRP/Steel joint FEA models.

Figure 7.10a and Figure 7.10b show the variation of the corresponding shear and peel stresses for the GFRP/Aluminium joints.
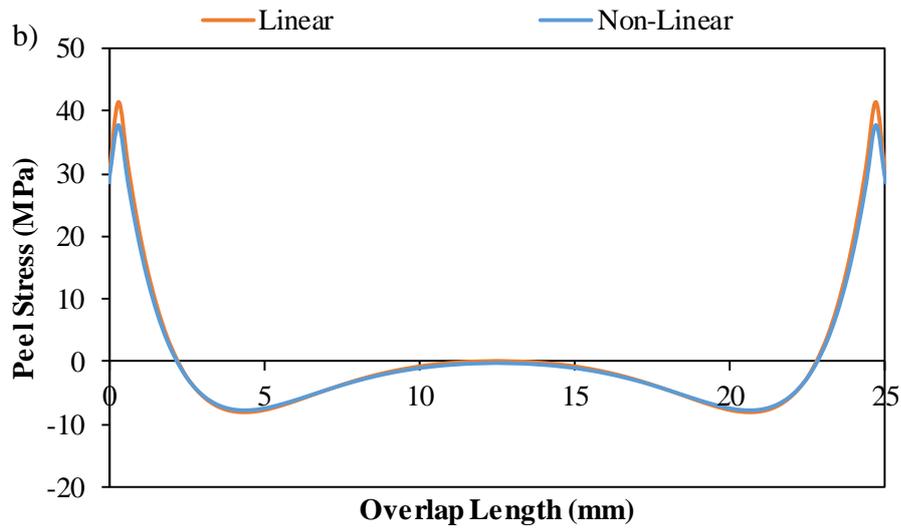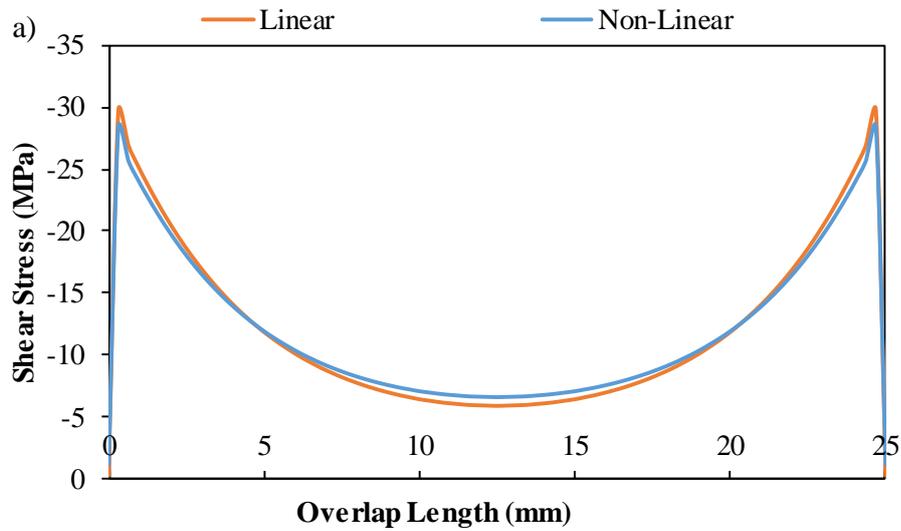
b)
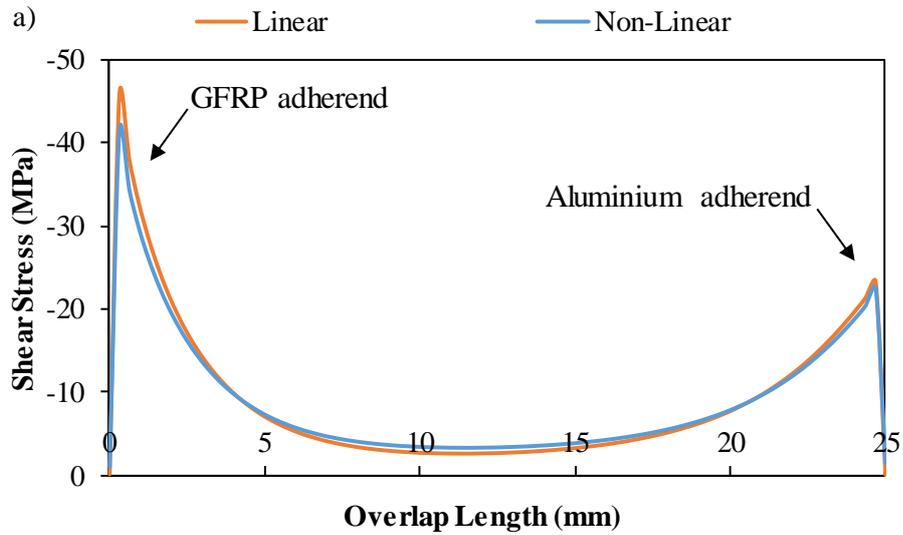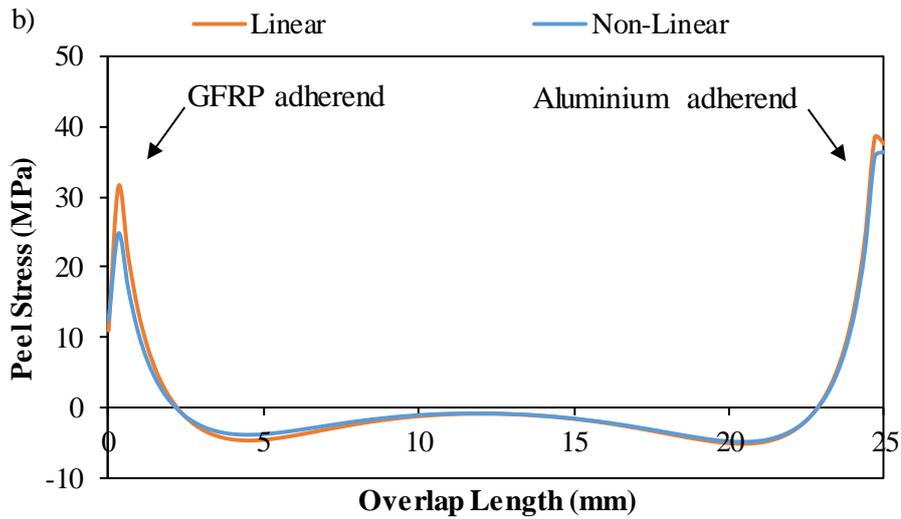
Figure 7.10: a) Shear stress and b) peel stress distributions from linear and non-linear GFRP/Aluminium joint FEA models.

Figure 7.11a and Figure 7.11b show the variation of the corresponding shear and peel stresses for the GFRP/Steel joints.
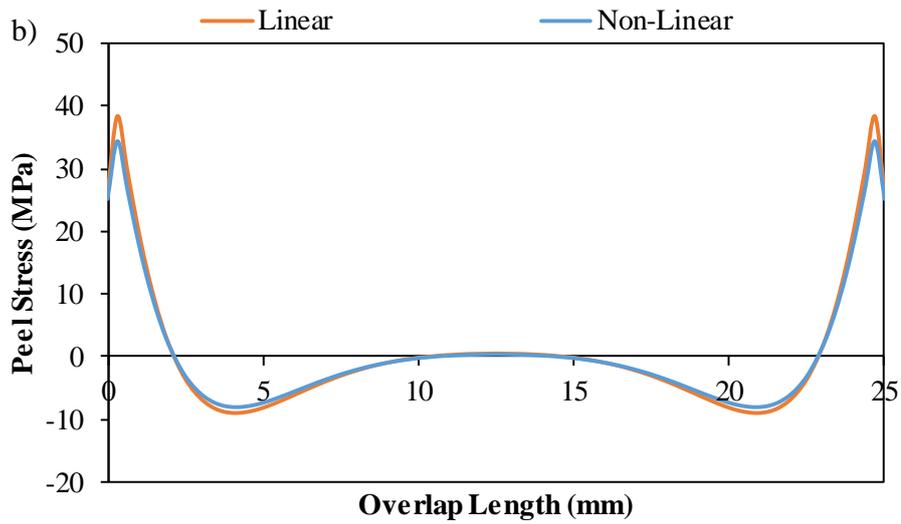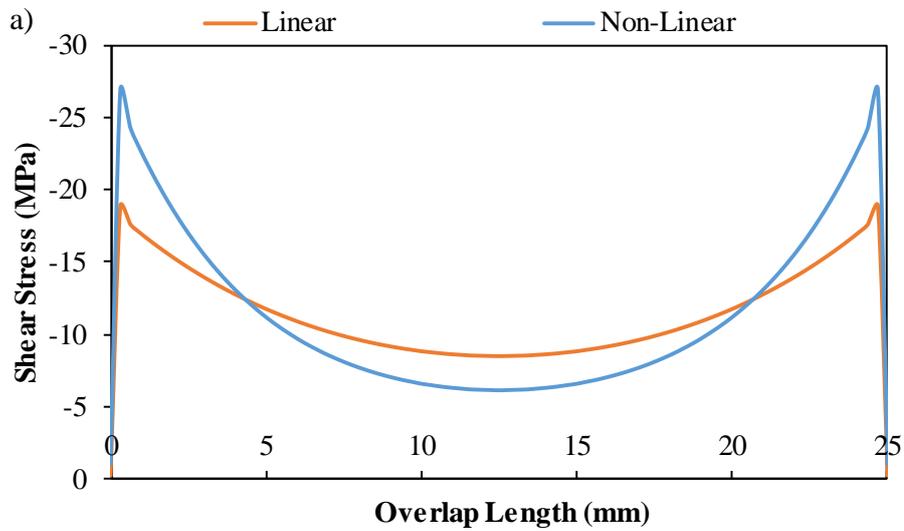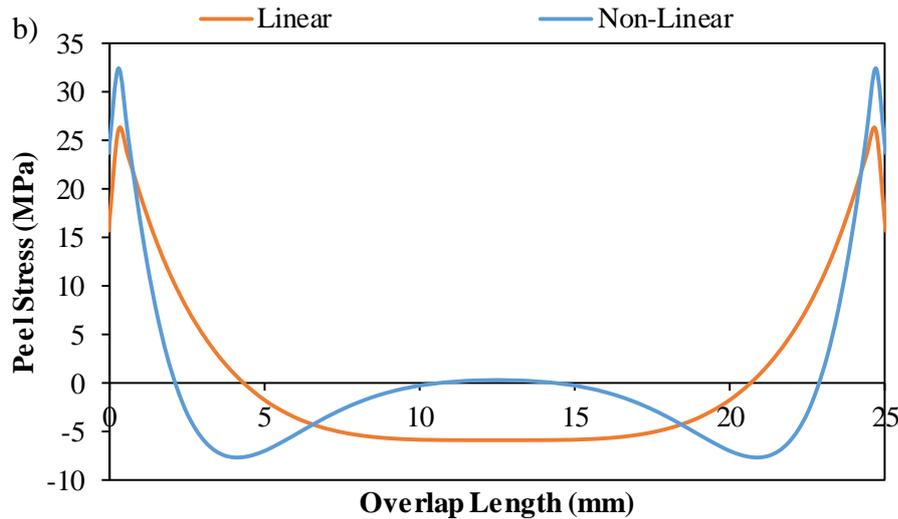
a)
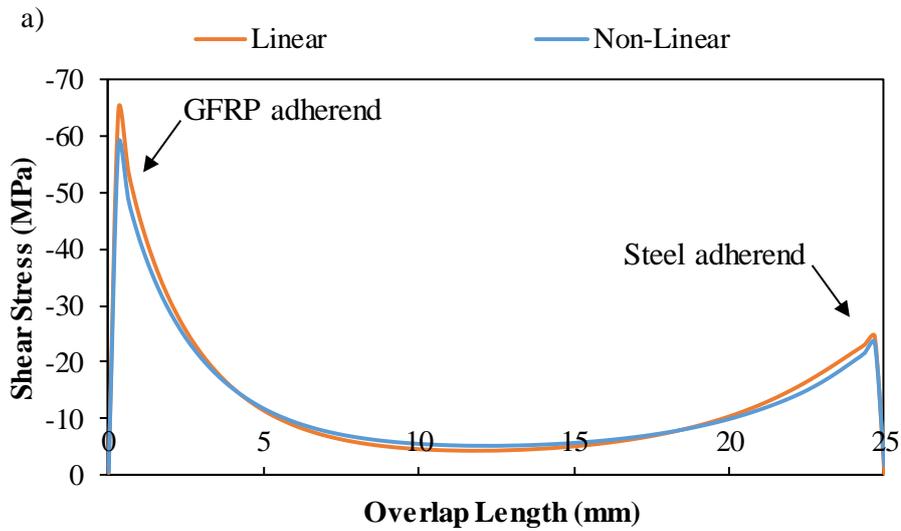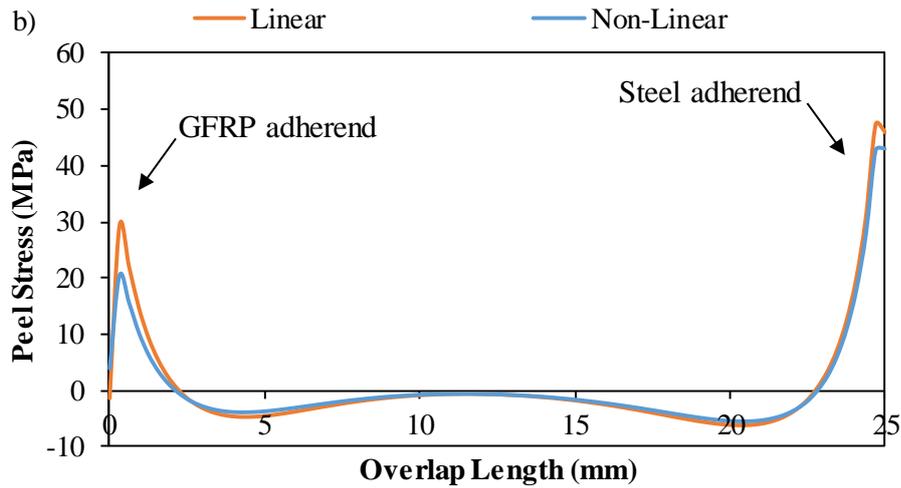
Figure 7.11: a) Shear stress and b) peel stress distributions from linear and non-linear GFRP/Steel joint FEA models.

From the stress graphs above, it is shown that the results between linear and non-linear models are very similar for all metal-to-composite joint configurations. Therefore, the stress results from the linear models are used for the failure criteria employed for the assessment of the joint strengths (section 7.1.4).

A load of 6000 N is applied on linear FEA models of all metal-to-composite joint configurations bonded with pure epoxy resin in order to investigate the effect of different overlap lengths i.e. 25mm, 40mm and 60mm. The variation of the shear stress field against the normalised distance along the overlap length is shown in Figure 7.12.
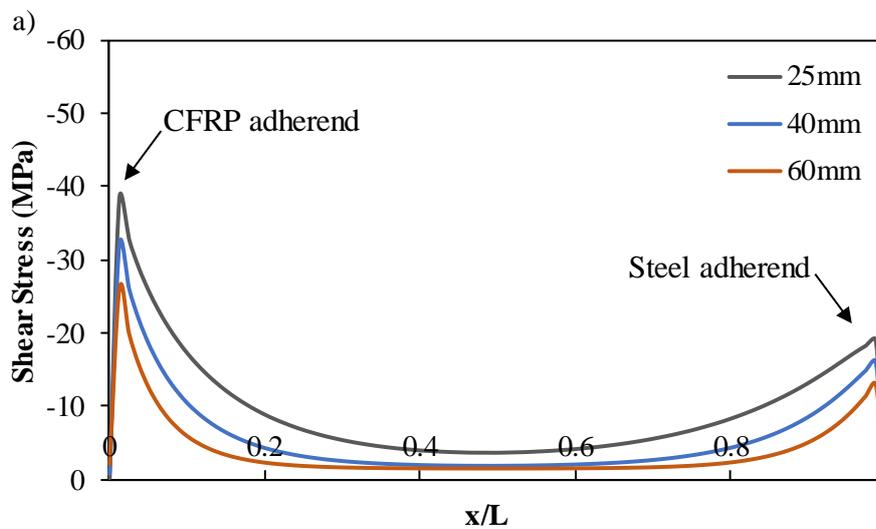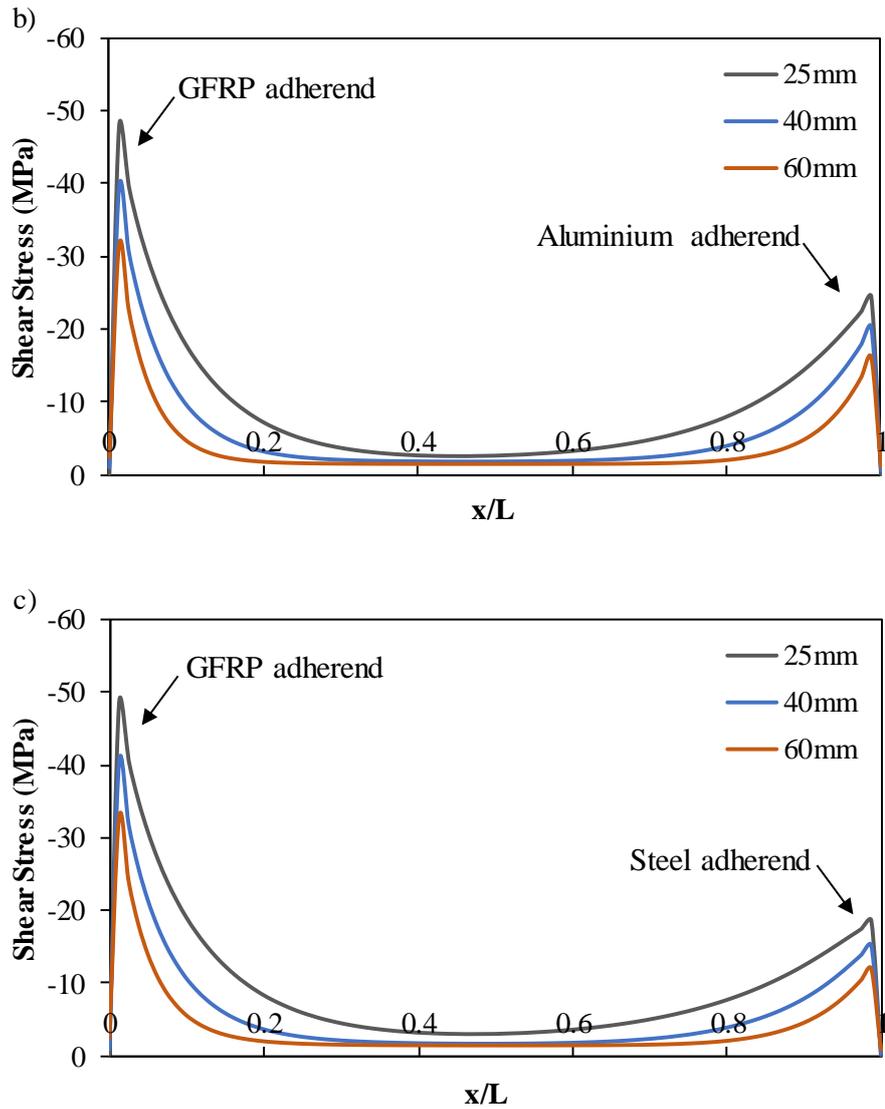
Figure 7.12: Shear stress distribution at the middle of the adhesive layer versus the normalised distance along the overlap length: a) CFRP/Steel, b) GFRP/Aluminium and c) GFRP/Steel.

The asymmetry in shear stress distribution observed is associated with the material mismatch of the adherends. For all types of joints and overlap lengths, shear stress values are much higher at the composite adherend side than those at the side of the metal adherend due to the lower Young's modulus of the former. This results in higher shear deformations of the adhesive and hence, in higher magnitude shear stresses towards the composite overlap end.

The CFRP/Steel single lap joints exhibit the lowest peak stresses because of the higher stiffness of CFRP and steel compared to GFRP and aluminium. The stiffer the adherends, the more uniform the shear stress distribution within the adhesive. This also leads to higher joint strengths, as seen from the experimental results (Table 7.8). The higher deformation of the

composite adherend compared to the metal adherend as obtained from FEA is shown in Figure 7.13.
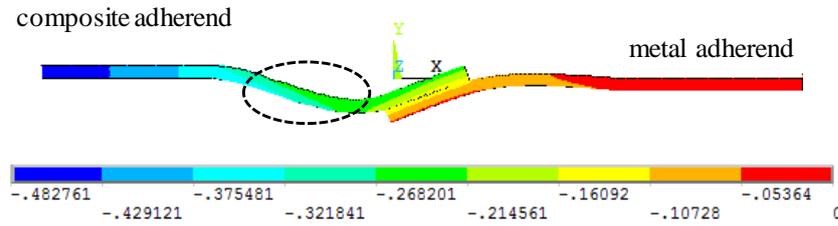
Figure 7.13: Deformed shape of metal-to-composite single lap joint.

In Figure 7.14, the peel stresses are plotted against the normalised distance along the overlap length.
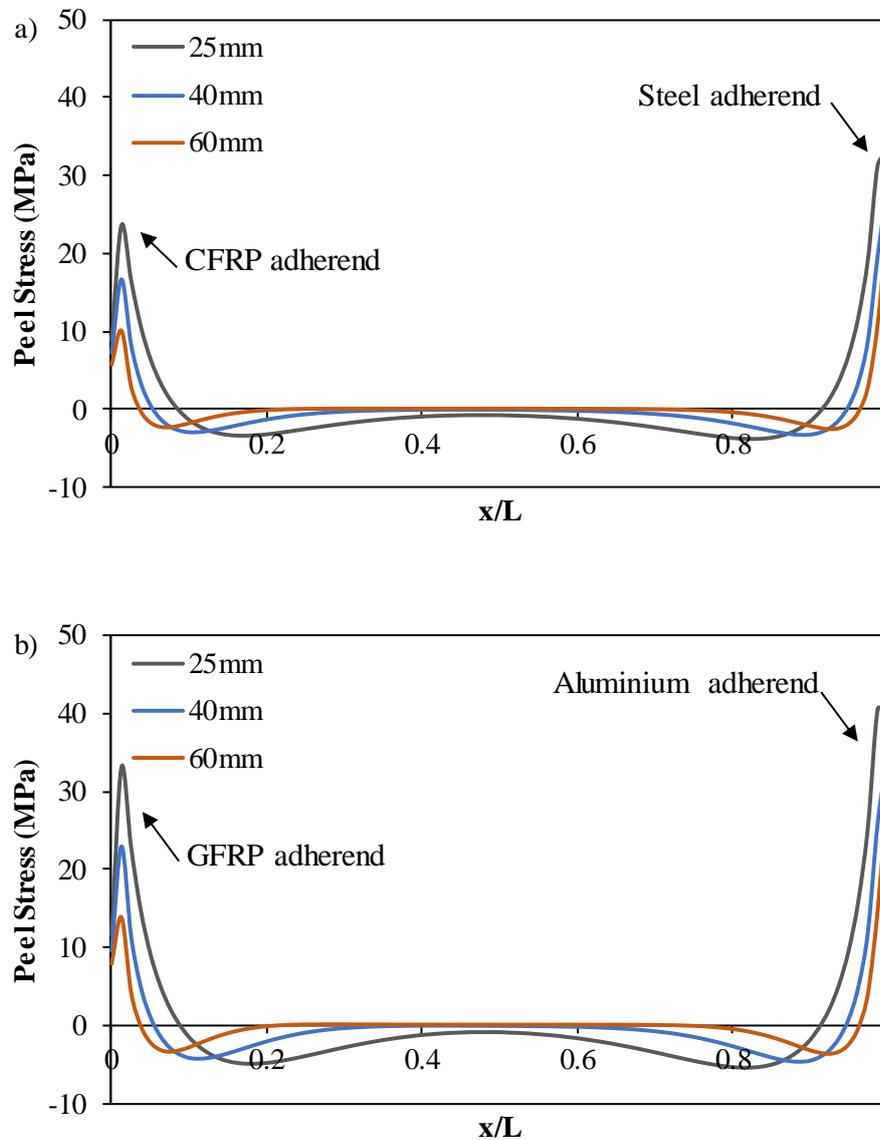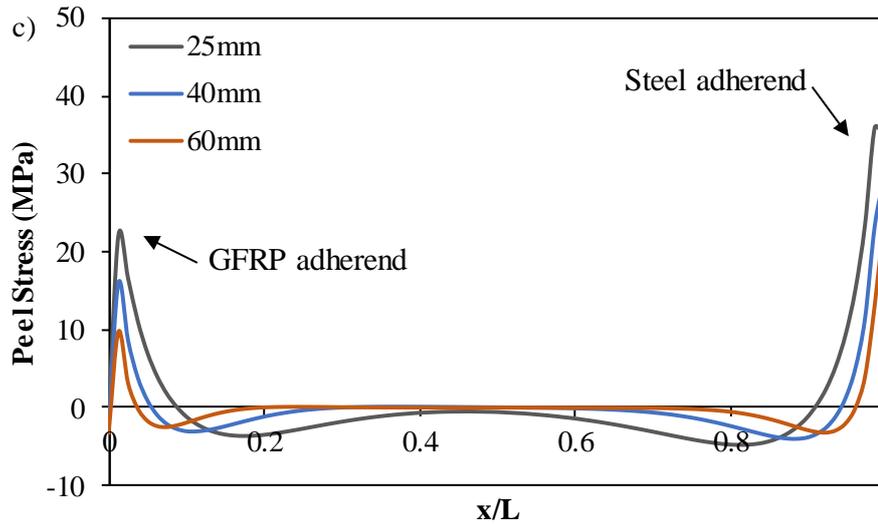
Figure 7.14: Peel stress distribution at the middle of the adhesive layer versus the normalised distance along the overlap length: a) CFRP/Steel, b) GFRP/Aluminium and c) GFRP/Steel.

GFRP/Aluminium joints exhibit higher peel stresses than the other two types of joints and this is due to the lower overall stiffness of the joint. Low adherend stiffness reduces the overall joint stiffness [34] and therefore, joints with stiffer adherends (Table 7.7) exhibit lower peak peel and shear stresses (i.e. GFRP/Aluminium peak stresses > GFRP/Steel peak stresses > CFRP/Steel peak stresses).

Axial Stiffness (N/m)			
Steel	Aluminium	CFRP	GFRP
104851.6	49281.4	30209.28	16702.4

Table 7.7: Axial stiffness of the adherends ($k = AE/L$, where A is the adherend cross-sectional area and L is the adherend length).

7.1.4 Failure Criteria for Metal-to-Composite Single Lap Joints

As in the case of metal-to-metal joints, metal-to-composite joints also exhibit brittle failure initiating at the overlap ends within the adhesive or at the adhesive/adherend interface (see Chapter 6). Maximum peel stresses are therefore used as a failure criterion.

The maximum peel stresses, as obtained from testing CFRP/Steel, GFRP/Aluminium and GFRP/Steel joints with 25mm overlap length and for all adhesive CNT contents, are shown in Table 7.8.

Joints	CNT Weight Fraction of Adhesive	Bulk Adhesive Tensile Strength (MPa)	Avg. Failure Load (N)	Max. Peel Stress (MPa)
CFRP/Steel	0 %	64.0	6380	34.4
	0.1%	62.8	8348	45.0
	0.3 %	52.2	9248	49.9
	0.5%	40.0	6844	36.9
	1%	44.6	7251	39.1
GFRP/Aluminium	0 %	64.0	5793	38.5
	0.1%	62.8	7566	50.3
	0.3 %	52.2	7178	47.7
	0.5%	40.0	8112	53.9
	1%	44.6	5681	37.7
GFRP/Steel	0 %	64.0	8053	47.3
	0.1%	62.8	7549	44.3
	0.3 %	52.2	7949	46.7
	0.5%	40.0	7529	44.2
	1%	44.6	7647	44.9

Table 7.8: Average joint failure load and maximum peel stresses in the adhesive for metal-to-composite joints with 25mm overlap length.

Table 7.8 shows that the strength of CFRP/Steel and GFRP/Aluminium joints increases after the incorporation of MWCNTs in the adhesive. It is also noted that the calculated maximum peel stresses at failure approach the bulk adhesive tensile strength with the increase of the CNT content. This indicates that there is a shift in failure mode, i.e. from adhesive/adherend interfacial failure (white area under red line) to failure within the adhesive (red area), as shown in Figure 7.15.
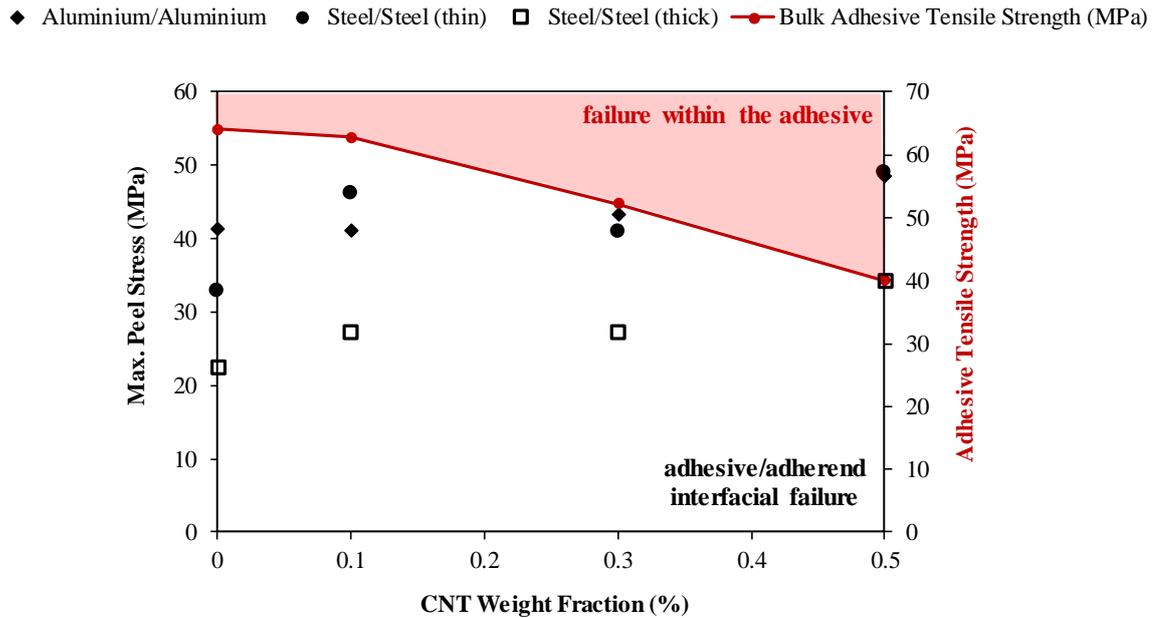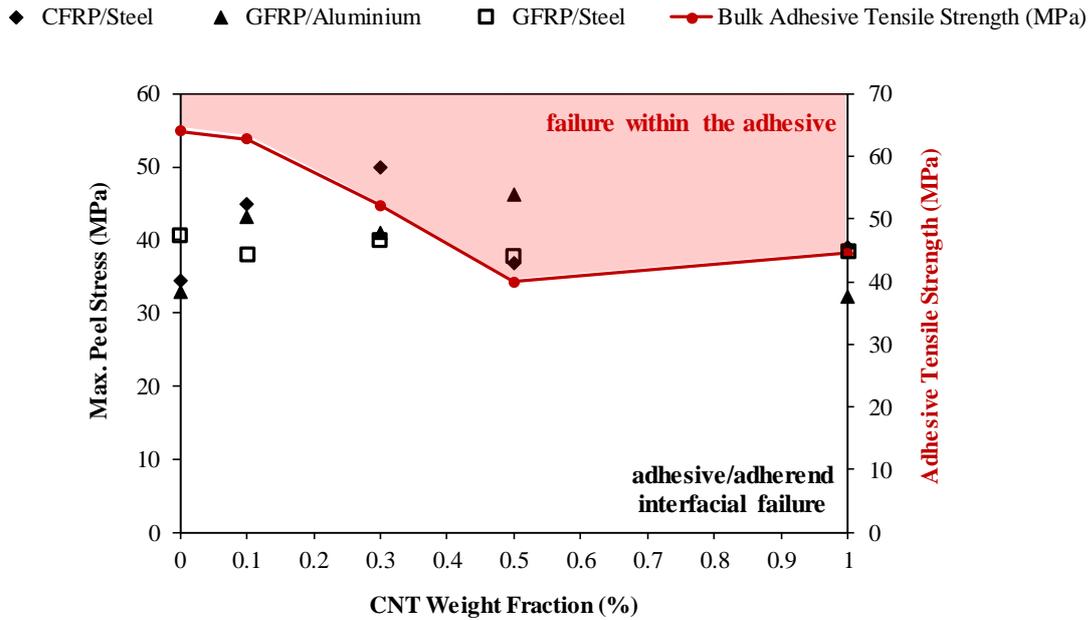
Figure 7.15: Variation of maximum peel stress and bulk adhesive tensile strength for metal-to-composite joint configurations with 25mm overlap length.

However, for the case of GFRP/Steel joints, there is no increase in their failure load with the addition of MWCNTs. This is because the maximum peel stress of the joint with pure epoxy adhesive is already close to the bulk adhesive tensile strength. The further enhancement of the adhesive/adherend interface with the addition of MWCNTs does not lead to increase in joint strength, because the failure is driven by the full utilisation of the adhesive.

The maximum peel stresses, as obtained from testing CFRP/Steel, GFRP/Aluminium and GFRP/Steel joints with 40mm overlap length and for all adhesive CNT contents, are shown in Table 7.9.

Lap Joints	CNT Weight Fraction of Adhesive	Adhesive Tensile Strength (MPa)	Avg. Failure Load (N)	Max. Peel Stress (MPa)
CFRP/Steel	0 %	64.0	9126	42.0
	0.1%	62.8	9618	44.2
	0.3 %	52.2	9308	42.8
GFRP/Aluminium	0 %	64.0	10784	60.0
	0.1%	62.8	10371	57.7
	0.3 %	52.2	10097	56.2
GFRP/Steel	0 %	64.0	10887	52.1

	0.1%	62.8	-	-
	0.3 %	52.2	8740	41.9

Table 7.9: Average joint failure load and maximum peel stresses in the adhesive for metal-to-composite joints with 40mm overlap length.

Table 7.9 shows that the strength of all metal-to-composite joint configurations with 40mm overlap length does not increase after the incorporation of MWCNTs in the adhesive. Due to the fact that the maximum peel stresses of all joints are already close to the bulk adhesive tensile strength, further enhancement of the adhesive/adherend interface via the incorporation of MWCNTs does not increase the joint strength (Figure 7.16).
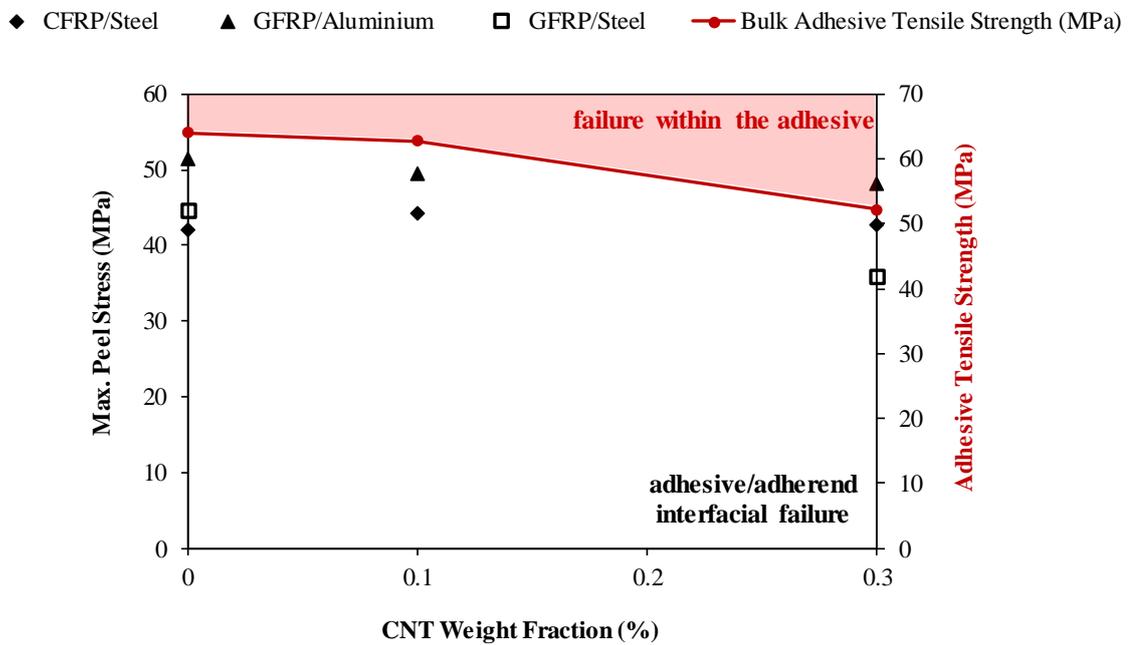
Figure 7.16: Variation of maximum peel stress and bulk adhesive tensile strength for metal-to-composite joint configurations with 40mm overlap length.

The maximum peel stresses as obtained from testing CFRP/Steel, GFRP/Aluminium and GFRP/Steel joints with 60mm overlap length and for all adhesive CNT contents are shown in Table 7.10.

Lap Joints	CNT Weight Fraction of Adhesive	Adhesive Tensile Strength (MPa)	Avg. Failure Load (N)	Max. Peel Stress (MPa)
CFRP/Steel	0 %	64.0	10218	39.3
	0.1%	62.8	10076	38.8
	0.3 %	52.2	10383	40.0
GFRP/Aluminium	0 %	64.0	12546	59.0
	0.1%	62.8	10668	50.1
	0.3 %	52.2	13938	65.5
GFRP/Steel	0 %	64.0	14292	56.2
	0.1%	62.8	-	-
	0.3 %	52.2	11309	44.4

Table 7.10: Average joint failure load and maximum peel stresses in the adhesive for metal-to-composite joints with 60mm overlap length.

Table 7.10 shows that the strength of GFRP/Aluminium and GFRP/Steel joint configurations with 60mm overlap length does not increase after the incorporation of MWCNTs in the adhesive, because the maximum peel stresses of these joints are already close to the bulk adhesive tensile strength (Figure 7.17).
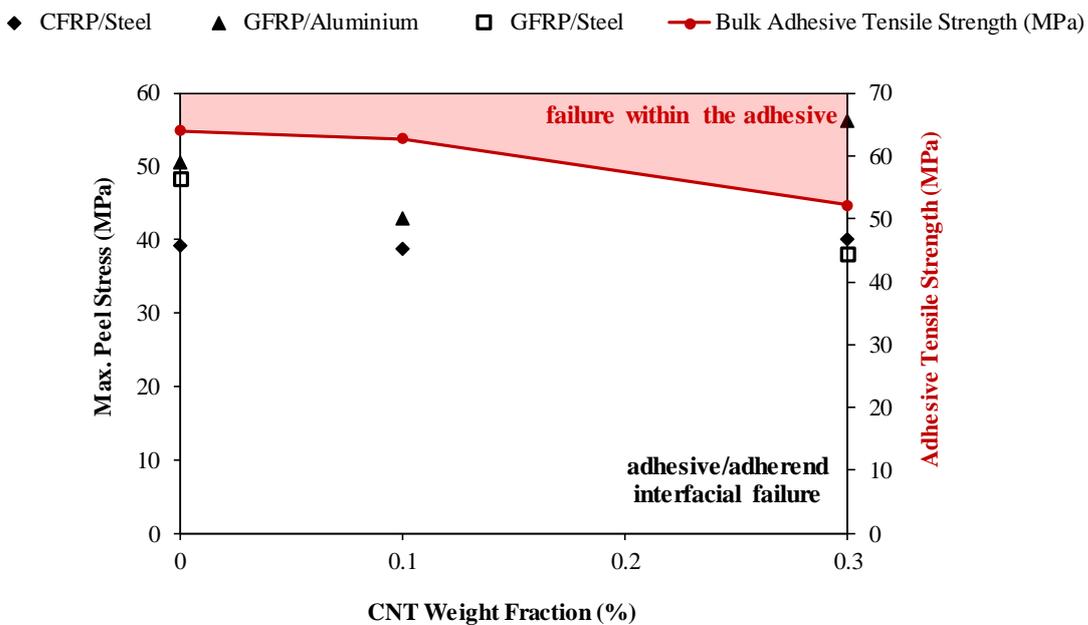
Figure 7.17: Variation of maximum peel stress and bulk adhesive tensile strength for metal-to-composite joint configurations with 60mm overlap length.

Regarding CFRP/Steel joints, the maximum peel stresses are lower than the bulk adhesive tensile strength for all CNT weight fractions. However, the fact that there is no increase in the failure load of these joints with the addition of CNTs indicates that the failure mode is too complex to be predicted via a simple maximum peel stress criterion.

7.2 Strain Energy Release Rate

Mode-I fracture has been investigated in joints bonded with pure epoxy resin and MWCNT filled epoxy resin (see Chapter 6). During the DCB test, opening load is introduced to the specimen and as the load increases, the crack extends. However, when the substrates have different flexural rigidities due to geometric and/or material differences, the DCB specimen does not deform symmetrically (Figure 7.18) and the tensile forces are no longer normal to the crack surface. The fracture mode thus shifts from opening to opening and shearing, i.e. mixed-mode failure [147]. Beam theory or modified beam theory, as proposed in the ISO standard [145], can only be used for the case of pure mode-I. Therefore, virtual crack closure technique (VCCT) is used instead for the calculation of the total strain energy release rate, G, which is the sum of mode-I, G_I and mode-II, G_{II}, energy release rates.
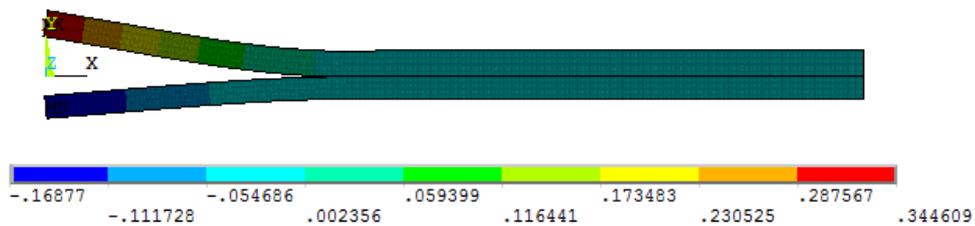
Figure 7.18: Variation of deformation along the y-axis.

The DCB joints are modelled as two-dimensional with plane strain solid elements. The loading and boundary conditions are shown in Figure 7.19.
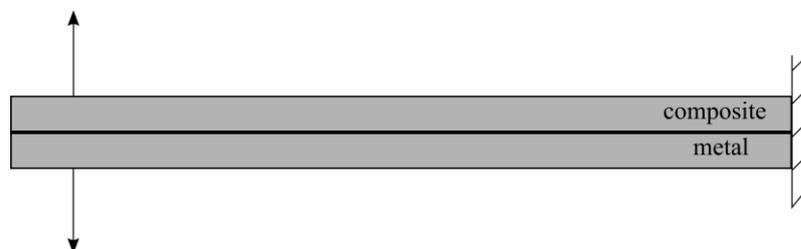
Figure 7.19: Loading and boundary conditions of DCB joint models.

In Figure 7.20, the total strain energy release rate is plotted against the CNT loading of the adhesive used to bond the various substrates.
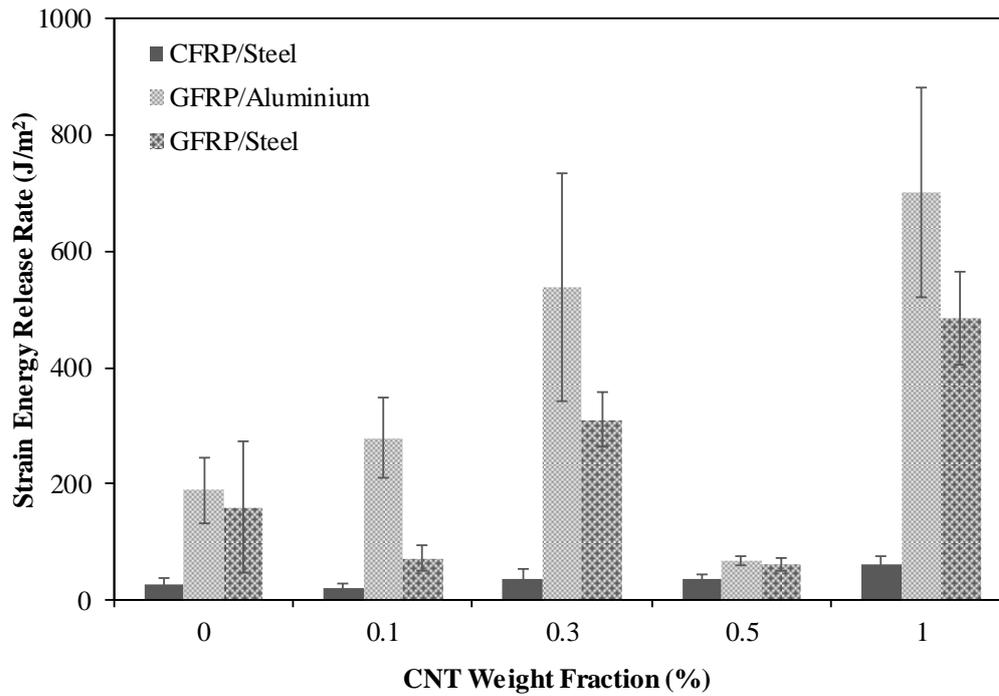
Figure 7.20: SERR versus the CNT weight fraction.

It can be observed that the incorporation of MWCNTs in the epoxy adhesive significantly affects the total SERR for all dissimilar material joints. As the CNT loading increases, the SERR of GFRP/Steel joints increases by 94% for 0.3 wt.% and the GFRP/Aluminium specimens exhibit a noteworthy improvement of 48% and 185% for 0.1 and 0.3 wt.% respectively.

Although the SERR of CFRP/Steel joints is enhanced by 45% for 0.3 and 0.5 wt.%, the obtained values are significantly lower than those of the other two joint configurations. This is an indication of poor adhesion between the steel and CFRP adherends, which has been verified after the visual inspection of the fracture surfaces of the tested specimens (Figure 7.21).
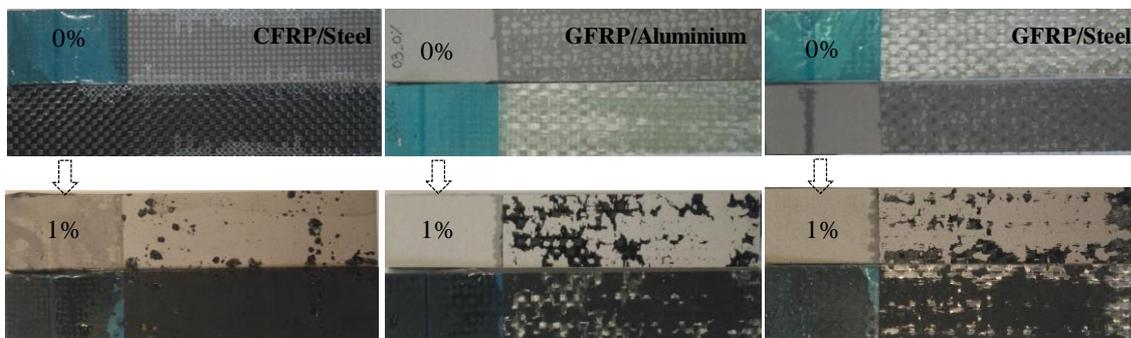
Figure 7.21: Bonding area of CFRP/Steel, GFRP/Aluminium and GFRP/Steel joints after failure.

In Figure 7.21, it can be observed that there is very little adhesive left on the metal substrate of the CFRP/Steel joints as opposed to the other two configurations, where the marks of the adhesive are clear on both adherends. This suggests that the crack that led to the failure of the CFRP/Steel joints propagated mostly through the adhesive and not through the interface. Therefore, any improvement in the adhesive/adherend interface of the CFRP/Steel joints will not result to significant increase in fracture toughness as in the case of GPRP/Aluminium and GFRP/Steel joints.

Significant drop of the SERR values at 0.5wt.% MWCNT content has been obtained for all dissimilar material joints and can be attributed to the low quality of the adhesive. As mentioned previously mechanical stirring and sonication have been used for the adhesive preparation. However, when mechanical stirring is used prior to sonication for high MWCNT weight fractions, such as 0.5wt.% many air bubbles are introduced to the mixture, which are unable to escape because of its high viscosity. Therefore, defects, i.e. as voids and big CNT agglomerations that are present in the adhesive assist the crack propagation and result in very low SERR values. In order to overcome this issue, the manufacturing of the 1 wt.% MWCNT adhesive has been carried out without the utilisation of mechanical stirring, which proved to be beneficial for the joint performance.

The highest SERR is attained for the highest CNT loading investigated in this study. An increase of 138%, 270% and 203% is achieved for the CFRP/Steel, GFRP/Aluminium and GFRP/Steel joints respectively. GFRP/Aluminium joints yield the highest SERR values followed by the GFRP/Steel, whereas the SERR of CFRP/Steel is much lower. This behaviour is a result of the flexural rigidity of the adherends.

In Table 7.11, the flexural rigidity ratio of the adherends used for each joint configuration is shown. The more rigid the adherends, the lower the deformation resulting to low SERR. Therefore, the GFRP/Aluminium joints, which exhibit the lowest ratio, achieve the highest SERR, as already shown in Figure 7.20.

	$EI_{composite\ adherend} / EI_{metal\ adherend}$
CFRP/Steel	0.525
GFRP/Aluminium	0.442
GFRP/Steel	0.453

Table 7.11: Flexural rigidity ratio of dissimilar material joints.

Finally, the total SERR obtained from FEA is compared to the SERR calculated using beam theory (G_{BT}) and the equation proposed by Soboyejo et al. [148]. According to this equation, the adherends of the DCB specimen are treated as separate cantilever beams and the strain energy release rate for mode-I is given by:

$$G_{TH} = \frac{6P^2a^2}{E_C b^2 t_C^3}\left(1 + \frac{1}{\beta_{CM}\beta_t^3}\right)(6)$$

$$\beta_{CM} = \frac{E_M}{E_C}\ (7)\ \text{ and }\ \beta_t = \frac{t_M}{t_C}\ (8)$$

Where, E_M and E_C are the Young's moduli of metal and composite adherends respectively, a is the crack length and b is specimen width. β_{CM} is the stiffness ratio between metal and composite substrates and β_t is the thickness ratio.

The results of the average SERR (in J/m^2) at the middle of the adhesive layer are summarised in Table 7.12.

CNT Weight Fraction (%)	CFRP/Steel			GFRP/Aluminium			GFRP/Steel		
	G_{FEA}	G_{BT}	G_{TH}	G_{FEA}	G_{BT}	G_{TH}	G_{FEA}	G_{BT}	G_{TH}
0	25.7	43.3	36.6	188.3	309.6	265.9	159.7	323	278.8
0.1	19.1	32.2	26.8	278.7	462.06	404.6	72.01	142.1	133.6
0.3	37.3	62.1	54.2	537.3	896.3	765.7	309.9	632.2	546.7
0.5	37.4	61.7	54.7	67.04	108.07	97.3	61.7	123.4	114.0
1	61.3	101.1	90.1	701.8	1177.7	1006.1	485.	991.4	887.3

Table 7.12: SERR obtained from FEA, beam theory and Soboyejo's equation.

The SERR calculated using the beam theory shows a large discrepancy from the FEA results for all joint configurations (Figure 7.22).
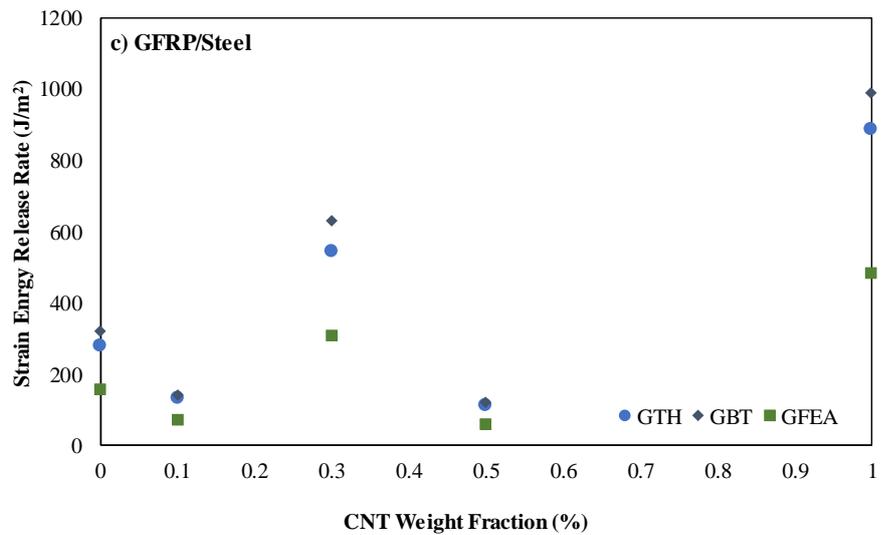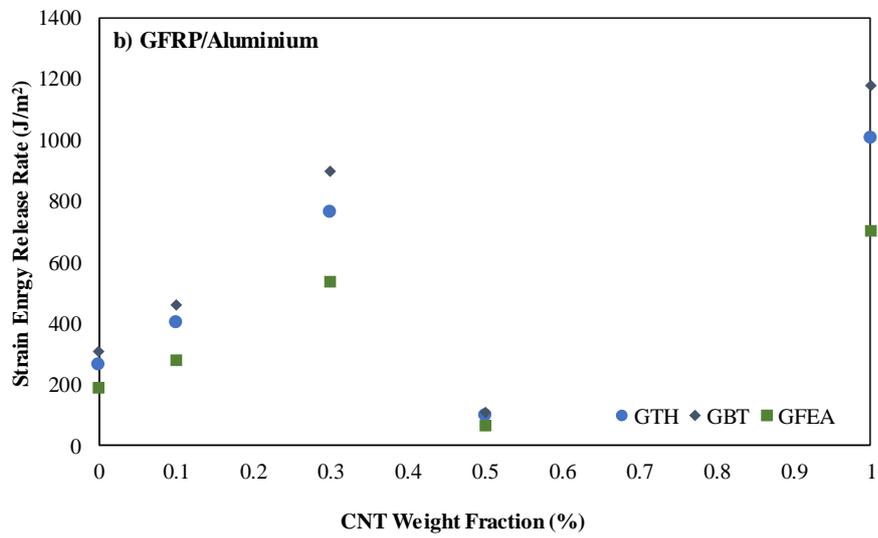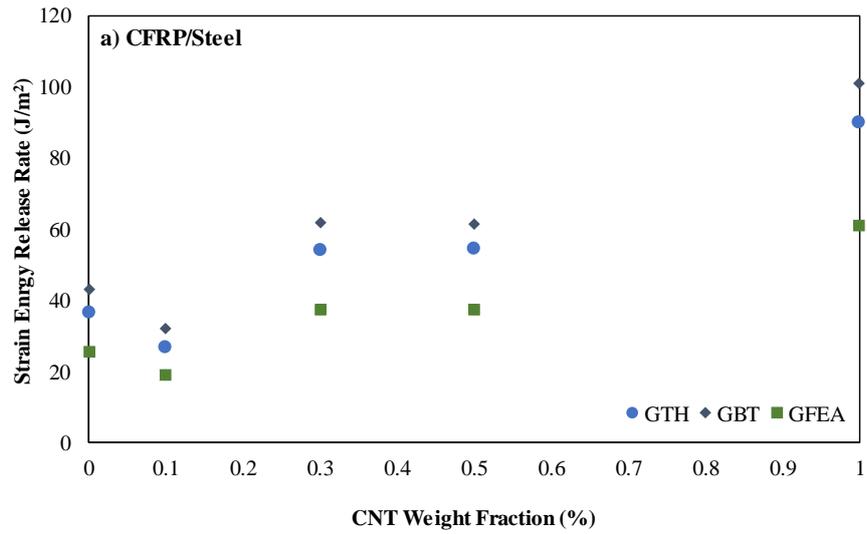
Figure 7.22: SERR of: a) CFRP/Steel, b) GFRP/Aluminium and c) GFRP/Steel joints versus the CNT weight fraction.

Although Soboyejo's equation [148] takes into account the stiffness of the substrates, it still overestimates the SERR compared to the FEA results. Both theoretical methods do not agree with the FEA results due to the fact that dissimilar material joints are under mixed-mode loading, i.e. coupling of tensile and shear deformations and therefore, mode-II SERR has to be also taken into account for the calculation of the total SERR.

7.3 Conclusions

A simple maximum peel stress criterion in conjunction with FEA analyses has been employed to assess the strength of a wide range of joint configurations, whereby different adherend materials, overlap lengths and adhesives with various CNT weight fractions have been used. Albeit not applicable for all joint configurations, this simple stress criterion provides a means to determine whether joints fail due to the full utilisation of the adhesive strength (i.e. adhesive failure mode) or earlier, which is most possibly an indication of poor adhesive/adherend interfacial strength (i.e. adhesive/adherend interfacial failure mode). The incorporation of MWCNTs in most of the joint configurations studied here indicates that there is a shift from adhesive/adherend interfacial failure mode to failure within the adhesive resulting in increased joint strengths.

Finally, the effect of MWCNTs on dissimilar material joints loaded in mixed-mode has been also studied. The crack length and the respective load values obtained from the DCB tests have been utilised for the calculation of the total strain energy release rate (SERR) via the VCCT method. As the CNT loading increases, the total strain energy release rate of all joints increases. The highest SERR is attained for 1 wt.% of CNT loading and increases by 138%, 270% and 203% for the CFRP/Steel, GFRP/Aluminium and GFRP/Steel joints respectively.

Chapter 8. Conclusions and Future Work

8.1 Summary

The incorporation of MWCNTs in the epoxy adhesive as an alternative method of improving the quality of dissimilar material bonded joints has been investigated. This study can be divided into three parts. In the first part, the characterisation of MWCNT reinforced composites is undertaken in order evaluate their properties. Different mixing methods are employed in order to obtain homogeneous dispersion of the nanofillers in the epoxy resin. The effect of the CNT loading (0, 0.1, 0.3, 0.5 and 1 wt.%) in respect to the mechanical properties is also assessed. After the completion of the first part, metal-to-metal single lap joints (Steel/Steel and Aluminium/Aluminium) are manufactured. Substrate surface preparation, which is the key factor for the realisation of durable joints is optimised and the failure loads obtained for the various CNT loadings of the epoxy adhesive are compared. The third and final part of this study is the fabrication of co-cured dissimilar material joints (CFRP/Steel, GFRP/Aluminium and GFRP/Steel), which are prepared with the surface preparation method determined previously and bonded with MWCNT reinforced epoxy adhesives, the manufacturing process of which has been optimised in the first part. The findings of this research are summarised below.

8.2 Conclusions

8.2.1 MWCNT filled Composites

Two epoxy resin systems have been investigated: RS and TW epoxy resin. TW/epoxy composites of 0.03, 0.1 and 0.3 wt.% have been fabricated using ultrasonication. It has been found that the addition of 0.03 wt.% CNT results in mechanical properties almost equal to pure epoxy resin. A further increase of the CNT content leads to significant reduction of the tensile and flexural strength despite the increase of sonication time from 15min to 30min. The poor mechanical performance of the nanocomposites is attributed to inhomogeneous dispersion and entrapped air in the CNT mixture that is impossible to remove because of the very high viscosity of the epoxy resin. Due to the problems occurring during the manufacturing process of TW epoxy resin, a second epoxy resin system with longer pot life and lower viscosity has been studied.

For the case of the RS epoxy resin system, various parameters, such as mixing time, dispersion techniques and CNT loadings have been evaluated via tensile, 3-point bend and

single edge notched beam tests. The variation of sonication time (15, 30 and 60min) shows a minimal effect on the mechanical properties suggesting that the dominant factor that influences the composite performance is the CNT loading. When the CNT content is up to 0.1 wt.%, the tensile strength exhibits almost similar values to the pure epoxy resin, whereas the modulus shows a moderate increase. However, increase of the CNT loading to 1 wt.% leads to the reduction of the mechanical properties suggesting that ultrasonication cannot manage to break completely the agglomerates, which later act as stress concentrators.

Ultrasonication has been also combined with mechanical stirring to enhance dispersion for higher CNT loadings and then, compared to the third dispersion method employed in this research work, ball milling. Young's modulus exhibits a marginal increase with the increase of the CNT loading for all dispersion methods. This finding indicates that sufficient load transfer between the matrix and the CNTs is achieved. Tensile and flexural strength almost remain unaffected up to 0.2 wt.% when either sonication or mechanical stirring/sonication are employed. The advantage of the utilisation of mechanical stirring prior to sonication is shown for the case of 0.3 wt.%, where it results in enhanced tensile strength. However, further increase of the loading to 0.5 wt.% leads to the reduction of the strength. The degradation of the tensile strength of nanocomposites with weight fractions up to 0.5% is avoided only when ball milling is employed,. The experimental results also reveal that the increase of the CNT content to 1 wt.% degrades the tensile and flexural properties for all dispersion methods due to increased agglomeration and void formation that lead to premature failure.

The images obtained from TEM complemented the experimental results. There is a noteworthy increase of the number and size of agglomerates when the CNT content increases. However, sonication seems to have an advantage over ball milling, since the CNTs exhibit more uniform particle distribution across the length and width of the samples. Another interesting finding is that although 1 wt.% CNT reinforced epoxy contain the highest number of defects causing significant deterioration of the tensile and flexural properties, it exhibits improvement in fracture toughness. This can be explained by the fact that due to the phenomenon of aggregation, CNT bundles of different sizes compensate for the imperfections and give rise to toughening mechanisms, such as pull-out.

Dispersion has been also assessed using DSC method according to which the total heat of cure is associated to the degree of dispersion. It has been found that the most homogeneous dispersion is achieved for 0.3 wt.% CNT content, where the individual MWCNTs act as hindrance to the cross-linking reaction and thus, reduce the heat of reaction. On the other

hand, the addition of 1 wt.% of CNTs in the matrix leads to the increase of agglomerates, which are much less efficient in blocking the chemical reactions, so higher values for the total heat of reaction are obtained. In addition, the shift of the exothermic reaction peak to lower temperatures after the incorporation of CNTs in the epoxy resin confirms previous studies according to which CNTs act as catalysts and accelerate the cure reaction. Finally, the addition of nanotubes does not significantly affect the glass transition temperature suggesting that although CNTs accelerate the cure reaction, they do not alter the overall degree of cure.

To conclude, none of the aforementioned methods managed to improve the mechanical properties of the nanocomposites, which verifies previous evidence that homogeneous dispersion and high interfacial strength between the matrix and the filler need to be ensured in order to transfer the exceptional properties of CNTs to the nano-modified composites. Nonetheless, such imperfections are proved to trigger energy dissipation mechanisms increasing thus the fracture toughness.

8.2.2 Metal-to-Metal Joints

For both types of metal-to-metal joints, namely Steel/Steel and Aluminium/Aluminium, the highest load bearing capacity is obtained when grit blasting is utilised and hence, it is the method also used for the fabrication of the co-cured dissimilar material joints. Despite the fact that the surface treatment is more prominent than the adhesive composition, the toughening effect of MWCNTs is also observed. For the grit blasted joints, the moderate increase of the joint strength with the increase of CNT weight fraction suggests that CNTs can positively affect the joint integrity via the increase of adhesive/adherend interfacial strength. However, this positive effect is only evident when the substrate surface preparation is optimised.

8.2.3 Metal-to-Composite Joints

The optimised surface preparation method and the MWCNT/epoxy adhesives are finally implemented into the manufacturing of co-cured dissimilar material joints. The variation of the overlap length and joint stiffness with respect to the CNT loading has been investigated.

This study has also confirmed the increase of the failure load with the increase of the overlap length for all joint configurations. The incorporation of MWCNTs in the epoxy resin adhesive is shown to increase the load bearing capacity of CFRP/Steel and GFRP/Aluminium single lap joints with 25mm overlap length. This is because for these joint configurations, the increase of CNT weight fraction results in a shift from adhesive/adherend interfacial failure to failure within the adhesive. On the contrary, GFRP/Steel joints do not show any improvement

after the addition of MWCNTs in the epoxy resin adhesive. This is most probably because these joints fail within the adhesive and hence, any enhancement in the adhesive/adherend interfacial strength through MWCNTs will not result in further improvement of the joint strength.

The effect of MWCNTs on dissimilar material joints loaded in mixed-mode has been also studied. As the CNT loading increases, the total strain energy release rate (SERR) of all joints increases. The highest SERR is attained for 1 wt.% of CNT loading and increases by 138%, 270% and 203% for the CFRP/Steel, GFRP/Aluminium and GFRP/Steel joints respectively.

One of the most significant findings of this study is the use of a simple failure criterion to determine the failure mode of dissimilar material adhesively bonded joints. Maximum peel stress criterion in conjunction with FEA analyses have been employed to assess the strength of a wide range of joint configurations, whereby different adherend materials, overlap lengths and adhesives with various CNT weight fractions have been used. Albeit not applicable for all joint configurations, this simple stress criterion provides a means to determine whether joints fail due to the full utilisation of the adhesive strength (i.e. failure within the adhesive) or earlier, which is most possibly an indication of poor adhesive/adherend interfacial strength (i.e. adhesive/adherend interfacial failure mode). The incorporation of MWCNTs in most of the joint configurations studied here indicates that there is a shift from adhesive/adherend interfacial failure mode to failure within the adhesive resulting in increased joint strengths.

In conclusion, a systematic and comprehensive study where experiments of the bulk adhesive (pure epoxy resin) and the adhesive reinforced with CNTs up to the joint structure have been performed in combination with FEA that shed light into the failure mode investigation. The strength of the adhesive/adherend interface is the main parameter defining the joint strength. Hence, optimisation of the substrate surface preparation and incorporation of CNTs in the adhesive/adherend interface can improve significantly the joint strength of metal-to-metal and metal-to-composite joints.

8.3 Future Work

The aforementioned findings provide insights for future research on the issues encountered in this study and also, additional ideas for further development on the following areas:

- Dispersion

- CNT/matrix interfacial adhesion

- CNTs used for damage sensing

- Effect of substrate surface preparation on different alloys

8.3.1 Dispersion

Various dispersion methods have been investigated in this study, such as sonication, mechanical stirring, ball milling and combination of those in order to prevent CNTs from clustering together. However, the phenomenon of aggregation was evident in all loadings examined. Calendering process has been employed by many researchers in order to disperse CNTs in epoxy matrix. In the majority of the articles, significant superiority of this dispersion method over sonication and high shear mixing has been reported, where the nanocomposites exhibit improved mechanical, electrical [115] and thermal properties. Gojny et al. [7] found that when calendering was employed, only some small agglomerates with exfoliated structure were observed, whereas after sonication the agglomerates did not exfoliate and maintained their condensed structure. Therefore, further investigation and experimentation into this dispersion technique is strongly recommended.

8.3.2 CNT/matrix Interfacial Adhesion

Apart from poor dispersion leading to no significant enhancement of the mechanical properties of the fabricated nanocomposites (as presented in Chapter 4), the lack of CNT/matrix interfacial adhesion, which is critical for load transfer, also affected the properties. A means to overcome these issues is the use of oxidative treatments that can improve the chemical compatibility between the matrix and the CNT fillers as well as dispersion. In [92] the dispersion of multi-walled carbon nanotubes was improved by the use of trifluoroacetic acid (TFA) as a co-solvent. The manufactured nanocomposites exhibited an extremely low percolation threshold of less than 0.006 wt.% MWCNT content, which is also an indication of improved dispersion. In [149], triethylenetetramine grafting was carried out creating athin layer on the MWCNT surface that contributed to homogenous dispersion and improvement of the MWCNT/epoxy interfacial interaction. Impact strength, bending strength and thermal conductivity were also enhanced. In [150], [151] and [152], it was shown that functionalised carbon nanotubes can efficiently enhance dispersion via chemical bonding to the epoxy resin. A strong correlation exists between the functionalisation, dispersion, wettability and re-agglomeration behaviour of CNTs and the mechanical properties of CNT/epoxy nanocomposites.

Additional work should therefore be done to establish whether CNT functionalisation can enhance the bond between the matrix and the fillers and consequently, the joint performance.

8.3.3 CNTs used for damage sensing

The electrical conductivity of MWCNTs would be also a useful property to explore. An additional advantage of CNTs due to their conductive nature is the potential to detect failure if conductive networks of carbon nanotubes are introduced to the composite substrate as well as the epoxy adhesive in similar or dissimilar (composite-to-metal) material joints. In situ electrical resistance measurements in conductive composites and adhesives can provide quantitative evidence of damage and can be also correlated with different damage modes [153]. The crack propagation can be therefore monitored by in-situ monitoring of the electrical resistance of the joint area. In [154], it was shown that different failure mechanisms of single lap joints possess a distinct resistance response, hence proving the ability to not only sense failure in situ, but also to distinguish the extent and nature of damage.

If successful implementation of this conductive CNT network to the composites and adhesives used for DCB tests is achieved, MWCNTs would not only be able to improve fracture toughness, but also detect failure real time.

8.3.4 Effect of Substrate Surface Preparation on Different Alloys

The joint manufacturing of all joints in this research work has been conducted by using only one type of steel and aluminium. Further research could be undertaken to fully understand whether the experimental results would differ if different metal alloys were utilised.

Substrate surface preparation, which the most important process step governing the quality of an adhesively bonded joints [155], could be either mechanical or chemical affecting not only the roughness, but also altering the composition of the alloys and hence, the bond strength of the joints. For instance, the effect of pre-treatments applied on the surface characteristics of aluminium substrates and on the adhesive strength of epoxy/aluminium joints was studied in [156]. The variation of the density, composition and aspect of the adherends were analysed as a function of the applied pre-treatment. Two different aluminium alloys were used, A1050 and A2024 in order to investigate the influence of the alloying elements. The etching treatment was found to affect the thickness, composition, aspect and porosity of the oxide layer formed, which also depend on the alloy nature. The presence of elements, such as Cu or Mg, enhanced the corrosion processes due to the different electrochemical potential of elements or intermetallic compounds formed. On the other hand, when abrasion was

employed, the adherends presented the same density as the non-treated ones. This is because the abrasion process is a mechanical treatment that increases the surface roughness without modifying the porosity or composition of the samples, also shown in [157]. For the mechanical treatments it has been concluded that the lower hardness of the metal, the higher roughness achieved (up to a threshold) and thus, higher bond strength values.

References

1. *MODERN AIRLINERS.* (http://www.modernairliners.com/boeing-787-dreamliner/boeing-787-dreamliner-specs/).
2. *Visby-class corvette.* (By Xiziz (talk) - I created this work entirely by myself., CC BY-SA 3.0, https://commons.wikimedia.org/w/index.php?curid=10071787).
3. *La Fayette-class frigate.* ({{GFDL}}Courtesy and autorisation of NetMarine.net).
4. Zhou, Y., et al., *Improvement in electrical, thermal and mechanical properties of epoxy by filling carbon nanotube.* Express polymer letters, 2008. **2**(1): p. 40-48.
5. Yu, N., Z.H. Zhang, and S.Y. He, *Fracture toughness and fatigue life of MWCNT/epoxy composites.* Materials Science and Engineering: A, 2008. **494**(1-2): p. 380-384.
6. Lau, K., et al., *Thermal and mechanical properties of single-walled carbon nanotube bundle-reinforced epoxy nanocomposites: the role of solvent for nanotube dispersion.* Composites Science and Technology, 2005. **65**(5): p. 719-725.
7. Gojny, F., et al., *Carbon nanotube-reinforced epoxy-composites: enhanced stiffness and fracture toughness at low nanotube content.* Composites science and technology, 2004. **64**(15): p. 2363-2371.
8. Srivastava, V.K., *Effect of carbon nanotubes on the strength of adhesive lap joints of C/C and C/C–SiC ceramic fibre composites.* International Journal of Adhesion and Adhesives, 2011. **31**(6): p. 486-489.
9. Kwon, Y.W., et al., *Enhancement of composite scarf joint interface strength through carbon nanotube reinforcement.* Journal of materials science, 2008. **43**(20): p. 6695-6703.
10. Yu, S., M.N. Tong, and G. Critchlow, *Use of carbon nanotubes reinforced epoxy as adhesives to join aluminum plates.* Materials & Design, 2010. **31, Supplement 1**(0): p. S126-S129.
11. Meguid, S.A. and Y. Sun, *On the tensile and shear strength of nano-reinforced composite interfaces.* Materials & Design, 2004. **25**(4): p. 289-296.
12. Matthews, F.L., P.F. Kilty, and E.W. Godwin, *A review of the strength of joints in fibre-reinforced plastics. Part 2. Adhesively bonded joints.* Composites, 1982. **13**(1): p. 29-37.
13. *Module 10: Special Topics, Learning Unit-1: M10.1 Mechanical Testing of Composites.* p. 16-26.
14. da Silva, L.F., A. Öchsner, and R.D. Adams, *Handbook of adhesion technology.* 2011: Springer Science & Business Media.
15. Adams, R.D., J. Comyn, and W.C. Wake, *Structural adhesive joints in engineering.* 1997: Springer Science & Business Media.
16. Banea, M.D. and L.F.M. Da Silva, *Adhesively bonded joints in composite materials: an overview.* Proceedings of the Institution of Mechanical Engineers, Part L: Journal of Materials Design and Applications, 2009. **223**(1): p. 1-18.
17. Quini, J.G. and G. Marinucci, *Polyurethane structural adhesives applied in automotive composite joints.* Materials Research, 2012. **15**(3): p. 434-439.
18. Khalili, S.M.R., et al., *Experimental study of the influence of adhesive reinforcement in lap joints for composite structures subjected to mechanical loads.* International Journal of Adhesion and Adhesives, 2008. **28**(8): p. 436-444.
19. Lucas F M da Silva, J.E.R., M V Figueiredo, and T R Strohaecker, *Influence of the Adhesive, the Adherend and the Overlap on the Single Lap Shear Strength.* Journal of Adhesion and Interface, 2006. **7**(4).
20. Banea, M.D. and L.F.M. da Silva, *Mechanical Characterization of Flexible Adhesives.* The Journal of Adhesion, 2009. **85**(4-5): p. 261-285.
21. da Silva, L.F.M., et al., *Effect of material, geometry, surface treatment and environment on the shear strength of single lap joints.* International Journal of Adhesion and Adhesives, 2009. **29**(6): p. 621-632.
22. V. A. Karatzas, Y.Z., N. G. Tsouvalis, M. K. Chryssanthopoulos, *A Parametric Investigation of the response of directly laminated Composite-to-metal Single lap joints.* ECCM-15, European Conference on Composite Materials, 2012.

23. Song, M.-G., et al., *Effect of manufacturing methods on the shear strength of composite single-lap bonded joints.* Composite Structures, 2010. **92**(9): p. 2194-2202.

24. Lucić, M., A. Stoić, and J. Kopač, *Investigation of aluminum single lap adhesively bonded joints.* Journal of Achievements in Materials and Manufacturing Engineering, 2006. **15**(1-2): p. 79-87.

25. Seong, M.-S., et al., *A parametric study on the failure of bonded single-lap joints of carbon composite and aluminum.* Composite Structures, 2008. **86**(1–3): p. 135-145.

26. Crocombe, A.D., Int. J. Adhes. Adhes., 1989(9): p. 145–153.

27. da Silva, L.F.M., et al., *Effect of Adhesive Type and Thickness on the Lap Shear Strength.* The Journal of Adhesion, 2006. **82**(11): p. 1091-1115.

28. Arenas, J.M., J.J. Narbón, and C. Alía, *Optimum adhesive thickness in structural adhesives joints using statistical techniques based on Weibull distribution.* International Journal of Adhesion and Adhesives, 2010. **30**(3): p. 160-165.

29. Bak, K.M., et al., *Effect of Adhesive Thickness Area of Single Lap Joints in Composite Laminate Using Acoustic Emission Technique and FEA.* Insight-Non-Destructive Testing and Condition Monitoring, 2012.

30. Davies, P., et al., *Influence of adhesive bond line thickness on joint strength.* International Journal of Adhesion and Adhesives, 2009. **29**(7): p. 724-736.

31. Pires, I., et al., *Performance of bi-adhesive bonded aluminium lap joints.* International Journal of Adhesion and Adhesives, 2003. **23**(3): p. 215-223.

32. Gledhill RA, S.S., Tod DA. , Int J Adhes Adhes 1990(10): p. 192.

33. Pinto, A.M.G., et al., *Single-Lap Joints of Similar and Dissimilar Adherends Bonded with an Acrylic Adhesive.* The Journal of Adhesion, 2009. **85**(6): p. 351-376.

34. Owens, J.F.P. and P. Lee-Sullivan, *Stiffness behaviour due to fracture in adhesively bonded composite-to-aluminum joints II. Experimental.* International Journal of Adhesion and Adhesives, 2000. **20**(1): p. 47-58.

35. Anyfantis, K.N. and N.G. Tsouvalis, *Loading and fracture response of CFRP-to-steel adhesively bonded joints with thick adherents–Part I: Experiments.* Composite Structures, 2013. **96**: p. 850-857.

36. Tsai, M.Y., J. Morton, and F.L. Matthews, *Experimental and numerical studies of a laminated composite single-lap adhesive joint.* Journal of Composite Materials, 1995. **29**(9): p. 1254-1275.

37. Lang, T.P. and P.K. Mallick, *Effect of spew geometry on stresses in single lap adhesive joints.* International Journal of Adhesion and Adhesives, 1998. **18**(3): p. 167-177.

38. Da Silva, L.F.M. and R.D. Adams, *Techniques to reduce the peel stresses in adhesive joints with composites.* International Journal of Adhesion and Adhesives, 2007. **27**(3): p. 227-235.

39. Mazza, J.J.A., Jason B. ; Kuhbander, Ronald J., *Grit-Blast/Silane (GBS) Aluminum Surface Preparation for Structural Adhesive Bonding.* 2003: p. 69.

40. Venables, J.D., et al., *Oxide morphologies on aluminum prepared for adhesive bonding.* Applications of Surface Science, 1979. **3**(1): p. 88-98.

41. Smith, C.J.E., *Advances in protective coatings and processes for aerospace applications.* Aircraft Engineering and Aerospace Technology, 1995. **67**(5): p. 13-16.

42. Davis, G., et al., *Application of surface behaviour diagrams to the study of hydration of phosphoric acid-anodized aluminium.* Journal of Materials Science, 1982. **17**(6): p. 1807-1818.

43. Venables, J.D., *Adhesion and durability of metal-polymer bonds.* Journal of Materials Science, 1984. **19**(8): p. 2431-2453.

44. Bjørgum, A., F. Lapique, and J. Walmsley, *AC anodising as pre-treatment prior to adhesive bonding of aluminium.* 2004.

45. Shin, K.C. and J.J. Lee, *Effects of manufacturing parameters on the tensile load bearing capacity of a co-cured single lap joint.* J Mater Process Technol, 2003. **138**(1-3): p. 89-96.

46. Park, Y.-B., et al., *Strength of carbon/epoxy composite single-lap bonded joints in various environmental conditions.* Composite Structures, 2010. **92**(9): p. 2173-2180.

47. Kim, K.-S., et al., *Failure mode and strength of uni-directional composite single lap bonded joints with different bonding methods.* Composite structures, 2006. **72**(4): p. 477-485.

48. Demczyk, B.G., et al., *Direct mechanical measurement of the tensile strength and elastic modulus of multiwalled carbon nanotubes.* Materials Science and Engineering: A, 2002. **334**(1–2): p. 173-178.

49.	Hedia, H.S., et al., *The influence of nanoadhesives on the tensile properties and Mode-I fracture toughness of bonded joints.* Engineering Fracture Mechanics, 2006. **73**(13): p. 1826-1832.

50.	Gude, M.R., et al., *Mode-I adhesive fracture energy of carbon fibre composite joints with nanoreinforced epoxy adhesives.* International Journal of Adhesion and Adhesives, 2011. **31**(7): p. 695-703.

51.	Hsiao, K.-T., J. Alms, and S.G. Advani, *Use of epoxy/multiwalled carbon nanotubes as adhesives to join graphite fibre reinforced polymer composites.* Nanotechnology, 2003. **14**(7): p. 791.

52.	Goh, C., et al. *The Influence of Nanofillers and Additives on the Adhesion Strength of Aluminum.* in *ASME 2010 International Mechanical Engineering Congress and Exposition.* 2010. American Society of Mechanical Engineers.

53.	Kahraman, R., M. Sunar, and B. Yilbas, *Influence of adhesive thickness and filler content on the mechanical performance of aluminum single-lap joints bonded with aluminum powder filled epoxy adhesive.* Journal of Materials Processing Technology, 2008. **205**(1–3): p. 183-189.

54.	Carbas, R., L. da Silva, and L. Andrés, *Functionally graded adhesive joints by graded mixing of nanoparticles.* International Journal of Adhesion and Adhesives, 2017.

55.	Kang, M.-H., J.-H. Choi, and J.-H. Kweon, *Fatigue life evaluation and crack detection of the adhesive joint with carbon nanotubes.* Composite Structures, 2014. **108**: p. 417-422.

56.	Burkholder, G.L., Y.W. Kwon, and R.D. Pollak, *Effect of carbon nanotube reinforcement on fracture strength of composite adhesive joints.* Journal of materials science, 2011. **46**(10): p. 3370-3377.

57.	da Silva, L.F.M., et al., *Analytical models of adhesively bonded joints—Part I: Literature survey.* International Journal of Adhesion and Adhesives, 2009. **29**(3): p. 319-330.

58.	da Silva, L.F.M., et al., *Analytical models of adhesively bonded joints—Part II: Comparative study.* International Journal of Adhesion and Adhesives, 2009. **29**(3): p. 331-341.

59.	He, X., *A review of finite element analysis of adhesively bonded joints.* International Journal of Adhesion and Adhesives, 2011. **31**(4): p. 248-264.

60.	da Silva, L.F.M. and A. Öchsner, *Modeling of adhesively bonded joints.* 2008: Springer.

61.	Volkersen, O., *Die Nietkraft Verteilung in Zugbeanspruchten mit Konstanten Laschenquerschritten.* Luftfahrtforschung, 1938(15): p. 41-47.

62.	Goland, M., and, Reissner, E. , *The stresses in cemented joints.* J. Appl. Mech., 1944. **Trans ASME**(66): p. A17-A27.

63.	Hart-Smith, L.J., *Adhesive-bonded single-lap joints.* 1973: Citeseer.

64.	Renton, W.J. and J.R. Vinson, *The efficient design of adhesive bonded joints.* The Journal of Adhesion, 1975. **7**(3): p. 175-193.

65.	Srinivas, S., *Analysis of Bonded Joints.* 1975, DTIC Document.

66.	Allman, D., *A theory for elastic stresses in adhesive bonded lap joints.* The Quarterly journal of mechanics and applied mathematics, 1977. **30**(4): p. 415-436.

67.	Adams, R. and V. Mallick, *A method for the stress analysis of lap joints.* The Journal of Adhesion, 1992. **38**(3-4): p. 199-217.

68.	Broughton, W., L. Crocker, and J. Urquhart, *Strength of adhesive joints: a parametric study.* 2001: National Physical Laboratory.

69.	Rodríguez, R.Q., et al., *Failure criteria for adhesively bonded joints.* International Journal of Adhesion and Adhesives, 2012. **37**: p. 26-36.

70.	Martiny, P., et al., *A maximum stress at a distance criterion for the prediction of crack propagation in adhesively-bonded joints.* Engineering Fracture Mechanics, 2013. **97**: p. 105-135.

71.	Reedy, E. and T. Guess, *Comparison of butt tensile strength data with interface corner stress intensity factor prediction.* International Journal of Solids and Structures, 1993. **30**(21): p. 2929-2936.

72.	Bogy, D.B., *Edge-Bonded Dissimilar Orthogonal Elastic Wedges Under Normal and Shear Loading.* Journal of Applied Mechanics, 1968. **35**(3): p. 460-466.

73.	Irwin, G.R., *Fracture dynamics.* Fracturing of metals, 1948. **147**: p. 166.

74.	Orowan, E., *Fracture and Strength of Solids.* Reports on Progress in Physics, 1948. **XII**: p. 185-232.

75.	Roylance, D., *Introduction to fracture mechanics.* Massachusetts Institute of Technology, Cambridge, 2001.

76. Gadala, M.S., *Chapter-3: Fatigue & Fracture Considerations in Design.* Mech-326: Mechanical Design-II, 2005.

77. Anyfantis, K.N. and N.G. Tsouvalis, *Loading and fracture response of CFRP-to-steel adhesively bonded joints with thick adherents–Part II: Numerical simulation.* Composite structures, 2013. **96**: p. 858-868.

78. Lin, G., *Crack growth simulation with VCCT technique in ANSYS.* 2011(ANSYS, Inc).

79. Sun, H., S. Rajendran, and D. Song. *Finite Element Analysis on delamination fracture toughness of composite specimens.* in *Proceedings of 2nd Asian ANSYS User Conference.* 1998.

80. Krueger, R., *Virtual crack closure technique: history, approach, and applications.* Applied Mechanics Reviews, 2004. **57**(2): p. 109-143.

81. Williams, J.G. and H. Hadavinia, *Analytical solutions for cohesive zone models.* Journal of the Mechanics and Physics of Solids, 2002. **50**(4): p. 809-825.

82. Blackman, B.R., et al., *The use of a cohesive zone model to study the fracture of fibre composites and adhesively-bonded joints.* International journal of fracture, 2003. **119**(1): p. 25-46.

83. Anyfantis, K.N., *On the failure analysis of bondlines: Stress or energy based fracture criteria?* Engineering Fracture Mechanics, 2014. **126**: p. 108-125.

84. Campilho, R.D.S.G., et al., *Strength prediction of single- and double-lap joints by standard and extended finite element modelling.* International Journal of Adhesion and Adhesives, 2011. **31**(5): p. 363-372.

85. Iijima, S., *Helical microtubules of graphitic carbon.* Nature 1991. **354**(56–58).

86. Prasek, J., et al., *Methods for carbon nanotubes synthesis—review.* Journal of Materials Chemistry, 2011. **21**(40): p. 15872-15884.

87. Qian, D., et al., *Mechanics of carbon nanotubes.* Applied Mechanics Reviews, 2002. **55**(6): p. 495-533.

88. Vidu, R., et al., *Nanostructures: a platform for brain repair and augmentation.* Frontiers in Systems Neuroscience, 2014. **8**(91).

89. Ma, P.-C., et al., *Dispersion and functionalization of carbon nanotubes for polymer-based nanocomposites: A review.* Composites Part A: Applied Science and Manufacturing, 2010. **41**(10): p. 1345-1367.

90. Rana, S., R. Alagirusamy, and M. Joshi, *A review on carbon epoxy nanocomposites.* Journal of Reinforced Plastics and Composites, 2009. **28**(4): p. 461-487.

91. Liu, L. and H.D. Wagner, *Rubbery and glassy epoxy resins reinforced with carbon nanotubes.* Composites Science and Technology, 2005. **65**(11-12): p. 1861-1868.

92. Chen, H., et al., *Dispersion of carbon nanotubes and polymer nanocomposite fabrication using trifluoroacetic acid as a co-solvent.* Nanotechnology, 2007. **18**(41): p. 415606.

93. Zhao, L. and L. Gao, *Stability of multi-walled carbon nanotubes dispersion with copolymer in ethanol.* Colloids and Surfaces A: Physicochemical and Engineering Aspects, 2003. **224**(1-3): p. 127-134.

94. Gkikas, G., N.M. Barkoula, and A.S. Paipetis, *Effect of dispersion conditions on the thermo-mechanical and toughness properties of multi walled carbon nanotubes-reinforced epoxy.* Composites Part B: Engineering, 2012. **43**(6): p. 2697-2705.

95. D638-14, A., *Standard Test Method for Tensile Properties of Plastics.* ASTM International, 2014.

96. Jin, F.-L. and S.-J. Park, *Recent advances in carbon-nanotube-based epoxy composites.* Carbon letters, 2013. **14**(1): p. 1-13.

97. Guo, W. and G. Chen, *Fabrication of graphene/epoxy resin composites with much enhanced thermal conductivity via ball milling technique.* Journal of Applied Polymer Science, 2014. **131**(15).

98. Zhang, S., et al., *Control of graphitization degree and defects of carbon blacks through ball-milling.* RSC Advances, 2014. **4**(1): p. 505-509.

99. Kónya, Z., et al., *End morphology of ball milled carbon nanotubes.* Carbon, 2004. **42**(10): p. 2001-2008.

100. Liu, C.-X. and J.-W. Choi, *Improved Dispersion of Carbon Nanotubes in Polymers at High Concentrations.* Nanomaterials, 2012. **2**(4): p. 329-347.

101. Huang, Y., S. Ahir, and E. Terentjev, *Dispersion rheology of carbon nanotubes in a polymer matrix.* Physical Review B, 2006. **73**(12).

102.   Ma, P.C., et al., *In-situ amino functionalization of carbon nanotubes using ball milling.* Journal of nanoscience and nanotechnology, 2009. **9**(2): p. 749-753.

103.   Caneba, G., et al., *Novel ultrasonic dispersion of carbon nanotubes.* Journal of Minerals and Materials Characterization and Engineering, 2010. **9**(03): p. 165.

104.   Khashaba, U.A., A.A. Aljinaidi, and M.A. Hamed, *Nanofillers modification of Epocast 50-A1/946 epoxy for bonded joints.* Chinese Journal of Aeronautics, 2014. **27**(5): p. 1288-1300.

105.   Song, Y.S. and J.R. Youn, *Influence of dispersion states of carbon nanotubes on physical properties of epoxy nanocomposites.* Carbon, 2005. **43**(7): p. 1378-1385.

106.   Thostenson, E.T. and T.-W. Chou, *On the elastic properties of carbon nanotube-based composites: modelling and characterization.* Journal of Physics D: Applied Physics, 2003. **36**(5): p. 573.

107.   Bai, J.B. and A. Allaoui, *Effect of the length and the aggregate size of MWNTs on the improvement efficiency of the mechanical and electrical properties of nanocomposites—experimental investigation.* Composites Part A: Applied Science and Manufacturing, 2003. **34**(8): p. 689-694.

108.   Rossell, M.D., et al., *Impact of sonication pretreatment on carbon nanotubes: A transmission electron microscopy study.* Carbon, 2013. **61**: p. 404-411.

109.   Cheng, Q., et al., *Ultrasound-assisted SWNTs dispersion: effects of sonication parameters and solvent properties.* The Journal of Physical Chemistry C, 2010. **114**(19): p. 8821-8827.

110.   K.L Lu, R.M.L., Y.K. Chen and M.L.H. Green, P.J.F. Harris and S.C. Tsang, *Mechanical Damage of Carbon Nanotubes by Ultrasound.* 1996.

111.   Huang, Y.Y. and E.M. Terentjev, *Dispersion of Carbon Nanotubes: Mixing, Sonication, Stabilization, and Composite Properties.* Polymers, 2012. **4**(4): p. 275-295.

112.   Vaisman, L., H.D. Wagner, and G. Marom, *The role of surfactants in dispersion of carbon nanotubes.* Advances in colloid and interface science, 2006. **128**: p. 37-46.

113.   Li, Q., M. Zaiser, and V. Koutsos, *Carbon nanotube/epoxy resin composites using a block copolymer as a dispersing agent.* physica status solidi (a), 2004. **201**(13): p. R89-R91.

114.   Cho, J., I.M. Daniel, and D.A. Dikin, *Effects of block copolymer dispersant and nanotube length on reinforcement of carbon/epoxy composites.* Composites Part A: Applied Science and Manufacturing, 2008. **39**(12): p. 1844-1850.

115.   Gojny, F.H., et al., *Evaluation and identification of electrical and thermal conduction mechanisms in carbon nanotube/epoxy composites.* Polymer, 2006. **47**(6): p. 2036-2045.

116.   Sandler, J., et al., *Development of a dispersion process for carbon nanotubes in an epoxy matrix and the resulting electrical properties.* Polymer, 1999. **40**(21): p. 5967-5971.

117.   Bal, S., *Dispersion and reinforcing mechanism of carbon nanotubes in epoxy nanocomposites.* Bulletin of Materials Science, 2010. **33**(1): p. 27-31.

118.   Gojny, F.H. and K. Schulte, *Functionalisation effect on the thermo-mechanical behaviour of multi-wall carbon nanotube/epoxy-composites.* Composites Science and Technology, 2004. **64**(15): p. 2303-2308.

119.   Hsieh, T., et al., *The effect of carbon nanotubes on the fracture toughness and fatigue performance of a thermosetting epoxy polymer.* Journal of Materials Science, 2011. **46**(23): p. 7525.

120.   Fidelus, J., et al., *Thermo-mechanical properties of randomly oriented carbon/epoxy nanocomposites.* Composites Part A: Applied Science and Manufacturing, 2005. **36**(11): p. 1555-1561.

121.   Puglia, D., L. Valentini, and J.M. Kenny, *Analysis of the cure reaction of carbon nanotubes/epoxy resin composites through thermal analysis and Raman spectroscopy.* Journal of Applied Polymer Science, 2003. **88**(2): p. 452-458.

122.   Tao, K., et al., *Effects of carbon nanotube fillers on the curing processes of epoxy resin-based composites.* Journal of Applied Polymer Science, 2006. **102**(6): p. 5248-5254.

123.   Kim, S.H., W.I. Lee, and J.M. Park, *Assessment of dispersion in carbon nanotube reinforced composites using differential scanning calorimetry.* Carbon, 2009. **47**(11): p. 2699-2703.

124.   Jahan, N., et al., *Effect of carboxyl functionalized MWCNTs on the cure behavior of epoxy resin.* 2013.

125.   Abdalla, M., et al., *Cure behavior of epoxy/MWCNT nanocomposites: the effect of nanotube surface modification.* Polymer, 2008. **49**(15): p. 3310-3317.

126. Xie, H., et al., *Cure kinetics of carbon nanotube/tetrafunctional epoxy nanocomposites by isothermal differential scanning calorimetry.* Journal of Polymer Science Part B: Polymer Physics, 2004. **42**(20): p. 3701-3712.

127. Fiedler, B., et al., *Fundamental aspects of nano-reinforced composites.* Composites science and technology, 2006. **66**(16): p. 3115-3125.

128. Patricia Irwin, W.Z., Yang Cao, Xiaomei Fang, and Daniel Qi Tan, *Chapter 6 Mechanical and Thermal Properties.* Dielectric Polymer Nanocomposites, 2009(Springer Science+Business Media).

129. Lange, F.F., *The interaction of a crack front with a second-phase dispersion.* Philosophical Magazine, 1970. **22**(179): p. 0983-0992.

130. Lachman, N. and H.D. Wagner, *Correlation between interfacial molecular structure and mechanics in CNT/epoxy nano-composites.* Composites Part A: Applied Science and Manufacturing, 2010. **41**(9): p. 1093-1098.

131. Kausch, H., *Deformation and fracture of high polymers.* 2013: Springer Science & Business Media.

132. Penumadu, D., et al., *Mechanical properties of blended single-wall carbon nanotube composites.* Journal of Materials Research, 2003. **18**(08): p. 1849-1853.

133. Lau, K.-t., S.-Q. Shi, and H.-m. Cheng, *Micro-mechanical properties and morphological observation on fracture surfaces of carbon nanotube composites pre-treated at different temperatures.* Composites Science and Technology, 2003. **63**(8): p. 1161-1164.

134. Gojny, F.H., et al., *Influence of different carbon nanotubes on the mechanical properties of epoxy matrix composites – A comparative study.* Composites Science and Technology, 2005. **65**(15–16): p. 2300-2313.

135. Chow, W.S. and P.L. Tan, *Epoxy/Multiwall Carbon Nanotube Nanocomposites Prepared By Sonication and Planetary Mixing Technique.* Journal of Reinforced Plastics and Composites, 2010. **29**(15): p. 2331-2342.

136. *Standard Test Method for Tensile Properties of Plastics.* 2014, ASTM International.

137. *Standard Test Methods for Flexural Properties of Unreinforced and Reinforced Plastics and Electrical Insulating Materials.* 2015, ASTM International.

138. *Standard Test Methods for Plane-Strain Fracture Toughness and Strain Energy Release Rate of Plastic Materials.* 2014, ASTM International.

139. Liao, Y.-H., et al., *Investigation of the dispersion process of SWNTs/SC-15 epoxy resin nanocomposites.* Materials Science and Engineering: A, 2004. **385**(1): p. 175-181.

140. Sichina, W.J., *Characterization of Epoxy Resins Using DSC.* Perkin Elmer Instruments, 2000(Thermal Analysis).

141. *AMS03_2 Cleaning and Preparation of Metal Surfaces.* SAE International, (Ams B Finishes And Fluids Committee): p. 45.

142. *BAC 5555.* US Patents 4,085012 & 4,793,903, 1974.

143. *BS 5350-C5:2002 Methods of test for adhesives - Determination of bond strength in longitudinal shear for rigid adherends.* London: British Standards Institution, 2002.

144. *Standard Test Method for Apparent Shear Strength of Single-Lap-Joint Adhesively Bonded Metal Specimens by Tension Loading (Metal-to-Metal).* 2010, ASTM International.

145. Organización Internacional de, N., *Adhesives: Determination of the Mode 1 Adhesive Fracture Energy of Structural Adhesive Joints Using Double Cantilever Beam and Tapered Double Cantilever Beam Specimens.* 2009: ISO.

146. Kim, T.-H., J.-H. Kweon, and J.-H. Choi, *An Experimental Study on the Effect of Overlap Length on the Failure of Composite-to-Aluminum Single-Lap Bonded Joints.* Journal of Reinforced Plastics and Composites, 2008. **27**(10): p. 1071-1081.

147. Boeman, R.G., et al. *A practical test method for mode I fracture toughness of adhesive joints with dissimilar substrates.*

148. Soboyejo, W., et al., *A modified mixed-mode bending specimen for the interfacial fracture testing of dissimilar materials.* Fatigue & Fracture of Engineering Materials & Structures, 1999. **22**(9): p. 799-810.

149. Yang, K., et al., *Effects of carbon nanotube functionalization on the mechanical and thermal properties of epoxy composites.* Carbon, 2009. **47**(7): p. 1723-1737.

150.   Shen, J., et al., *The reinforcement role of different amino-functionalized multi-walled carbon nanotubes in epoxy nanocomposites.* Composites Science and Technology, 2007. **67**(15-16): p. 3041-3050.

151.   Gojny, F.H., et al., *Surface modified multi-walled carbon nanotubes in CNT/epoxy-composites.* Chemical physics letters, 2003. **370**(5-6): p. 820-824.

152.   Ma, P.-C., et al., *Dispersion, interfacial interaction and re-agglomeration of functionalized carbon nanotubes in epoxy composites.* Carbon, 2010. **48**(6): p. 1824-1834.

153.   Friedrich, S.M., et al., *Damage mode characterization of mechanically fastened composite joints using carbon nanotube networks.* Composites Part A: Applied Science and Manufacturing, 2011. **42**(12): p. 2003-2009.

154.   Lim, A.S., et al., *Damage sensing of adhesively-bonded hybrid composite/steel joints using carbon nanotubes.* Composites Science and Technology, 2011. **71**(9): p. 1183-1189.

155.   Baldan, A., *Adhesively-bonded joints and repairs in metallic alloys, polymers and composite materials: adhesives, adhesion theories and surface pretreatment.* Journal of materials science, 2004. **39**(1): p. 1-49.

156.   Prolongo, S.G. and A. Ureña, *Effect of surface pre-treatment on the adhesive strength of epoxy–aluminium joints.* International Journal of Adhesion and Adhesives, 2009. **29**(1): p. 23-31.

157.   Khan, M.H., Gali, O. A.,Edrisy, A.,Riahi, A. R., *Effect of oxidation and surface roughness on the shear strength of single-lap-joint adhesively bonded metal specimens by tension loading.* Applied Adhesion Science, 2016. **4**(1): p. 21.

Publications

1. Konstantakopoulou M., Kotsikos G., "Effect of MWCNT filled epoxy adhesives on the quality of adhesively bonded joints", Plastics, Rubber and Composites, 1-7, 2016.

2. Konstantakopoulou M., Deligianni A., Kotsikos G, "Failure of dissimilar material bonded joints", Physical Sciences Reviews, 2016.

3. A. A. Mahuof, M. Konstantakopoulou, A. G. Gibson, and G. Kotsikos, "Preparation of novel nanocomposites using the ultra-sonication technique", In Students on Applied Engineering (ICSAE), International Conference for, pp. 383-391. IEEE, 20-21 October 2016.

4. Konstantakopoulou M., Kotsikos G., "Adhesive Property Modification through Addition of MWCNTs for Dissimilar Material Joint Applications", Proceedings of ECCM 17, Munich, Germany, 23-30 June 2016.

5. Konstantakopoulou M., Kotsikos G., "Investigation of the Effect of MWCNT Filled Epoxy Adhesives in Enhancing the Quality of GFRP/Aluminium Bonded Joints", Proceedings of ICCM 20, Copenhagen, Denmark, 19-24 July 2015.